Quasi-Static and Fatigue Strength of Helically Wrapped Structures

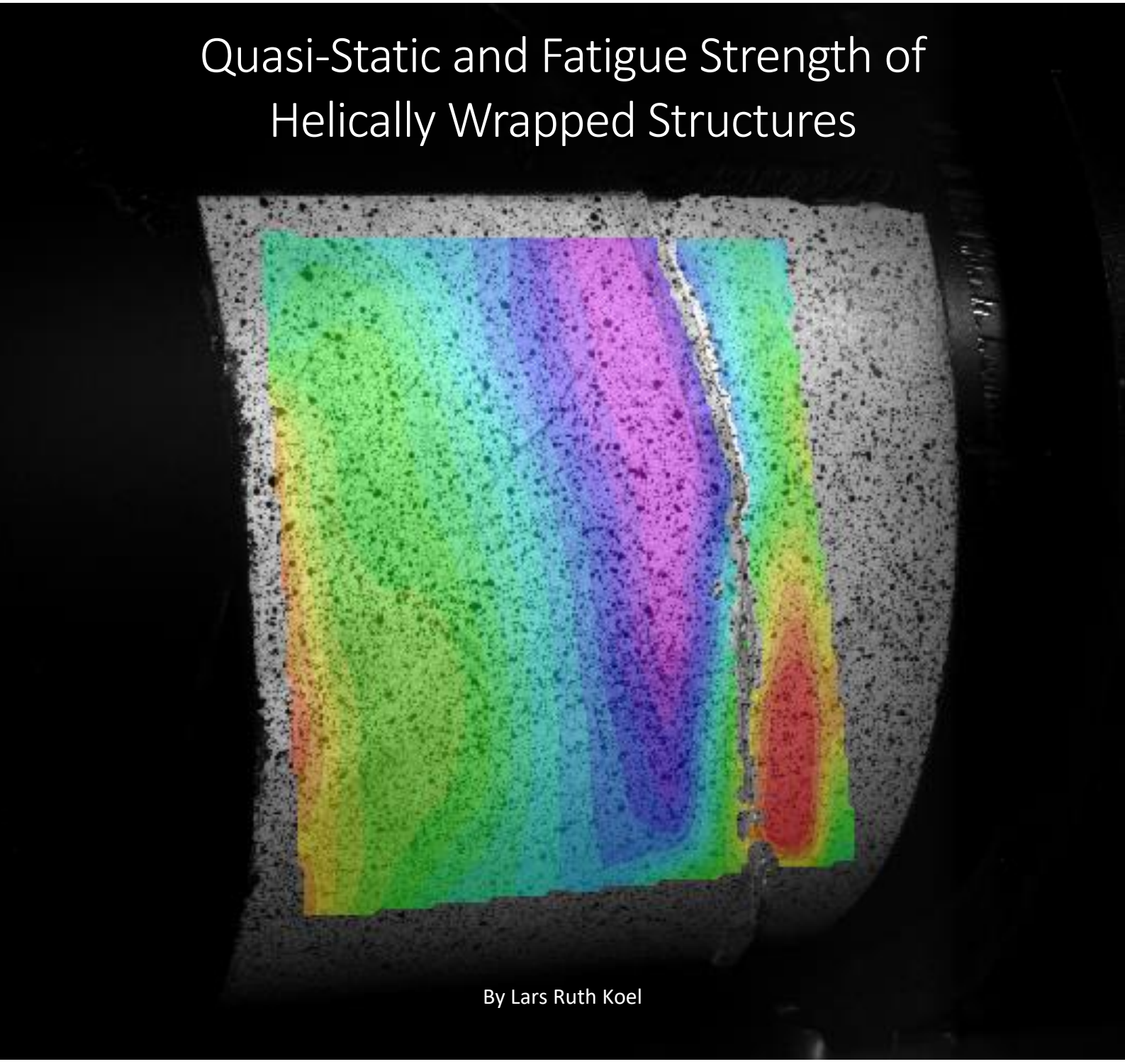

By Lars Ruth Koel

HUYGENS ENGINEERS

TU Delft

Faculty of Aerospace Engineering

Delft University of Technology

Quasi-Static and Fatigue Strength of Helically Wrapped Structures

By Lars Ruth Koel

Technical University of Delft
Aerospace Engineering

Aerodynamics and Wind Energy

Aerospace Structures and Materials

March 3, 2023

Summary

The structural performance of a structure is determined by the applied material and geometry. Mechanical structures in the aerospace and renewable energy industry are produced with composites nowadays. Huygens Engineers was inspired to design a mechanical structure to be manufactured for a wind energy application. A helically wrapped structure with overlapping adhesively bonded interfaces was invented and has been researched for this master thesis. The helically wrapped structure is a composite made from a thin strip of metal and is bonded with a strong structural adhesive, providing a lightweight, strong, and cost-friendly solution.

Despite the advantages of helically wrapped adhesively bonded structures, they are anisotropic and contain stress concentrations. The strength and fatigue lifespan of this conceptual structure is unknown and requires research. The stress distribution through an adhesive joint is non-linear, making strength and fatigue analysis complex. The objective of this research is to predict the fatigue life of the helically wrapped structure and determine whether either the adherend or the adhesive is the critical factor in this design.

The literature described an energy-based method to analyse non-homogeneous materials. The strain energy release rate which originated from the work of Griffith is the preferred method to predict fatigue crack growth in non-homogeneous structures. The literature described a method to express the delamination growth rate in an adhesive interface as a power-law function of the strain energy release rate. A finite element model employing the virtual crack closure technique calculates the strain energy release rate in the helically wrapped structure with predefined cracks in the adhesive joint. It was found that the crack front propagated like an oval shape through the joint under fatigue loading.

This research was supported by experimental testing to validate the fatigue predictions. Multiple helically wrapped structures were manufactured in a self-designed wrapping machine. Tweaking the wrapping machine and machining special parts enabled the production of identical helically wrapped structure test specimens. The structure was tested in a self-designed four-point bending test setup employing a 60 kN fatigue bench. The test setup was found not suitable to transfer the desired loads through the helically wrapped structure. The bolts in the clamps kept breaking and the helically wrapped structure endured local buckling deformations near the clamps. Nevertheless, the structure did endure half the amount of fatigue cycles the adherend could withstand. It did not disprove the number of predicted fatigue cycles the structure would endure, but further validation is required.

Quasi-static analyses of single lap joints employing the shear-lag model of Volkersen, and basic normal stress and shear stress definitions were used to determine whether the adherend or the adhesive fails. It was found that the adherend reaching yield strength caused too much strain for the adhesive to withstand, leading to instant failure of the joint. The adhesive single-lap-joint shear strength derived from the ASTM D1002-10, as provided by many manufacturers, is not suitable as a design allowable. A range of overlap length and adherend thickness ensures the adherend to be dominant for the strength and not the adhesive.

The fatigue life predictions of the helically wrapped structure showed that the adherend and not the adhesive is the critical factor. Supported by experimental data an overestimated prediction of the fatigue crack growth of the adhesive in the structure was found to be conservative. Here it was concluded that the adherend is the critical factor. The found design rules for a limited range of configurations ensure fatigue life predictions need only be done for the adherend materials. For these cases, the adherend is guaranteed to be critical.

Contents

List of tables

List of Figures

1 Introduction

1.1 Mechanical Structures

The structural performance of a structure is determined by the applied material and geometry. Structures like columns, beams, trusses, and arches are structural elements which are known to be strong for their intended application due to its shape. However, the chosen material is equally important since it determines the ability to distribute stress through the geometry. For example, a beam made of steel can withstand higher loads instead of wooden beams.

Mechanical structures in aerospace and renewable energy industry are produced with composites nowadays. Composites are materials produced from dissimilar materials that create enhanced structural properties unlike the individual elements. Reinforced concrete, plywood, fibre-reinforced polymers, and cardboard pipes are examples of composite materials. Cardboard pipes can be seen as a composite because it is made of cardboard and the interfaces are adhesively bonded. Hence, the composition of different materials result in a strengthened structure. It would be interesting to know what other applications this cardboard pipe structure can offer, if it is made of different materials. Therefore, derived from the cardboard pipe but using different materials, a helically wrapped structure as a load carrying structure is researched for this thesis. The structural strength, rigidity and lightweight of this structure could be utilised for several applications. A helically wrapped structure could be used in a wind energy application, for example.

Aside the advantages of composites, a negative aspect is that composites are anisotropic and generally expensive. The anisotropic property makes a composite strong in a desired direction but lack the ability to withstand transverse forces. Therefore, composite structures require detailed analyses of the stress distribution through the structure. General fracture mechanics cannot be easily applied to analyse this helically wrapped structure. There is no knowledge or methods available to perform calculations on this structure, to predict the quasi-static strength or the fatigue life. Therefore, modelling is required to analyse the structural strength and fatigue life. The fatigue life and quasi-static strength is either dependent on the adherend or the adhesive. Therefore, research on a method to predict the quasi-static and fatigue strength of a helically wrapped structure is required.

1.2 Fatigue Failure

Fatigue is a damage accumulation phenomenon where the repetition of cyclic fluctuating loads is responsible for the complete failure of a structure, even when the applied load is far below the critical strength of the structure [1]. Cyclic fluctuating loads, such as wind turbulence, thermal expansion, or rotational excitations acting on a structure, like an aircraft or wind turbine, make it particularly susceptible to fatigue failure. Therefore, fatigue failure has become an important subject for several areas of engineering, like aerospace engineering, and the renewable energy industry, since it might prevent the loss of massive constructions or even lives.

Fatigue failure is known to initiate at material defects or stress concentrations due to structural discontinuity. Discontinuities on structures are encountered in areas like joints, or

changes in structural geometry. These are considered potential areas for failure and demand higher attention on design and maintenance.

The helically wrapped structure is initially designed to carry fluctuating loads and functions as a mechanical structure. Adhesively bonded structures behave differently than traditional mechanical joining techniques like rivets or welds. The stress concentration is reduced and the area to transfer load or distribute stress is larger. Consequently, fatigue behaviour in a joint can benefit from the utility of an adhesively bonded joint, Figure 1.1.

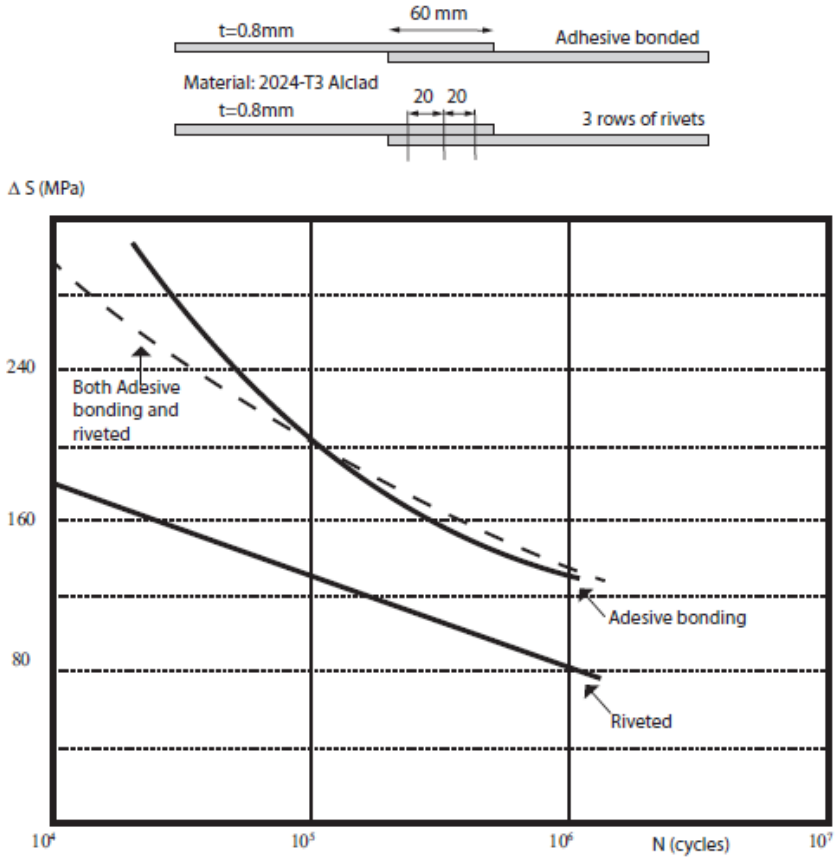

Figure 1.1 Comparison between the S-N curves (R=0.1) of a riveted, bonded and riveted and bonded joint for similar geometries [2].

1.3 Project Scope

This research is focussed on helically wrapped structures which are adhesively bonded. The structure must function as a load carrying structure. The scope of this project can increase rapidly so choices are made to focus on aspects being most valuable for this conceptual design.

There are different techniques to helically wrap a structure, but only one type of helical wrapping technique is researched. A mould is required to wrap around. Machining of this mould is expensive and time consuming, so only one wrapping technique must be picked.

The quasi-static and fatigue properties are analysed for only one load case, because costs to create this structure and being able to test it, increase rapidly. The worst-case scenario load level must be applied to obtain useful information about the operational envelope.

Only debonding of the adhesive joint must be simulated, because detailed analyses of the stress concentration along a joint requires heavy computational work when the entire helically wrapped structure is modelled. The objective is to predict the fatigue life of the structure which does not require a model of the damage degrading properties of the adhesive. Only modelling debonding of the adherend surfaces provides sufficient information to determine the crack growth rate.

This project is divided into two parts. The first part is to manufacture the helically wrapped structure. The first objective is figuring out how to manufacture and design a machine to create a helically wrapped structure. The second part is to validate the helically wrapped structure's quasi-static strength and fatigue life. Validation must be done in a fatigue bench that must be adapted to be able to apply the loads accordingly. The objective is to validate the predicted quasi-static strength and fatigue life.

First a chapter is devoted to describing the present literature about helically wrapping structures, adhesive bonding, linear elastic fracture mechanics, and fatigue crack growth prediction. This describes the required knowledge for this project and reveal knowledge gaps to be researched. The research question is given at the end of the literature review. Then the helically wrapped pipe structure is elaborated in the up-following chapter. The different wrapping techniques, manufacturing and chosen geometry of the helically wrapped structure is elaborated here. Chapter 4 is devoted to the description of the quasi-static strength of the helically wrapped structure. Here it becomes clear whether the adherend or the adhesive is the critical factor in this design. Chapter 5 describes the fatigue analysis of the helically wrapped structure. The method to determine the crack growth rate and to predict the fatigue life is explained here. After that the validation of the quasi-static strength and the fatigue life of the helically wrapped structure is described in the last chapter. Finally, the report is then wrapped up by the conclusions and recommendations.

2 Literature Review

A literature review was conducted before starting on the research for this thesis. The objective was to determine the current knowledge about helically wrapped structures and adhesive joints. Wrapping techniques are currently found in structures that are not meant for high strength applications. Various wrapping techniques and structures are discussed in this chapter. To prove the potential of this conceptual design of the helically wrapped structure, fatigue performance must be analysed. Various models to predict fatigue failure and damage growth are discussed.

2.1 Present Wrapping Techniques

There are several wrapping techniques to create a tubular structure from sheet materials. Cardboard tubes and spiral ducts are the most common helically wrapped structures, see Figure 2.1. They both share one technique to helically wrap the structure but differ in the joining method. Cardboard tubes are adhesively joined by several sheets wrapped around each other. Steel ventilation ducts are joined by interlocking and forming the edges to create a mechanical joint. They both share one wrapping technique. The individual metal strips are helically wrapped along the same diameter without overlapping its own surface, hence the edges of the sheet connect after one revolution while simultaneously axially translating a length of the strip width.

A *B*

Figure 2.1 Helically Wrapped structures. A: Cardboard pipe. B: Steel duct [3]

Another wrapping technique is found in the reinforcement or repairing of gas or liquid transmission pipelines. Several patents describe helically wrapping of composites, but they consist of fibre reinforced materials. Patent number US10890276B2, with the title: ‘metal strip winding continuous reinforced thermoplastic composite pipe’, is similar to this project, but uses different and multiple materials. Also the metal strip is not bonded and can move within the structure [4]. The helically wrapping of a strip of material is also used in this thesis. It ensures an increase in hoop and axial strength of the tube and thereby increasing the compressive capacity of it. Up until this point no research has been found about a wrapping technique where one metal strip, helically wrapped, overlaps its own surface after one revolution while axially advancing less than a strip width and adhesively bond the interfaces.

2.2 Stress Analysis of Adhesive Joints

The stress distribution through an adhesive joint is affected by many variables, making it difficult to quickly apply it for design purposes. Adhesive joints can be used in different configurations. For instance, different dissimilar materials can be joined but also different joint geometries can be used. The type of adhesive determines the possibility to bond to certain materials. Despite the many possibilities, all adhesives withstand shear loads better than normal loads. Counter-intuitively, loads on a lap joint result in a peeling force component due to secondary bending.

This is a feature to be avoided as much as possible since adhesives perform less well in peel stress loading.

A few scientists have dedicated their research to analytically approximating the shear and peel stresses within an adhesively bonded joint. The first important contributor is Volkersen [5], and his approach is described in paragraph 2.2.1. Other scientists successfully improved on his approximation, at the expense of more time consuming and computationally heavy solutions. These contributions are considered in paragraph 2.2.2.

2.2.1 Volkersen's analysis

The analytical shear-lag model from Volkersen was a first step to assess the shear strength of an adhesively bonded structure [5]. He approximated the adhesive to only deform in shear and the adherend to only deform in tension. Later it became apparent that this model was inaccurate for short overlap lengths, as it did not account for the out-of-plane rotation of the outer edges of the adherend. This out-of-plane rotation of the outer edges caused the adhesive to be loaded in peel stress. Adhesives tend to endure shear stress better than peel stresses [6]–[8]. Nevertheless, this approximation proved valid to determine the peak stress for single lap joint structures for overlap lengths larger than 10 millimetres.

Volkersen's analysis gives good insight into how the load is transferred through a thin adhesive. Figure 2.2, shows the parameters used in the analytic expression for the peak stress equation (1).

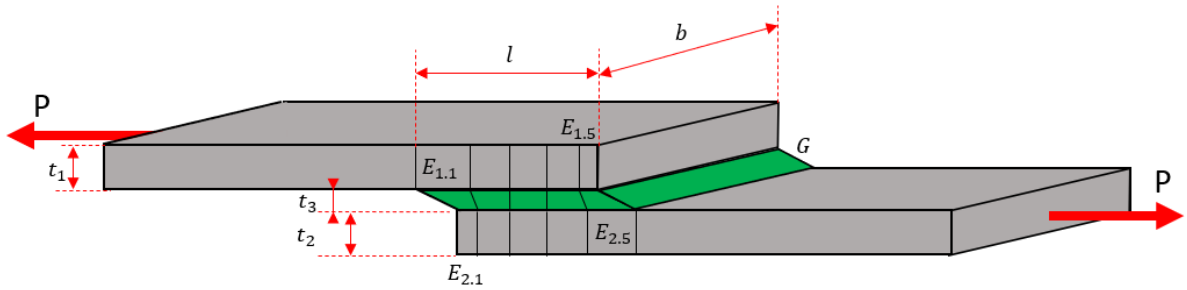

Figure 2.2 Single lap Joint parameters

$$p_{max} = 2\, b\, \tau_{adh} \sqrt{\frac{E * t * t_3}{2 * G}} * \tanh \sqrt{\frac{G * l^2}{E * t * t_3}} \qquad (1)$$

Here the peak load is p_{max} $[N]$, b is the width of the adherend $[m]$, τ_{adh} is the adhesive shear strength $[\frac{N}{m^2}]$, E is the Young's modulus of the adherend $[Pa]$, t is the thickness of the adherend ($t_1 = t_2 = t, in\ the\ figure$) $[m]$, t_3 is the adhesive thickness $[m]$, G is the shear modulus of the adhesive $[Pa]$ and l is the overlap length $[m]$.

Figure 2.3 shows a plot of the maximum failure load versus overlap length. The trend of the graph is applicable to any arbitrary adhesive joint.

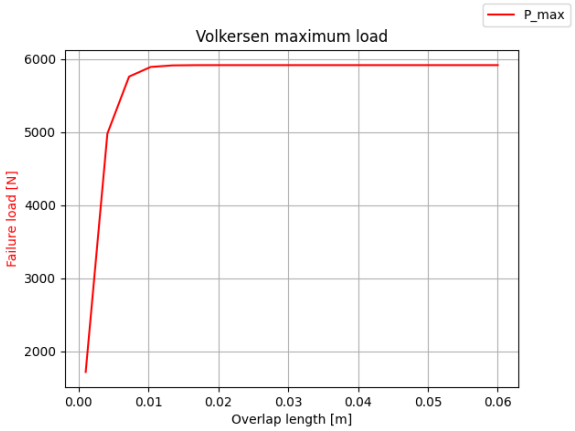

Figure 2.3 Volkersen's shear lag model, maximum failure load

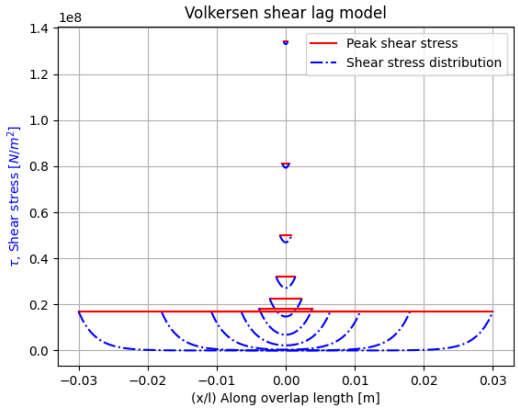

Figure 2.4 Shear stress distribution by Volkersen

When the overlap length is below 10 mm, the total load that can be applied to the single lap joint is lower than for longer overlap lengths. However, increasing the overlap length will only increase the total load up to a maximum load because it stagnates. This is caused by the maximum retainable shear stress at the edges of the joint. This feature is determinant for any adhesive joint and therefore very important to account for when designing a structure with adhesive joints. This will be the limiting factor for the load applied to the helically wrapped structure. The reason for this stagnating maximum load is due to a mechanism that causes a concentration of the shear stress at the edges of the joint.

Figure 2.4 shows this mechanism of how the shear stress along the joint is distributed; the mechanism is more visible in Figure 2.2. The low shear modulus of the adhesive causes the shear stress to increase from the middle of the lap joint to a maximum value closer to the edges. At the very edge of the joint, at the transition from upper adherend to adhesive to lower adherend, the normal stress is distributed through the adhesive to the beginning of the lower adherend. In the vicinity of the beginning of the lower adherend no load is transferred. An infinitesimal small distance next to this beginning of the lower adherend the load can be transferred. When the applied load and thus peak stress exceeds the maximum peak stress of the joint, it fails immediately. A too short overlap length causes the applied load to exceed the allowable peak stress too soon, also leading to failure. When the overlap length is increased, the centre of the overlap of the joint carries a decreasing amount of load. Most of the load is carried at the edges of the joint.

The strain of a joint clarifies the load distribution also illustrated in Figure 2.2. The strain at E1.1 is higher than at E1.5. The same but opposite view is true for the lower adherend, (strain E2.1 < E2.5). There is no straining present in the middle of the joint. Hence, all straining occurs at the edges of the joint. Therefore, a bathtub shape of the shear stress distribution is obtained along the overlap length of the joint. Due to the constant maximum allowable peak stress an adhesive can withstand, depending on the joint geometry and adherend material, there is always a limit to the amount of applied load to an adhesive joint.

According to the Volkersen approximation, the maximum adhesive shear stress occurs at the ends of the joint and is calculated by equation (2)[8]. One can see that the maximum shear stress, τ_{max}, is independent of overlap length for the terms outside the hyperbolic cotangent. Only the limit of overlap length approaching zero causes the hyperbolic cotangent and thus

shear stress to go to infinity. Therefore, Volkersen's approximation is not accurate for very low overlap lengths. Nevertheless, it is still a good approximation for a longer overlap length.

$$\tau_{max} = \frac{P}{l * b}\sqrt{\frac{G * l^2}{2 * E * t * t_3}} * Coth\left(\sqrt{\frac{G * l^2}{2 * E * t * t_3}}\right) \quad (2)$$

The research done by Volkersen assumed the peel and shear stress to be constant across the adhesive thickness, the shear was maximum (and not zero) at the overlap ends and the shear deformation of the adherends was neglected. However, the shear stress at the overlap-end must be zero because at the very end of the adherend face there is no material anymore and thus it cannot bear any load. Experiments verify that bending of the outer edges of the adherend occurs at a single lap joint test. When there is a bending moment present, compressive and tension forces must be present inside the adhesive layer as well. These are phenomena that were either neglected or assumed to be constant.

2.2.2 Improvements on Volkersen's analysis

Multiple other scientists tried to improve the approximation of Volkersen's analysis. A few of these scientist are Goland and Reissner (1944)[9], Hart-Smith (1973)[10], Adams and Mallick (1992)[11].

Goland and Reissner did account for rotation in the joint by applying a bending factor into the equation. Later they also included the option to calculate bonding strength for different adherend materials.

Hart-Smit improved and extended the classical approach by Goland and Reissner. He overcame the deficiency in the determination of the critical bending moment in the adherends at the ends of the overlap. He then extended the approach by Goland and Reissner by including additional factors like adhesive plasticity, stiffness imbalance between adherends, and influence of laminated filamentary composite adherends. The last addition provides a distinction from isotropic metal adherends.

Adams and Mallick developed a more advanced analysis for both single and double lap joints. They did take bending and different adherend materials into account for the calculations of the stress distributions. The equations can only be solved explicitly and numerically and must be verified with experimental data.

Since the improved solutions are rather a time expensive solution, it would be best suited to proceed with the analytical formulas supplied by Volkersen or Hart-Smit. These approximations are still the reference work. With the relatively fast analytical method, Volkersen's method is considered for the thesis work. Though, this method still provides a good approximation of the stresses through an adhesive joint.

2.3 Linear Elastic Fracture Mechanics and Adhesive Joints

Linear Elastic Fracture Mechanics (LEFM) studies the development and propagation of cracks in materials. It uses methods of analytical solid mechanics to calculate the driving force on crack growth and those of experimental solid mechanics to characterize the material's resistance to fracture[12]. The current approaches to understand fatigue crack growth have their roots in the

work of Griffith[13]. Griffith was looking for a theory that would explain the failure of structures containing cracks. He made its breakthrough when he took energy, rather than stress, as a controlling parameter. Griffith proposed that the critical stress at which a crack would extend, could be derived from the balance between released and consumed energy.

Generally accepted formulation of the present development in this field of research is combined in a parameter known as the Strain Energy Release Rate (SERR). The SERR is the derivatives of the external work and strain energy [14]:

$$G = \frac{d(F - U)}{dA} \tag{3}$$

where F is the work done on a body by external forces, U the strain energy in a body, and A is the crack surface area. The SERR is equal to the difference between the reduction of strain energy per unit of crack growth and the external work performed per unit of crack growth. If this difference exceeds the amount of energy required per unit of crack growth, unstable fracture can occur. Crack growth will occur if:

$$G \geq G_c \tag{4}$$

where G_c is a critical SERR value.

Irwin demonstrated an equivalence of the SERR and the Stress Intensity Factor (SIF, K) [15]. They can be used interchangeably in fracture mechanics by the following relation:

$$G = \frac{K^2}{E'} \tag{5}$$

$$E' = E \qquad \text{plane stress} \tag{6}$$

$$E' = \frac{E}{1-\nu^2} \qquad \text{plane strain} \tag{7}$$

where E is the Young's modulus of the material, ν is the Poisson ratio. Consequently, Fatigue Crack Growth (FCG) models originally developed for metals, (SIF based models), are adapted to be used in FCG models when the use of the SERR is preferred. Due to the difficulty of calculating the K for non-homogeneous materials, G is often used in models for FCG in adhesives and composites. However, because these models are originally developed for using K, G in this case is interpreted as indicative of the crack-tip stress field, rather than as a energy parameter [16].

This information can be applied to fatigue in composites and adhesives. For quasi static loading conditions, equation (4) can be used to predict when a crack will grow. However, under fatigue crack loading conditions, cracks will grow even below the critical G_c values measured in quasi static loading test. Paris et al. proposed a method for predicting FCG which is currently the most successful method [17]. The SIF range, $\Delta K = K_{Max} - K_{Min}$, was proposed as a similitude parameter for FCG and with the use of experimental crack growth data he proposed the following relationship:

$$\frac{da}{dN} = C(\Delta K)^n \tag{8}$$

where a is the crack length, N is the number of fatigue cycles, and C and n are curve fitting parameters. As mentioned before, the K is generally used for FCG in metals, hence

homogeneous materials. The G is an energy-based method and thus the preferred method to predict FCG in non-homogeneous materials like adhesive bonds. By using the relation in equation (5), the proposed preferred relationship for the prediction of debonding under fatigue loading of adhesively bonded metals is:

$$\frac{da}{dN} = C(G_{Max})^n \tag{9}$$

where G_{Max} is the SERR calculated from the maximum applied stress S_{Max}.

2.4 Crack Opening Modes and Directions

There are three different crack opening modes defined for different types of loading, Figure 2.5. Fatigue cracks in service usually grow in a direction macroscopically perpendicular to the tensile stress that tries to open the crack [1]. This kind of crack opening is called 'Mode-I'. All modes are generally assessed separately for a specific application. Experience has shown that small cracks, nucleated under pure shear loading, quickly exhibit a transition to fatigue crack growth in tensile mode i.e. mode-I.

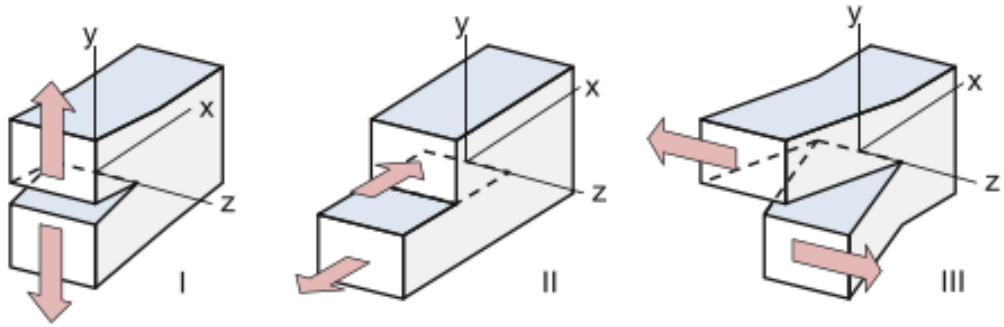

Figure 2.5 Crack opening modes, (left) Mode-I opening by tension or peeling forces, (middle) Mode-II opening by in-plane shear, (right) Mode-III opening by transverse shear [18].

Predicting the fatigue behaviour of a bonded joint for its use in a damage tolerance design philosophy remains a problem with no satisfactory solution. Often, the joint is subjected to a combination of peeling and shearing stresses. Hence, one of the most important factors influencing the fatigue behaviour of an adhesively bonded joint is the Mode Ratio [2]. Since the evaluation of the mode mix of a helically wrapped structure is a three-dimensional problem, complexity increases rapidly. The literature is not clear about the assessment of the direction of FCG. Generally, researchers take the normal of the crack front or the stress gradient as the crack growth direction. However, FEA models can calculate the SERR and derive the mode mix to estimate the crack growth direction.

2.5 Fatigue Crack Growth Prediction with FEA

Fatigue Crack Growth (FCG) can be predicted with the use of FEA software. The SERR or SIF is usually the quantity involved with the calculation of fatigue crack growth predictions. These models in FEA-software have their advantage and disadvantages. The three main models are the Extended Finite Element Method (XFEM), the Cohesive Zone Model (CZM), and Virtual Crack Closure Technique (VCCT).

2.5.1 Extended Finite Element Method

The Extended Finite Element Method (XFEM) is a finite element technique that allows more flexible modelling of crack growth. This method allows the crack path not to be confined to element edges or special interface elements from the mesh. Instead, enrichment functions are added to certain nodes, allowing the crack to grow arbitrarily through the element, rather than just along the edge. Hence, there is no need for a predefined crack path in the model [19].

2.5.2 Cohesive Zone Model

The Cohesive Zone Model is a failure model in FEA-software and is used in fracture mechanics of adhesively bonded joints. The stress singularity at a crack tip is removed, by applying a softening relation between the stress and relative displacement of the crack faces. A traction - separation law represents the relationship between the surface tractions and the relative separation at an interface where the crack might occur. The traction – separation law requires data about the critical SERR, cohesive stiffness, cohesive strength, critical separation, and separation at final failure. This is not convenient from a design perspective, because these values must either come from literature or experimental data. Once these values are known tweaking of the traction separation law is still required to include fatigue degrading effect in this model. The positive side of this model is no requirement for remeshing.

2.5.3 Virtual Crack Closure Technique

The Virtual Crack Closure Technique (VCCT) criterion uses the principles of LEFM and can be used for crack propagation analysis along a predefined surface. It assumes that the strain energy released when a crack is extended by a certain amount is the same as the energy required to close the crack by the same amount. According to Abaqus documentation[20] the SERR is calculated as follows:

$$G_I = \frac{1}{2}\left(\frac{v_{1,6}F_{v,2,5}}{b\ d}\right) \tag{10}$$

where G_I is the pure first mode SERR, b is the width and d is the length of the elements at the crack front, $F_{v,2,5}$ is the vertical force between the nodes 2 and 5, and $v_{1,6}$ is the vertical displacement between nodes 1 and 6. This is shown in Figure 2.6.

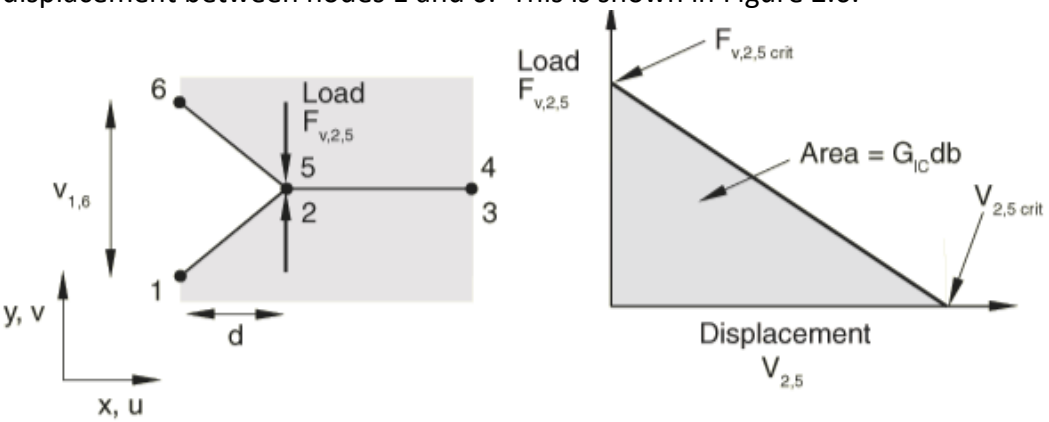

Figure 2.6 Calculation of the SERR pure mode-I

The calculation of the SERR employing the VCCT is dependent on the forces and displacement of the structure. This function requires a predefined initial crack. When the critical SERR, G_{IC}, is exceeded the nodes are separated and the crack is propagated. Once the crack is extended the mesh needs to be re-meshed. However, when the critical SERR is never reached, no crack propagation occurs but the SERR for that initial crack length is obtained. When consecutive initial crack areas are modelled in different simulations the SERR along the crack front is obtained. Employing the Paris relation about the amount of crack growth per fatigue cycle for a given SERR, allows for the prediction of the fatigue crack growth.

2.6 Research question

No research is conducted on helically wrapped structures with adhesively joined interfaces. Helically wrapped structures are at this point only available as structures transferring air, like air ducts, or as pipe cardboards to roll up paper. When it is made of metal and a continuous

structural adhesive joint is used it can function as a load carrying structure. This conceptual design must prove its utility as a load carrying structure.

This thesis objective is to prove the potential of this concept by researching the static and fatigue performance of this structural component. A method to predict the fatigue life must be found to be applicable to other helically wrapped structures. Researching the behaviour of fatigue crack propagation must clarify whether the adherend or the adhesive fails sooner in fatigue loading. Therefore, the following research question must be answered:

What is the fatigue life of a helically wrapped, adhesively joined, structure and how does fracture propagate through the joint?

To achieve the research goal, the following questions must be answered:

1. Is it possible to create a load carrying helically wrapped structure?
2. For fatigue, when is either the adherend or the adhesive the limiting factor in the concept?
3. How do fatigue cracks of a helically wrapped structure propagate?
4. What method should be used to predict the fatigue life?
5. If the adherend is the part limiting fatigue life, can fatigue analyses of the adhesive be neglected?

3 Helically wrapped pipe structure

The design and manufacturing of helically wrapped structure is elaborated in this chapter. Three wrapping techniques can be used to create a helically wrapped structure. A wrapping machine was built to manufacture the helically wrapped structure. This chapter is closed by the chosen geometry to be researched and tested in this thesis.

3.1 Wrapping Techniques

There are three techniques to helically wrap the sheet material into a tubular shape. One technique utilises two or more long rectangular strip sheet materials which are helically wrapped without overlapping of the individual sheets, see Figure 3.1. This is like the examples given in Figure 2.1. An additional helically wrapped patch or sheet material is required to join the first wrapped layer if the seam is adhesively bonded as shown in the cross-section. Every revolution the sheet is axially shifted by the width of the sheet material. Hence, a dependency between the pitch and the sheet width is present. During the wrapping a feed-in angle for the sheet material is required to avoid overlapping of the sheet material. Therefore, the feed-in angle of the sheet material is dependent on the sheet width, and tube radius.

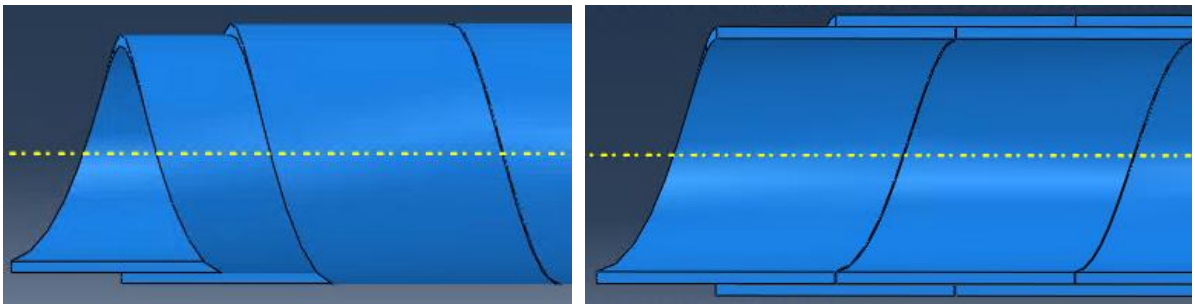

A B

Figure 3.1 Helically wrapped structure with helical patch. A: Top view. B: Cross-section.

The second technique utilises a curved sheet of material to be wrapped in a tubular shape, Figure 3.2. The sheet must be wrapped such that a continuous overlap is created every revolution. To create the overlap by wrapping around its own surface a conical shape is required. During manufacturing I discovered that a curved strip instead of straight sheet material is required. The initially used straight strip of material deviated from the helical guidance of the mould. After some revolutions the straight strip of material fully overlapped itself instead of a small section. Due to the partial overlap and inherently required cone, a remaining average constant diameter tube is obtained. For illustration purposes the sheet thickness is large, but a smaller wall thickness yields a very small deviation in the tubular diameter.

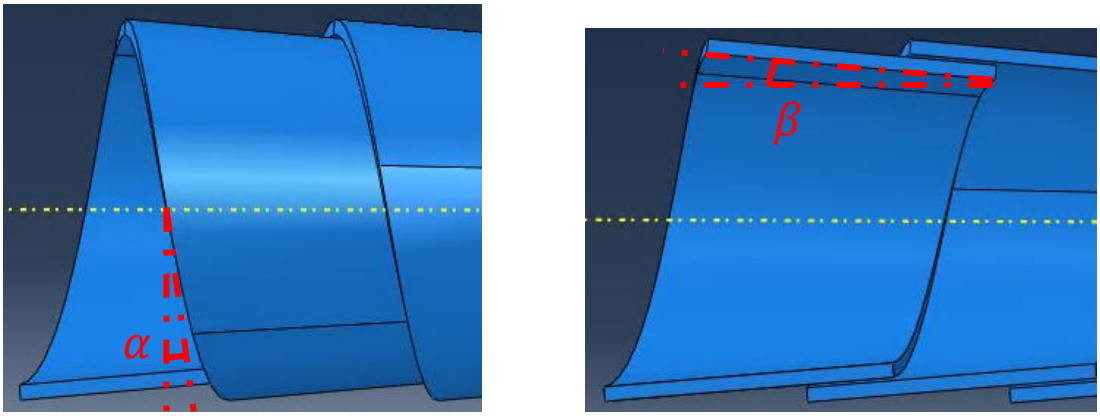

A B

Figure 3.2 Conical helically wrapped structure with constant average diameter. A: Top view. B: Cross-section.

To helically wrap a strip of material with this technique one must take the thread angle, α, and cone angle, β, into account. These angles are indicated in Figure 3.2. The thread, α, is dependent on the sheet width minus the desired overlap length and the circumference of the smallest radius of the cone. The cone angle, β, is dependent on the smallest radius of the cone, the sheet width minus the desired overlap length, and the sheet thickness. The pitch or helix angle is calculated by equation (11):

$$\alpha = \tan^{-1}\left(\frac{L_p}{2\,\pi\,r}\right) \tag{11}$$

where α is the angle of the helix or thread angle [rad], L_p is the lead of the helix or distance covered along the helix axis by shifting one strip-width minus the overlap length to complete one revolution [mm], and r is the inner radius of the helix [mm].

Due to the conus shape of the helically wrapped structure, a cone angle is introduced, indicated in Figure 3.2. One single strip of material must be wrapped around itself every lead distance. Therefore, the width of the metal strip minus the desired overlap length must be equal to the lead distance. To keep the minimal radius constant to obtain a constant average tubular diameter after one revolution, the radius of the metal strip along the width must increase. In other words, due to the axial repetitive conical shape, one thickness of the metal strip must increase the radius of the tube. The cone angle is calculated by equation (12):

$$\beta = \sin^{-1}\left(\frac{t}{l_w - l_o}\right) \tag{12}$$

Where, t, is the thickness of the metal strip [mm], l_w is the width of the metal strip [mm], and l_o, is the overlap length of the desired bonded area [mm].

The third technique utilises a rectangular strip of sheet material and helically wrap it around its own surface while expanding the outer diameter. This technique allows for an overlap and thus the use of only one strip of material without the need of a conical shape. This technique requires a spirally expanding but still helically wrapped tapered tube. The overlap must be joined either mechanically or with adhesives.

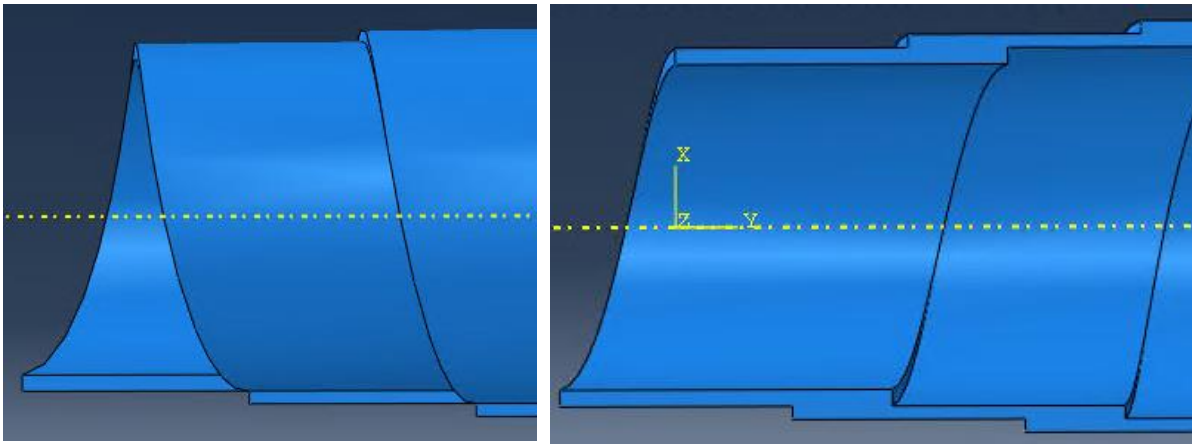

A B

Figure 3.3 Helically wrapped tapered structure. A: Top view. B: Cross-section

3.2 Producing the Helically Wrapped Structure

To make the helically wrapped structure and be able to apply adhesive between the interfaces a machine was made, Figure 3.4. The technical drawings of the individual parts designed for this project are included in the appendix. The second wrapping technique was chosen to manufacture the helical wrapped structures. This technique requires only one curved strip of material to be wrapped around itself. Due to guidance from a mould, geometrically identical specimens are created leaving less scatter in results due to manufacturing faults. Also, this technique was not available in the literature, so its application had to be developed as part of this thesis.

The overlapping interfaces must be adhesively joined to create a complete solid structure. The curved strip of material is mechanically fastened to the mould by two screws. The adhesive is applied on both sides of the curved strip of material. One side of the curved strip of material is provided with adhesive at the edge near the smaller radius. The other side is provided with adhesive at the edge near the larger radius. After wrapping one revolution the adhesive on both sides come together.

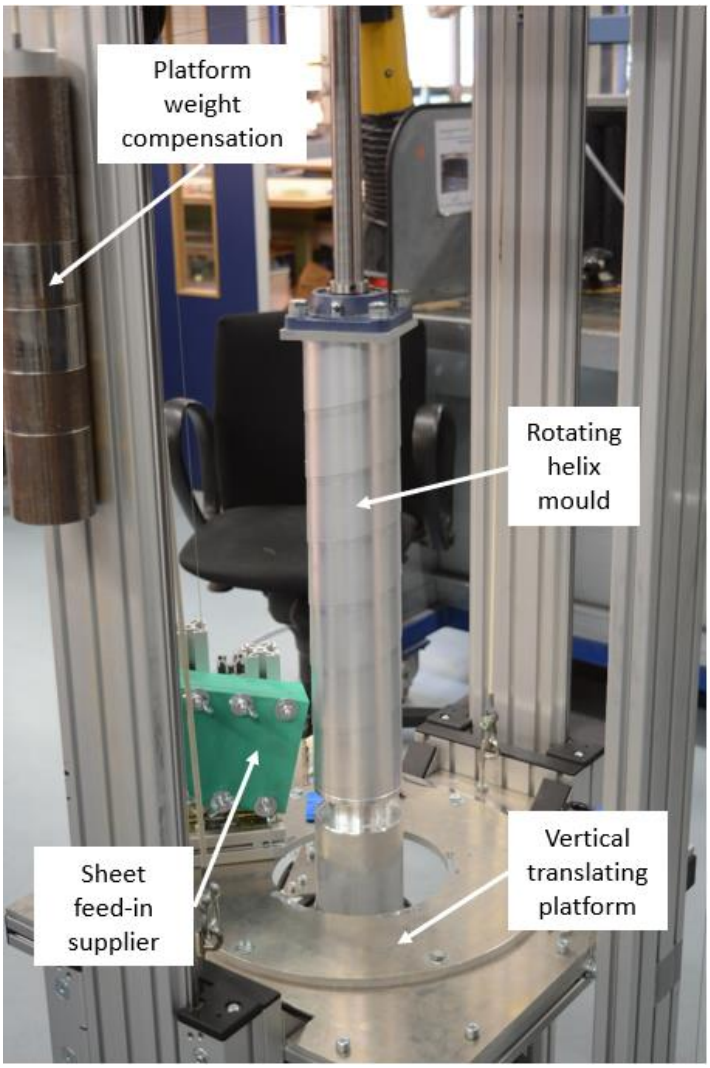

Figure 3.4 Wrapping machine.

The wrapping machine guides the metal strip through the green block shown in Figure 3.4. This block is set to an insert angle, α, that follows exactly the thread angle of the mould. The green block applies pressure to the strip to create resistance when the metal strip goes through the block. Once the mould starts to rotate by the manual crank, Figure 3.5, it bends the metal strip and pulls it through the green block. While the mould rolls up the metal strip, a vertical translating platform is elevated simultaneously.

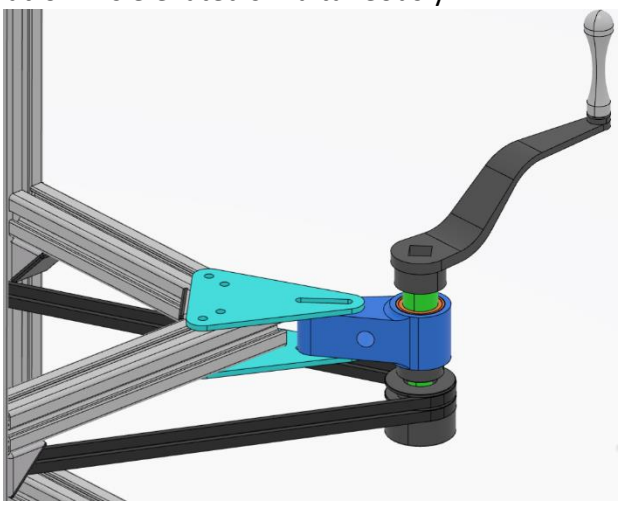

Figure 3.5 Manual crank on the wrapping machine

The platform containing the supplier that guides the metal strip is elevated by each revolution. Via a steel cable a connection is made between the rising platform and the rotating mould. This makes the platform to rise each revolution by the lead distance of the helix. The cable is rolled up by the circumference of a winder that is equal to the lead distance, see technical drawing in the appendix "pitch regulator". The following equation takes this into account:

$$r_{winder} + r_{cable} = \frac{L_p}{2\,\pi} \tag{13}$$

Where r_{winder} is the radius of the winder [mm] attached underneath the helical mould, and r_{cable} is the radius of the cable [mm].

The cone angle is used to calculate the required length of the curved strip of material to manufacture a desired length of the complete tube. Therefore, an arclength, L_R, is calculated by dividing the inner radius of the tube by the sine of this cone angle, β. The covered circumferential distance along the minimal radius of the tube for one revolution while advancing one thread length axially, is divided by this cone angle to obtain the arc angle, γ, of the curved metal strip. This covered circumferential distance is the long edge of a triangle and is calculated by using Pythagoras's theorem. The short edges of the triangle are the circumference of the tube and the axial advanced length after one revolution. The long edge of the triangle can be multiplied with the desired number of revolutions, f, to obtain the required curved strip length. To clarify these calculations, Figure 3.6 is added. The equation takes the following form:

$$\gamma = \frac{f * \sqrt{(2\pi r)^2 + (l_w - l_0)^2}}{L_R} \tag{14}$$

where f is the desired number of revolutions [-], r, $l_w$and l_0 are explained in equation (11) and (12), and L_R is the arc length and is calculated by:

$$L_R = \frac{r}{\sin(\beta)} \tag{15}$$

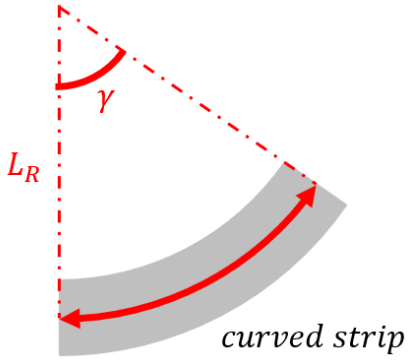

Figure 3.6 illustration of the dimension and arc angle of the curved strip

3.3 Chosen Geometry

One geometry for the helically wrapped structure was chosen to analyse the quasi-static and fatigue properties. A FEA model of the helically wrapped model is described in the next chapters. The full-scale specimen is created to validate the FEA model.

The diameter of the tube was chosen to be 100 mm. This is done to minimize the amount of bending required to form it into a tubular shape. Without quantification it was thought that

plastic deformation was reduced. Hence the fatigue life of the bend structure is affected as little as possible. Also, the amount of springback is minimized due to a relatively large diameter, thus the amount of peel stress to be endured by the adhesive is minimized. Therefore, the adhesive is loaded in shear as much as possible, which is the preferred loading condition for adhesives.

The overall length of the tube was chosen to be 350 mm. The mould to guide the metal strip is difficult to be manufactured since it requires a milling machine with multiple axis. Therefore, the mould is made to be 500 mm long. For the validation with the 4-point-bending tests it was thought that this length was sufficient. During testing it became clear that the required forces to create a bending moment in the structure was too high due to the length of the structure. It is recommended that a longer tube or a smaller diameter is taken for future testing.

The aluminium alloy 5754-h22 (AlMg3) was chosen for the metal strip [21]. This type of aluminium alloy has good cold forming abilities, making it easy to bend at room temperature. The ultimate strength and yield strength are relatively high making the stress range for fatigue testing large enough to pick a sufficient load level. During this project material costs went through the roof so choosing higher graded aluminium was not an option.

The adhesive from Huntsman corporation, Araldite AW4858/HW4858 two component epoxy adhesive was chosen for this project [22]. It presented the highest shear strength in its catalogue and performs best on aluminium. The curing temperature was around room temperature making it easy to apply while wrapping the metal strip in the machine. Also, the application window was 60 minutes, giving time to helically wrap and apply the adhesive. Curing was done at 40 degrees Celsius for a minimum of 16 hours curing time, since the manufacturer achieved the highest shear strength at this temperature and curing time. The adhesive contains spacers to ensure a minimum bond line thickness of 0.05 mm. This is the thickness where greatest lap shear strength was reached according to the technical data.

4 Quasi-Static Strength Properties

The quasi-static strength of the helically wrapped structure is analysed in this chapter. It becomes clear whether either the adherend or the adhesive subjected to a certain load, fails. The helically wrapped structure was invented for a wind energy application. The aerodynamic force creates a bending moment of the structure. Therefore, a bending moment load case is considered for the helically wrapped structure. This load case can be tested on a four-point bending test setup. A four-point bending analyses is therefore elaborated in this chapter. A numerical model is initially created to determine the maximum obtainable strength a tubular shaped object can endure. The calculations from the four-point bending setup are used further on in this thesis.

4.1 Adhesive failure due to Material Yielding

Adhesives tend to fail upon yielding of the adherend material. It is well established by Volkersen and his successors that the adhesive joint breaks when the adhesive peak stress exceeds adhesive peak strength. However, technical data sheets supplied by adhesive manufacturers, indicate the maximum average tested shear strength an adhesive can endure, which might underestimate the true limit as a result from testing constraints. This is for design purposes a problem since the full potential of the adhesive strength might not be clear.

Metal-to-metal bonding strength tests are done according to ISO 4587 or ASTM D1002-10. These standards specify the required dimensions of the specimen to be 114 x 25 x 1.6 mm (length x width x thickness) with an overlap length of 12.5 mm. This determines the bond area to be around 312.5mm^2. Since the dimensions are constant, one can determine whether the adhesive strength test failed as a consequence of adherend material yielding.

To verify this assumption, the definition of tensile stress and shear stress are required for static equilibrium conditions, equation (16) and (17). The applied load and width of the single lap joint specimen are kept constant to set the tensile and shear stress equal with a factor, equation (18). Figure 4.1 indicates the used parameters.

$$\sigma = \frac{P}{b * t_1} \tag{16}$$

$$\tau = \frac{P}{b * l} \tag{17}$$

$$\frac{P}{b} = \sigma * t_1 = \tau * l \tag{18}$$

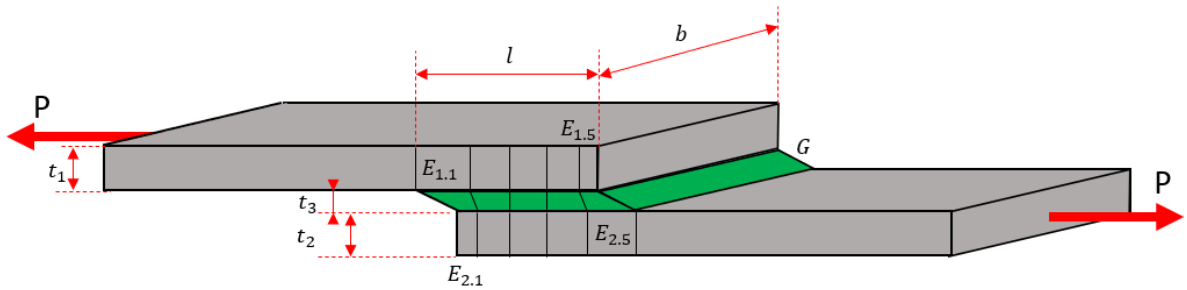

Figure 4.1 Single lap joint parameters definition

Equation (18) specifies a direct relation between the tensile and shear stress with a factor $\frac{t_1}{l}$. The static equilibrium principle can be applied to validate this assumption. The tensile stress in the adherend far away from discontinuities must be equal to the total shear stress in the joint to distribute and transfer all the load. This is valid up to the shear strength of the adhesive while being dependent on the adherend material. From literature it is known that the shear stress along the joint overlap length is distributed with peak shear stresses on the edges of the joint and minor shear stress between the peaks [5], [10], [23]. Therefore, equation (18) is not valid upon breaking of the adhesive layer.

Using equation (18) and comparing the shear strength of the adhesive and the material yield strength, shown in Table 1, one can see that the provided shear strength failed at material yielding. The third column contains the manufacturer tested adhesive maximum shear strength. The fourth column multiplies the adhesive maximum shear strength with the overlap length and thickness of the specimen to get the maximum tensile stress. The tensile stress is compared with the material yield strength in the last column. Within 11% deviation of the material yield strength, for these shown cases, it can be assumed that material yielding is the main cause of quasi-static adhesive failure. Hence, the provided adhesive shear strength cannot be trusted as a true strength as it would have been different when adherend yielding did not occur for different specimen dimensions.

Table 1 Comparing the manufacturer tested adhesive shear strength with the adherend material yield strength [22]

Adhesive	Adherend material	Shear strength [MPa]	$\tau * \frac{l}{t_1}$ [MPa]	Yield strength [MPa]
Scotch-weld DP410	Alu 2024-T3 - Etched	38	297	290
Scotch-weld DP420	Alu 2024-T3 - Etched	38	297	290
Araldite AW4858	Aluminium – pretreat & sand blasted	37	289	290
Araldite AW4858	Steel 37/11 – pretreat & sand blasted	27	211	235
Araldite AW4858	Stainless steel v4a – pretreat & sand blasted	27	211	250
Araldite 2019	Aluminium – pretreat & sand blasted & degreasing	33	258	290
Araldite 2019	Steel 37/11 – pretreat & sand blasted & degreasing	27	211	235
Araldite 2019	Stainless steel v4a – pretreat & sand blasted & degreasing	27	211	250

To conclude, the specified maximum shear strength an adhesive can withstand is dependent on the yield strength of the adherend material. Hence, these values are merely a tool for comparison purposes than rather being a useful design parameter. It is recommended that manufacturers of adhesives should present technical properties of adhesives in parameters like the SERR or SIF, for design purposes. Having this information at hand, a designer can much more easily design a structure with adhesive joints.

As described in the literature review, the maximum load that can be applied to an adhesive joint is limited by the peak shear stress of an adhesive, equation (2). This peak shear stress is dependent on the geometry and properties of the adhesive and adherend. The peak stress of an adhesive is constant beyond a certain sufficient overlap length. Therefore, the overlap length was chosen to be 30mm. This is long enough for the peak stress to be constant. The redundant overlap length, where a part of the adhesive initially transfers no load, provides space for crack growth of the adhesive thus increasing fatigue life.

Increasing the thickness of the adherend decreases the maximum shear stress of the adhesive, equation (2). Therefore, the thickness and overlap length of the adherend must be chosen such that the adhesive maximum shear stress is never reached. Hence, the overlap length and adherend thickness provides control for either the adherend or the adhesive to be a limiting factor.

The overlap length and adherend thickness was chosen such that the adherend material is the critical factor. Since the adherend material was chosen to be critical instead of the adhesive shear strength, there is no need to research the adhesive strength any further. The crack propagation through the adhesive is analysed by the stress distribution in the adherend. The adherend material is determinant to whether the adhesive fails. Therefore, for the remaining analyses of the quasi-static strength and fatigue life of the helically wrapped structure for this thesis, the adherend material is analysed because this is the critical factor.

4.2 Pipe Bending Analysis

The helically wrapped structure is tested in a 4-point bending test setup. The helically wrapped structure was invented for a wind energy application. The aerodynamic force creates a bending moment on the structure. Therefore, a bending moment load case is considered for the helically wrapped structure. Although, due to a spinning motion from the aerodynamic device, fluctuating bending loads are dominant instead of static loads. A homogeneous pipe structure is analysed as reference for the maximum load the helically wrapped structure can withstand. The simple analytical equations for 4-point bending can be applied to the helically wrapped structure as a reference. Though, the helically wrapped structure will be less stiff and therefore also less strong.

Analytical calculations of the homogeneous pipe structure determine the maximum tension due to bending, assuming the homogeneous pipe structure is stronger than helically wrapped adhesively bonded structure. It is stronger because the helically wrapped structure is anisotropic and thus has stress concentrations. Also due to the adhesive more flexibility in the helically wrapped structure is present making it less stiff. A homogeneous pipe structure with the following dimensions is analysed for reference. The geometry is identical to the helically wrapped pipe structure, Table 2.

Table 2: Geometry and material properties of the homogeneous pipe structure

Material	***Aluminium 5754-h22 (AlMg3)***	
E, Young's modulus	70000	$[MPa]$
Tensile Yield strength	190	$[MPa]$
Tensile ultimate strength	240	$[MPa]$
Elongation at break	14	$[\%]$
Shear modulus	25900	$[MPa]$
Poisson's ratio	0.33	$[-]$
Length pipe	300	$[mm]$
Radius outer wall	50	$[mm]$
Thickness wall	1	$[mm]$
Cross-sectional area	311	$[mm^2]$
Inertia (I_x)	381074.40	$[mm^4]$

The maximum bending moment that can be applied until this homogeneous pipe structure reaches the yield stress is 1.448 kNm. This is calculated according to (19) along with the convention indicated in Figure 4.2.

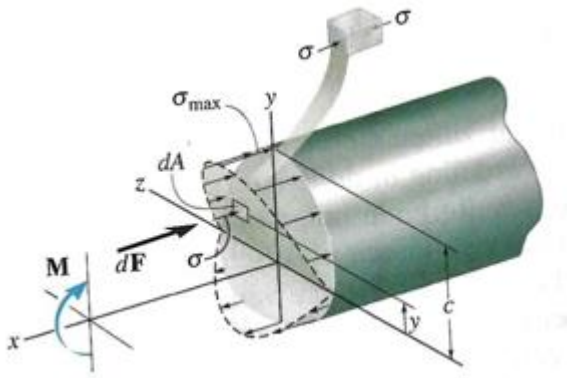

Figure 4.2: Sign convention and maximum tension in a pipe structure [24]

$$\sigma_{max} = \sigma_{yield} = \frac{Mc}{I} \tag{19}$$

The free body diagram, indicated in Figure 4.3, is used to derive the shear force and bending moment diagram along with its equations. To reach the maximum stress in the pipe structure a load of 38.615 kN is required. This is calculated with equation (24).

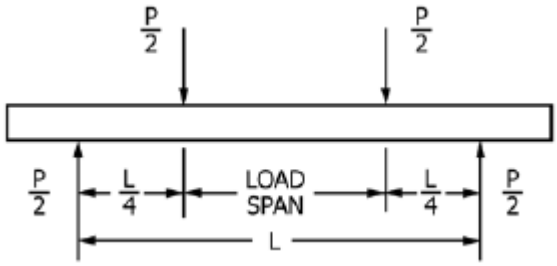

Figure 4.3: Free Body Diagram homogeneous pipe structure [25]

$$+\uparrow \sum F_y = 0\,;\; V = \frac{p}{2} \qquad \text{Domain:}\{0 < x < \tfrac{L}{4}\} \tag{20}$$

$$+\uparrow \sum F_y = 0\,;\; V = 0 \qquad \text{Domain:}\{\tfrac{l}{4} < x < \tfrac{3L}{4}\} \tag{21}$$

$$+\uparrow \sum F_y = 0\,;\; V = -\frac{p}{2} \qquad \text{Domain:}\{\tfrac{3L}{4} < x < L\} \tag{22}$$

$$\circlearrowleft + \sum M_z = 0\,;\; M = \frac{px}{2} \qquad \text{Domain:}\{0 < x < \tfrac{L}{4}\} \tag{23}$$

$$\circlearrowleft + \sum M_z = 0\,;\; M = \frac{PL}{8} \qquad \text{Domain:}\{\tfrac{l}{4} < x < \tfrac{3L}{4}\} \tag{24}$$

$$\circlearrowleft + \sum M_z = 0\,;\; M = \frac{PL}{8} - \frac{px}{2} \qquad \text{Domain:}\{\tfrac{3L}{4} < x < L\} \tag{25}$$

Figure 4.4 shows the results of the shear forces and bending moments through the pipe structure tested in a 4-point bending test setup. The maximum bending moment is obtained between the middle two loads or supports. All shear forces are created at the edges of the pipe structure leaving no shear forces in the middle section of the pipe structure.

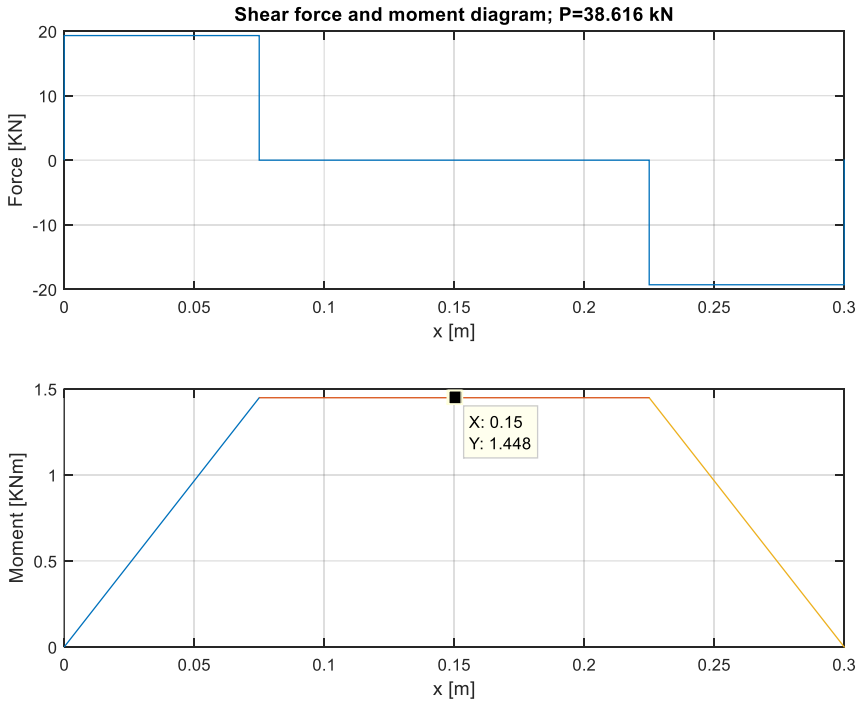

Figure 4.4: Shear force and bending moment diagram of a homogeneous pipe structure.

4.3 Numerical model of a homogeneous pipe

This result is checked with a finite element method model. The geometry details are copied from Table 2. Reference point 1 was fixed and a moment was applied through reference point 2. The reference points are independently coupled by a constraint to the base and top surface providing a continuous distribution of the boundary condition and applied moment. This approach is later used for the helically wrapped model. The mesh reached a maximum aspect ratio of 1.02 which indicates almost perfect cubic mesh elements. The shortest and longest edge was set to 1 and 1.02 mm.

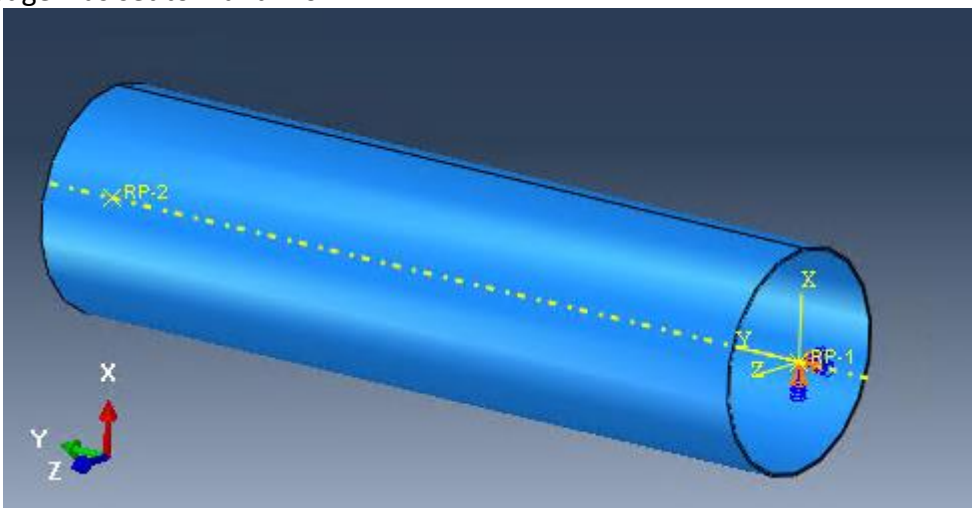

Figure 4.5: Pipe structure in Abaqus

The Mises stress distribution of the homogeneous pipe structure is shown in Figure 4.6. The maximum stress is reached at the lower and upper side of the pipe structure due to the bending moment along the z axis. This confirms that the model is setup correctly because the yield strength was expected to be at 190 MPa when a bending moment of 1.448 kNm was applied. The FEA model reaches a maximum tensile stress of 186.5 MPa, hence a deviation of 1.84%.

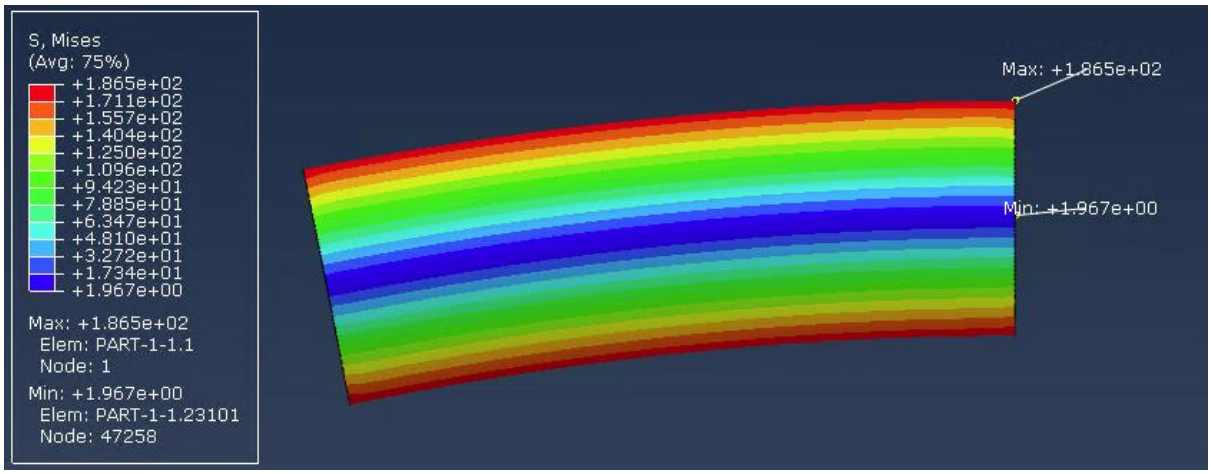

Figure 4.6 Stress distribution in a pipe structure due to bending moment.

A convergence analysis was done to verify when the model generates reliable results. Figure 4.7 shows the results of the convergence analysis. After 4 iterations the global mesh size had 5 mm long mesh edges and a total of 3840 elements. At this simulation the displacement and maximum tensile stress reached convergence since it deviates only within 1% of the result for the largest mesh size.

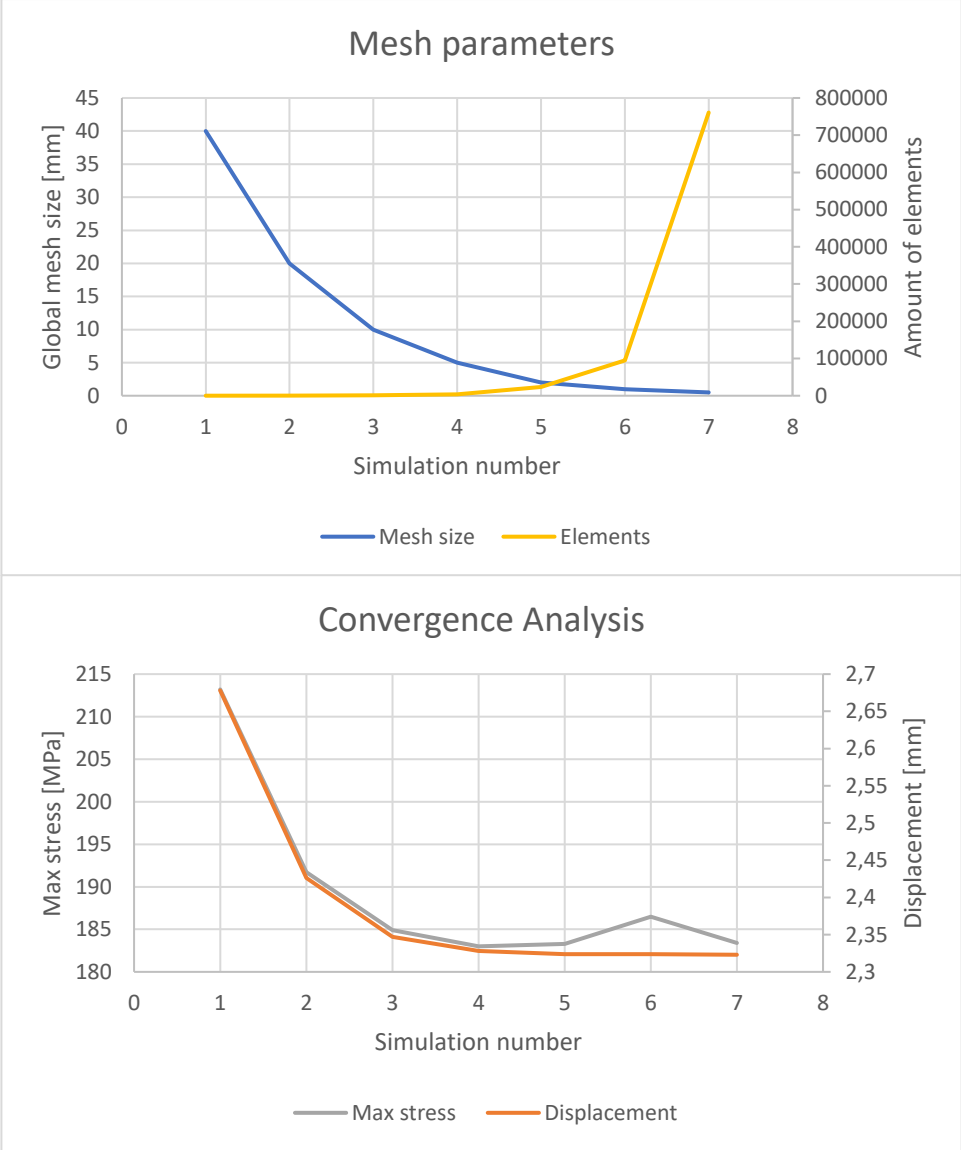

Figure 4.7 Convergence analysis of the stress and displacement of the numerical model

5 Fatigue Prediction

From the quasi-static strength analysis of the helically wrapped structure it is clear what overlap length and adherend thickness is required to limit analyses to the adherend and not the adhesive. It was found that the adherend reaching yield strength causes the adhesive to fail. This is not necessarily the case for fatigue loads below the yield strength of the adherend. Therefore, the objective is to determine whether either the adherend or the adhesive fails under fatigue loading.

The SN-curve of the adherend material is required to determine when it fails after a certain number of stress cycles at an associated stress level. This already narrows the operational envelope of the helically wrapped structure in terms of load and number of fatigue cycles. When the adherend material is critical instead of the adhesive, it is allowed to only focus to the fatigue properties of the adherend to predict the fatigue life. If the adhesive is critical under fatigue loads the operational envelope is even more narrowed. In this case detailed analysis of the fatigue crack growth propagation in the adhesive is required. This was the chosen approach to determine the operational envelope and thus fatigue life of the helically wrapped structure.

5.1 Method to predict fatigue crack growth

To predict the fatigue life of the helically wrapped structure one would require the information about the strain energy release rate, G, and the delamination growth rate $\frac{da}{dN}$. The method used for this project is supported by empirical data. It is derived from the thesis of J.A. Pascoe [26]. It requires two functions:

$$G = f(a, \sigma) \tag{26}$$

$$\frac{da}{dN} = C(G)^m \tag{27}$$

where G can be any expression of the SERR as appropriate. The first function calculates G which is dependent on the delamination growth and the applied forces on the structure, equation (26). FEA results of the SERR, employing the VCCT, are created for several pre-defined fixed crack sizes. A fourth order curve is then fitted through these results to get the function for the SERR. Subsequently, the Paris relation between the SERR and the crack growth rate is required to predict fatigue life, equation (27). This relation requires empirical data to determine the material specific parameters C and m. These parameters are determined by curve fitting a power law through the $\frac{da}{dN}$ versus G graph, generated from separate tests. Then with the Paris relation and the function for the SERR, a crack growth rate $\frac{da}{dN}$ for the helically wrapped structure is found. The crack growth rate is used in an iterative process to match the pre-defined crack sizes to yield a final fatigue life estimation. Hence, an adhesive joint length can endure a limited amount of crack propagation per cycle at a certain crack length and load.

The VCCT is employed in FEA software to calculate the SERR at several pre-defined fixed crack lengths. First the surfaces that are adhesively bonded are joined by a surface-to-surface contact condition. From this bonded area, a small section is selected as initial crack. The pre-

defined fixed crack length was chosen for several iterations. Between every iteration a step size of 5mm was taken as crack growth propagation. The critical crack propagation values are set at an unrealistic high number, preventing crack propagation, and avoiding re-meshing. This allows for control of the crack propagation. Re-meshing is a VCCT property that is required when a crack propagated beyond or outside a mesh grid, slowing down the simulation time and increasing the computational work.

5.2 Fatigue Properties of aluminium AlMG3-H22

The aluminium used to create this helically wrapped structure is AlMg3-H22 (EN) or 5754-H22 (USA). This is an aluminium alloy suitable for cold forming and has an ultimate strength of 239 MPa, and a yield strength of 190 MPa [27], [28]. The fatigue properties of this aluminium alloy AlMG3-H22 are determined from the literature. The fatigue tests to validate the FEA model are done at a stress ratio, R, of 0.1. This is done to keep a minimum load on the structure such that it cannot move. Consequently, the mean stress not equal to zero. Hence, provided fatigue properties presented on a stress amplitude scale are lower than the general S_a vs N data for $R = 0$.

Using data from Ref. [27], [28], the Basquin relation is used to reconstruct the S_a vs N curve in Figure 5.1. The provided fatigue stress range, $\Delta\sigma\ (= 2S_a)$, of AlMg3-H22, tested at $R = 0.1$, is 133.3 MPa and is reached after $1.037 * 10^6$ fatigue cycles. The stress amplitude for this test was 66.68 MPa. Following the stress cycle definitions, the maximum stress was 148 MPa and the minimum must be 14.8 MPa. This means the test was done at a mean stress level of 81.5 MPa to determine the fatigue limit at $R = 0.1$. The ultimate stress provided by the manufacturer was 239MPa. This value translates, for the fatigue test done at $R = 0.1$, to a stress amplitude of 107.4 MPa in the graph[1]. When the maximum stress is set equal to the yield strength for the fatigue tests at $R = 0.1$, the stress amplitude in the graph becomes 85.5 MPa and fails after $2 * 10^5$ fatigue cycles. Since an adhesive tend to fail when the yield strength of the adherend is reached, the range of interest for stress amplitudes, where the adhesive can fail sooner than the adherend, is below this stress amplitude of 85.5 MPa. Therefore, for validation purpose, fatigue tests are done at 90% of the yield strength stress amplitude, (at $R = 0.1$) to determine whether the adherend or the adhesive fails earlier. According to the calculations based on literature, for this stress amplitude the adherend should fail after $4 * 10^5$ cycles.

[1] Note that the ultimate stress in Figure 5.1 for a stress ratio, R=0.1, is reached at $\pm$44000 cycles. This means that the first knee point is reached relatively late, but it is in accordance with the source. The horizontal lines are created by the writer of this thesis.

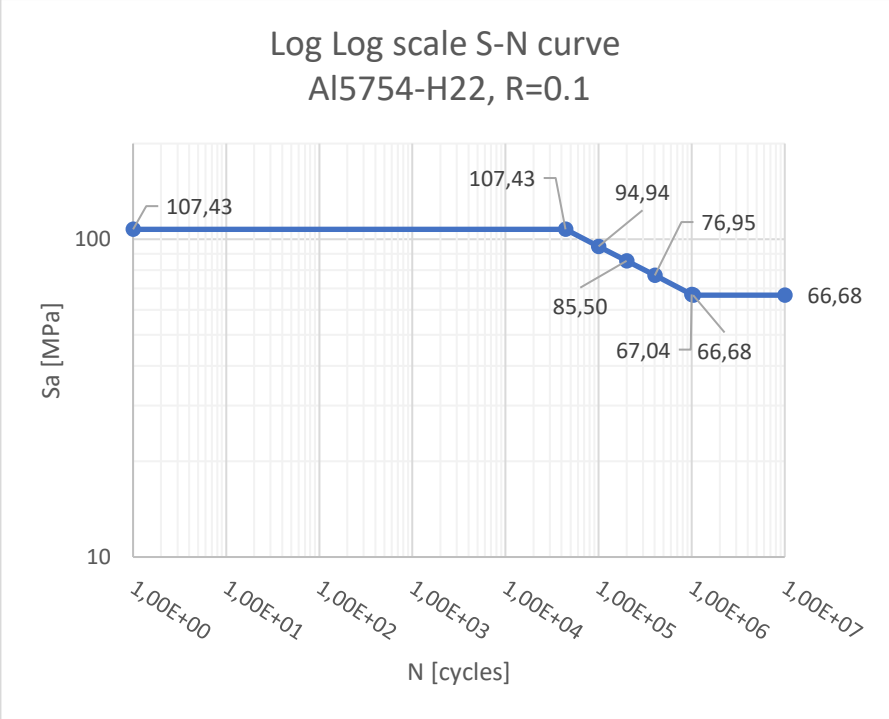

Figure 5.1 Reconstructed S-N curves for Continuous Casted Aluminium 5754-H22 [27].

5.3 Numerical Modelling of the Helically Wrapped Structure

Developing an analytic formula to calculate the SERR is too complex due to the axially repetitive joined sections, the conus shape, and the adhesive joint itself. The continuous metal strip is joined to itself after one revolution. Therefore, it cannot be assumed to behave as one homogeneous section, which makes it complex to describe analytically. Assumptions are made to analyse a small section of the joint which could then be extrapolated to the complete structure. However, this would result in the analysis of an axially bent single lap joint. It is then more convenient to test and analyse a normal non-bend single lap joint according to available test standards. Although, both the bend simple single lap joint or non-bend variant require empirical evidence and validation with the full-scale model. Therefore, an analytical description of the stress distribution in this structure is not easily obtained.

A Model of the helically wrapped structure in FEA software (Abaqus) is required to calculate the SERR. This structure must be analysed for a bending load case since the application will be subjected to it most frequently. The begin and end of the 1080-degree revolved strip part is cut off to create a flat surface where the load and boundary conditions can be applied to, Figure 5.2.

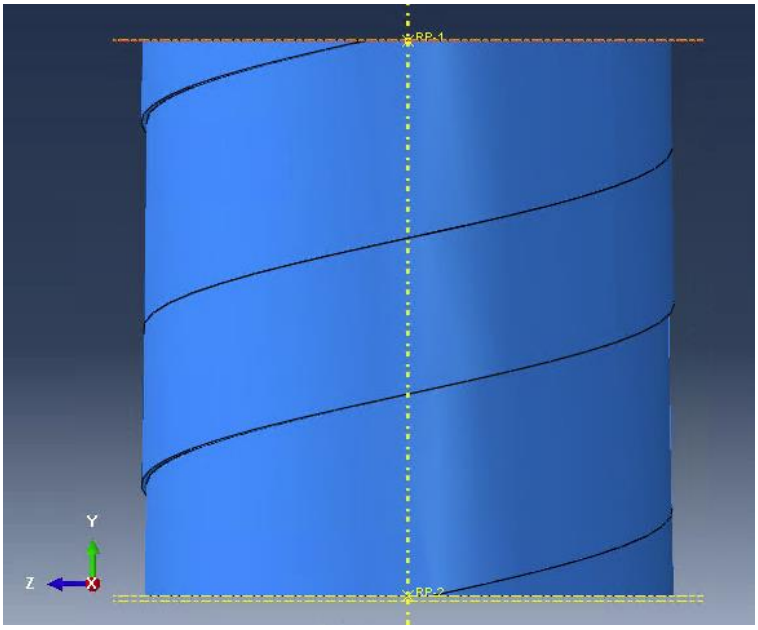

Figure 5.2 Model of the helically wrapped structure with flush ends.

The width of metal strip is divided in three separated metal strips along the entire strip length, Figure 5.3. This is done to control alignment of the mesh nodes of the master and slave contact interfaces. The surface-to-surface contact property in Abaqus is used to join and simulate the bonded surfaces. Individual mesh nodes must be assigned to be bonded or delaminated. This determines the delamination area and is used to calculate the SERR at different crack propagations.

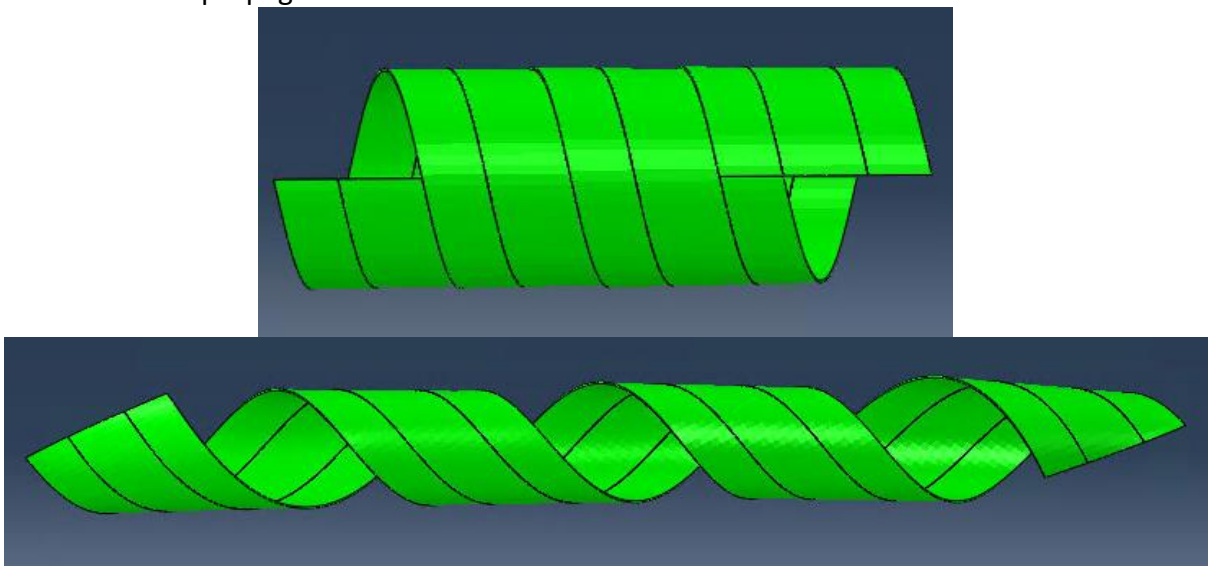

Figure 5.3 Model of the three individual metal strips. Upper: Undeformed section with the master and slave surface bonded. Lower : Deformed section without bonded surfaces

The three separate strips are tied together along the edges with a *Tie* constraint and behaves like one single metal strip. The tie constraint is checked for functionality without the adhesive layer, Figure 5.4. An axial force is applied to this completely delaminated model to check the functionality of the tie constraint and check if the stress is distributed along the width of the tied strip. The is a 3D stress element type family was used. The outer modelled strips contain 8750 elements each. C3D8 elements were used in this model, these are 8-node linear bricks. This means so a total of 140000 nodes were created. The middle strip model contained C3D6 elements, meaning a 6-node linear triangular prism. This middle metal strip does not require

alignment of nodes with another surface. Therefore, triangular elements were used. This decreased required computational time. A total of 54305 elements were created, so 325830 nodes were created for the middle strip model.

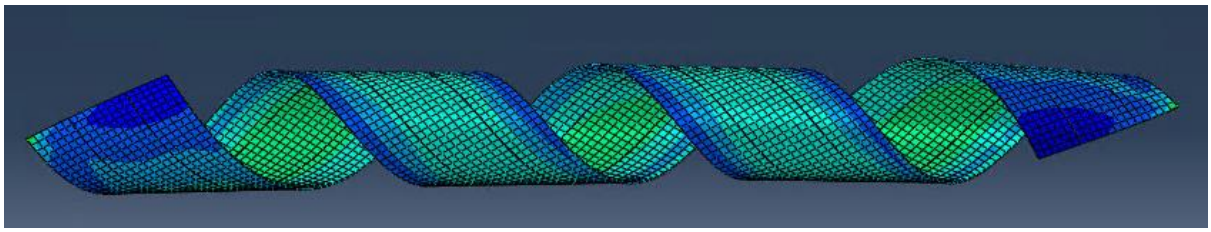

Figure 5.4 Model to check the functionality of the tie constraint between the edges of three individually modelled metal strips. One can see that the deformed solution behaves like a single homogeneous metal strip.

A kinematic coupling constraint was used to evenly distribute the bending moment applied at one control point to the flanges of the tube, Figure 5.5. The control point was at placed at the intersection between the axial axis and the plane of the flange. The same was done for the encastre constraint at the other side of the tube flange. This means no rotations or displacements of the control point.

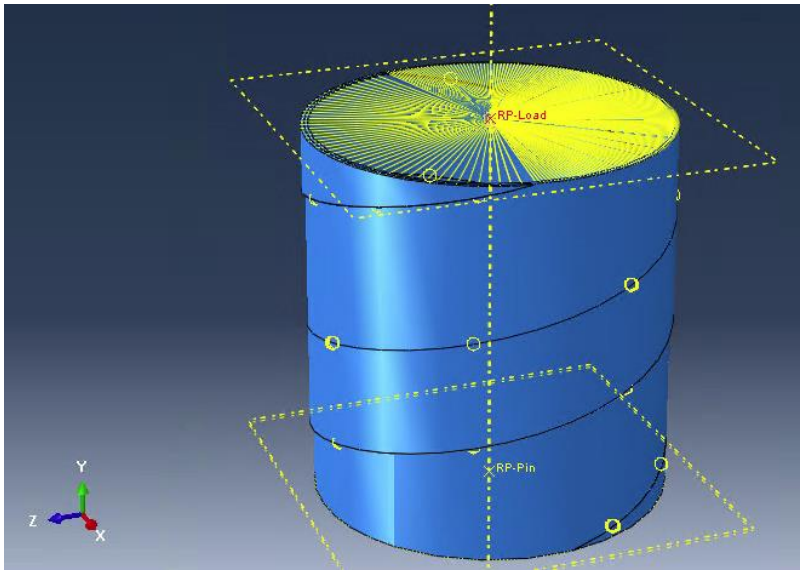

Figure 5.5 Coupling constraint distributing the boundary condition and bending load evenly to the flanges of the tube

5.4 FEA to Calculate the SERR as a Function of Crack Length Employing the VCCT

FEA software is used to calculate the SERR employing the VCCT. Adhesives tend to fail once the yield strength of the adherend is reached. Therefore, loads below the yield strength are analysed, to determine whether the adherend or the adhesive fails after a number of fatigue cycles. The applied load must be above the adherend fatigue limit to determine the unknown section where either the adherend or the adhesive fails earlier. Therefore, a bending moment is applied to analyse the SERR-distribution at a load level 90% of the yield strength of the material, see paragraph 5.2.

Figure 5.6 contains the helically wrapped structure with a bending moment applied to the edges of the tube. A bending moment of $1.053 * 10^6$ Nmm is required to create a tension of 171 MPa on the furthest fibre from the neutral axis. Comparing to the homogeneous pipe, a lower stress is obtained for the same bending moment. This is because there are stress concentrations in the helically wrapped anisotropic structure. The stress on the neutral axis

is coloured blue and shows a decrease in stress once the bonded metal strip is reached in axial direction. The single centre metal strip, without adhesive elements, distributes the stress evenly like a homogeneous pipe structure would do.

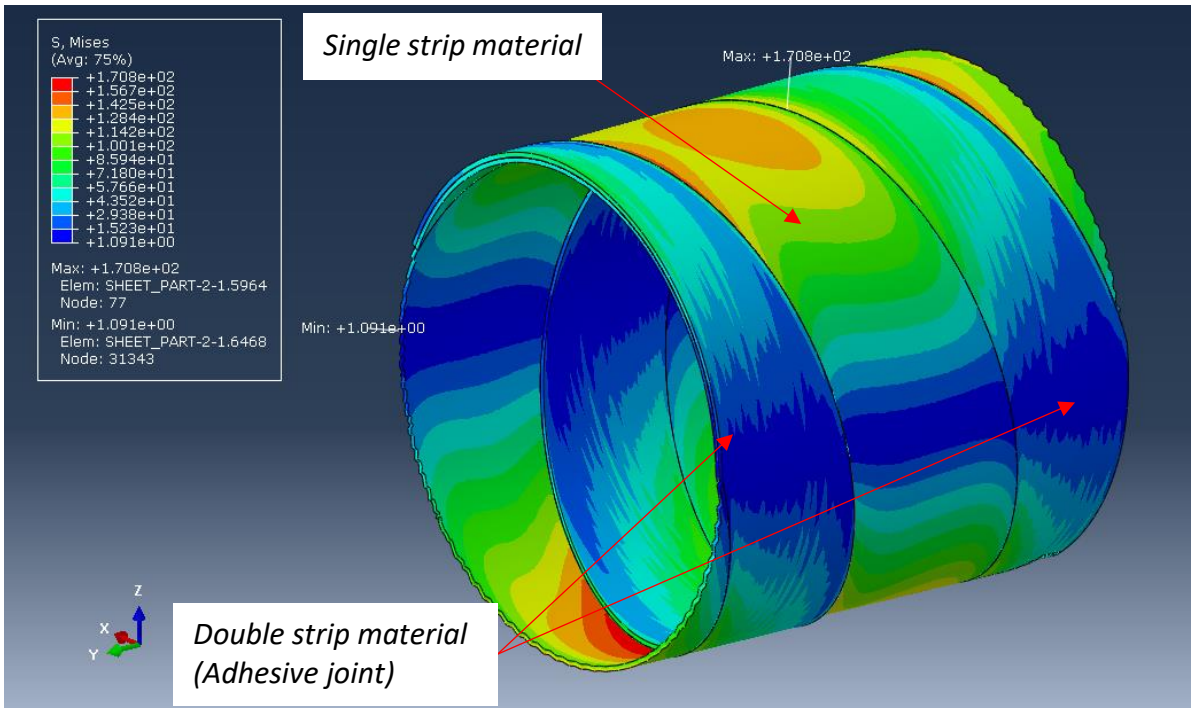

Figure 5.6 Bend helically wrapped structure. Due to diamond shaped mesh elements the stress distribution is less smooth. The single metal strip is meshed with triangular elements and show better stress distribution.

An initial crack is created at the edge of upper circumferential half of the helical joint. The highest value of the G_{Max} distribution along a crack front at the initial fixed delamination area is substituted in the Paris relation once the power law parameters are known. This provides the fatigue crack growth rate, $\frac{da}{dN}$, for this single highest G_{Max} value along the crack front. This fatigue crack growth rate value is divided by a crack size propagation of 5mm to obtain the amount of fatigue cycles. The remaining but lower G_{Max} values along the crack front are also substituted in the Paris relation to get the fatigue crack growth rate at the remaining nodes along the crack front. These are then multiplied with the obtained required fatigue cycles to propagate the crack. This results in the remaining nodes along the crack front to propagate as well but less then 5mm. Now the cack front has propagated, another simulation with the new crack area is required. This consecutive iteration follows the exact same procedure to calculate the fatigue crack propagation.

Iteratively analysing SERR along the crack front of the initial delamination, starting with one disconnected node, resulted in the largest value of $G_{II,Max}$ on the edges of the crack and slowly spreading out in circumferential direction, Figure 5.7. After some iterations a crack front shaped like an oval is formed.

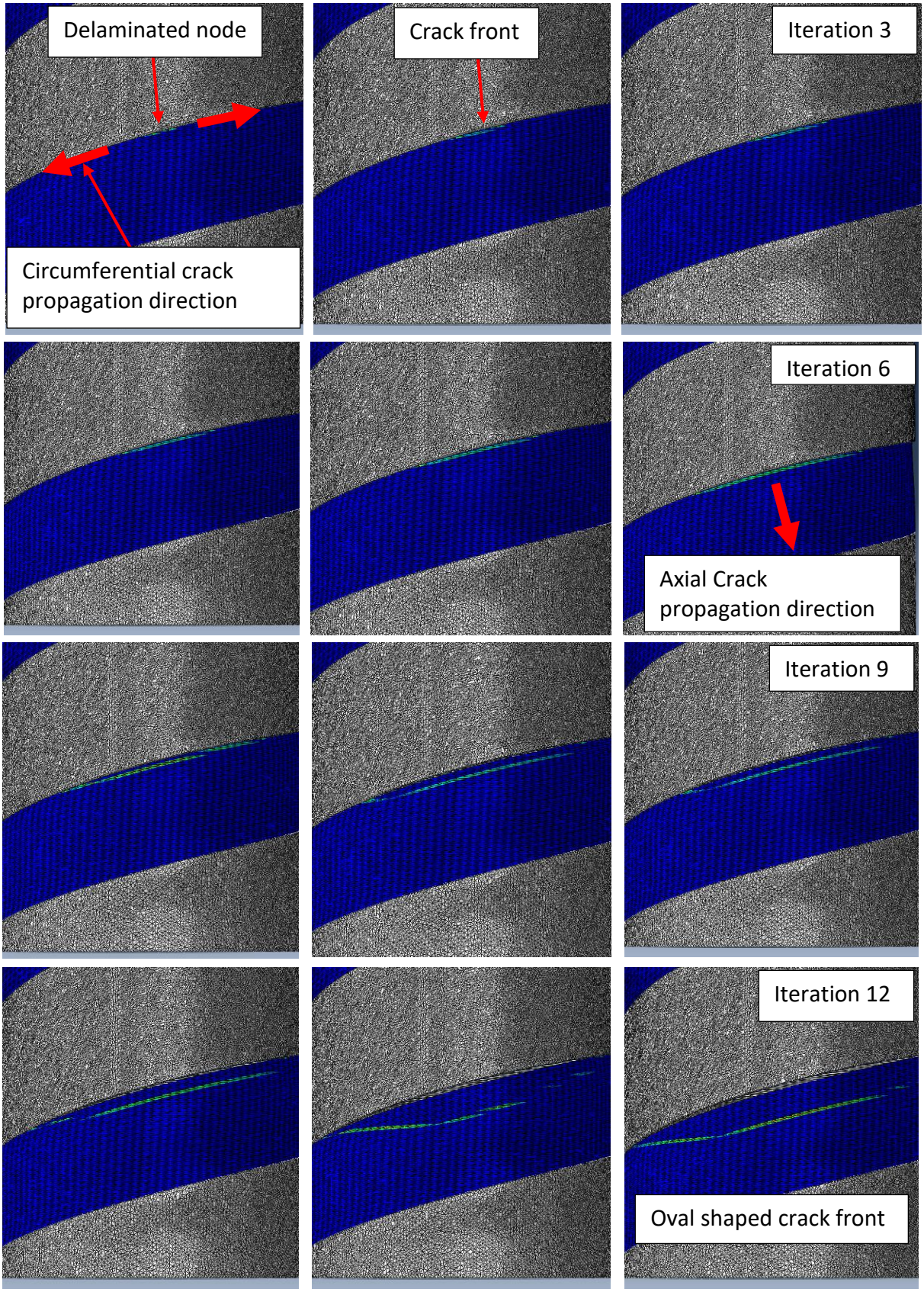

Figure 5.7 Iterations of the fatigue crack front growth propagation of the helically wrapped model. The propagation of the crack is indicated by thick red arrows. Initially one node was delaminated leading to $G_{II,Max}$ values being largest in circumferential direction. The sixth iteration shows that the crack front propagates in axial direction since the dominant $G_{II,Max}$ values are largest there. Finally, the crack front is shaped like an oval.

Figure 5.8 till Figure 5.10 show the distribution of G_{Max} along the crack front per node per iteration. For each iteration a nodal path along the crack front is drawn to plot the $G_{II,Max}$ values on. Each consecutive iteration contains more nodes because the crack propagates. The centre of the crack front is the horizontal axis (node=0) in the contour plot. The positive valued nodes along the crack front correspond to a crack propagation direction in Figure 5.7. Step sizes of 5 to 10mm per iteration were taken to obtain the distribution of $G_{II,Max}$ along the delaminated front. A step size of 10mm is taken when no change in magnitude or distribution of G_{Max} was found in previous two iterations for computational efficiency.

From the three contour plots is concluded that the dominant mode, of the G_{Max} distribution along the crack front, is the second mode, (in-plane shear). Due to the required diamond shaped mesh elements no smooth distribution of G_{Max} along the crack front is obtained. The first few iterations showed peak values at the edges along the crack front. At a crack length of 50mm in width along the crack front (iteration 6), the $G_{II,Max}$ values increased, along the middle of the crack front, indicating crack propagation in axial direction. The last iteration clearly shows an increment of $G_{II,Max}$ values along the centre of the crack front.

Figure 5.10 showed that $G_{III,Max}$ values along the crack front increased at the edges of the oval shaped delamination area. These peak values are obtained at the sharp edge of the diamond shaped mesh elements and believed to be a model error; hence it is neglected. These values are only obtained at the latest iteration.

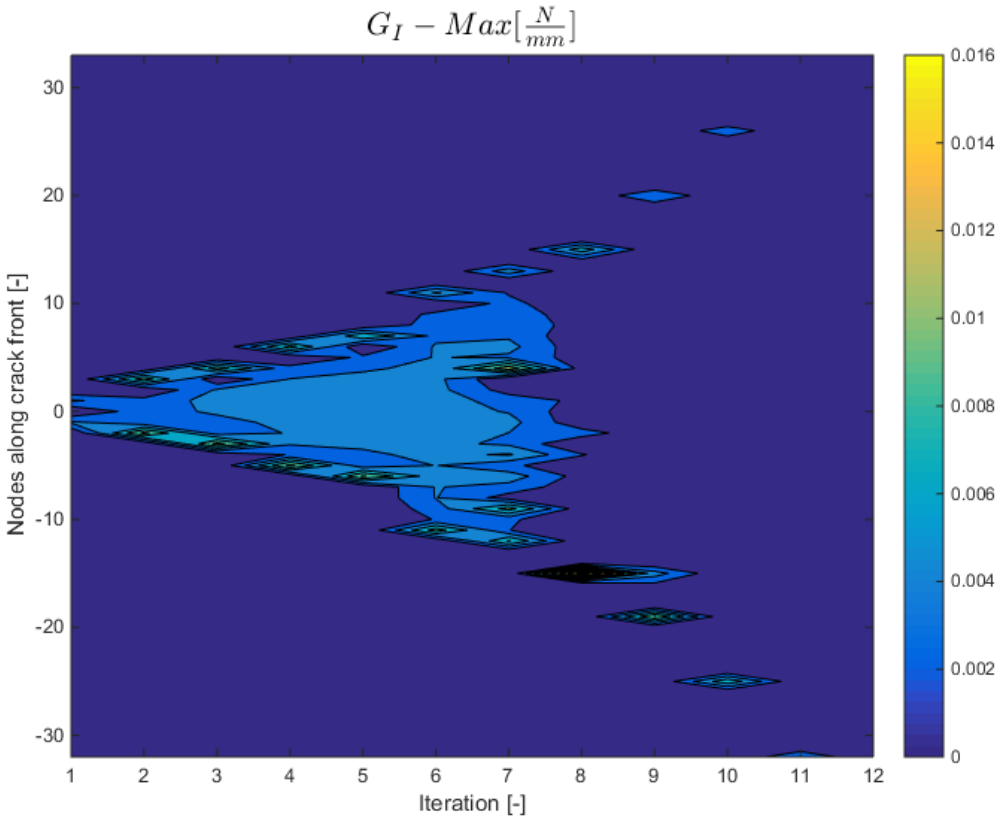

Figure 5.8 $G_{I,Max}$ distribution along the crack front per iteration and per node.

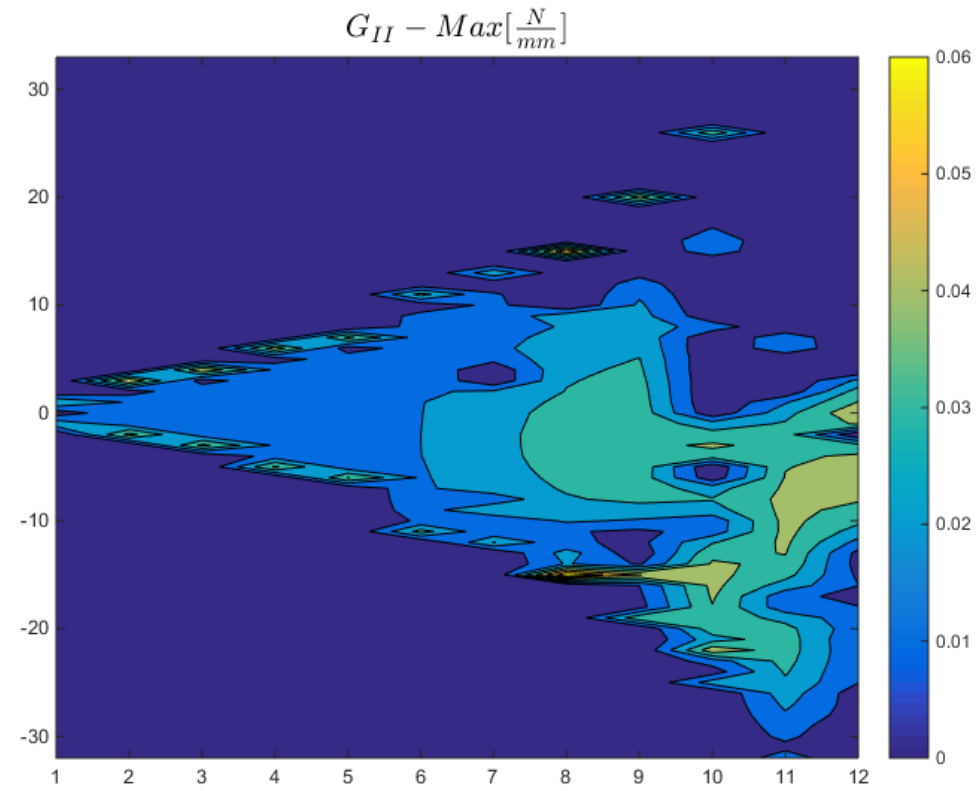

Figure 5.9 $G_{II,Max}$ distribution along the crack front shown per iteration.

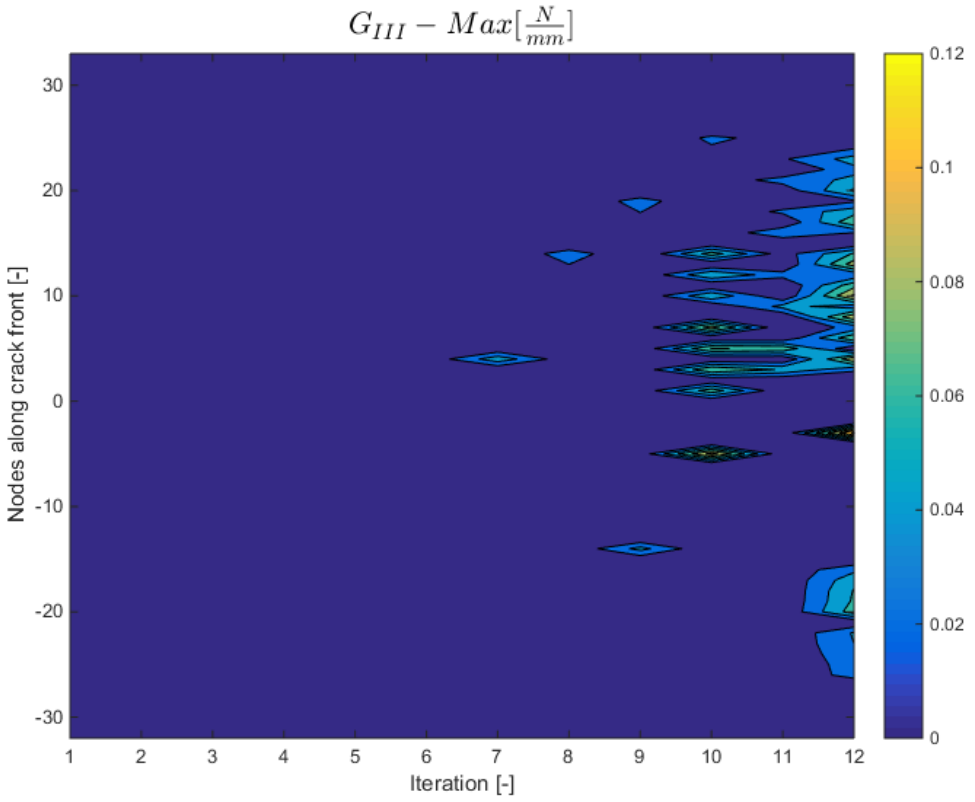

Figure 5.10 $G_{III,Max}$ distribution along the crack front per iteration and per node

A second approach employed the introduction an initial crack line along the entire circumferential edge (first line of nodes). A smooth distribution of the $G_{II,Max}$ is obtained along the crack front also indicating crack propagation in axial direction, Figure 5.11. This $G_{II,Max}$ distribution is a function of the distance from the centre of the crack front along the circumferential length, Figure 5.12. The centre of this distribution (a=0) is the location of maximum stress due to bending. Here, the largest value of $G_{II,Max}$ is obtained. This indicates that the crack propagates in an oval shape in axial direction. The following iteration included an increase, with a step size of 10mm, of the crack front in axial direction according to the $G_{II,Max}$ distribution. After this crack propagation the same delaminated area is obtained like the eleventh iteration in previous approach.

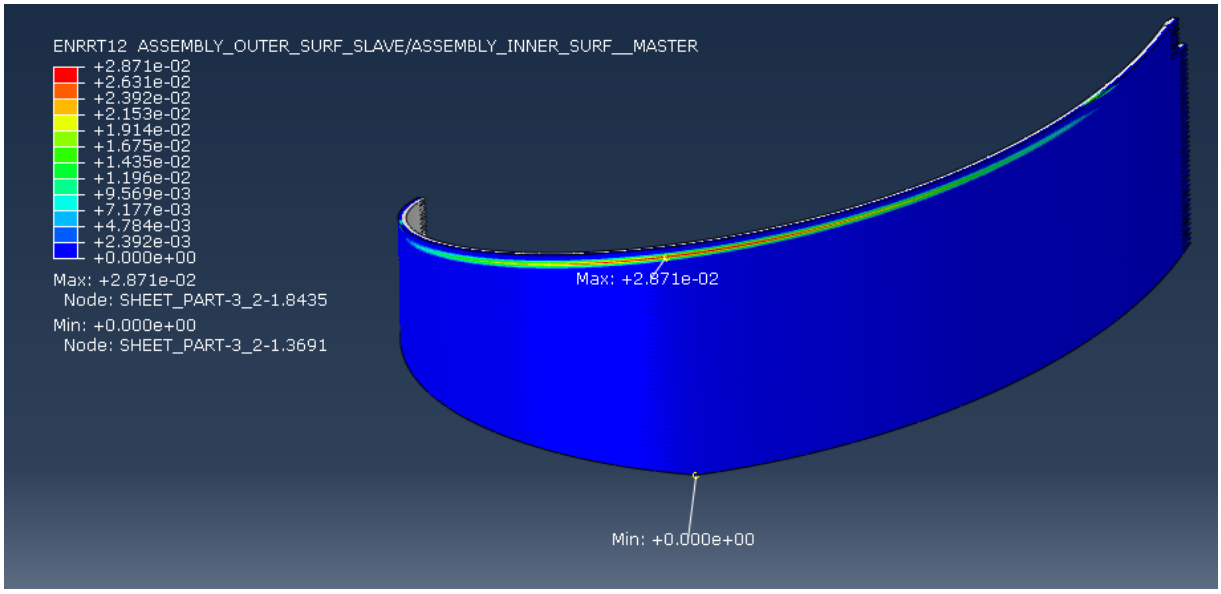

Figure 5.11 G_{Max} Mode-II distribution along the circumference of the upper helically wrapped structure

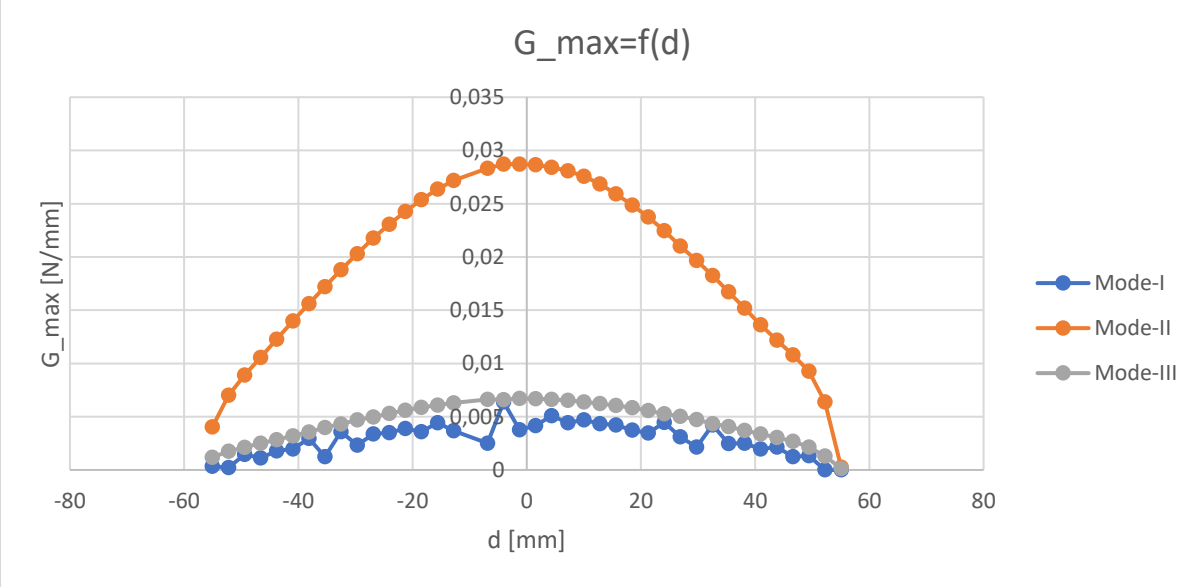

Figure 5.12 G_{Max} mode-II distribution along the circumferential distance of the upper half of the tube.

The ratio of the modes is 15%, 70%, 15%, respectively for Mode-I to Mode-III. The only remaining unknown information to estimate the fatigue life, is the Paris-relation. The mixed mode bending test provides this information and is elaborated in the next paragraph.

5.5 Methodology of acquiring mixed mode I – mode II Paris parameters

This section describes the required steps and test setup to generate required data to determine the parameters of the power law. This power law is the Paris relation between the delamination growth rate and the SERR, equation (27). These results are used for the fatigue prediction of adhesively bonded aluminium structures. This data represents identical behaviour for the helically wrapped structure when the adhesive, aluminium, and mode mix are identical. The test provides results about the SERR for a fixed mode mix. Testing at several loads yields a different SERR at a different crack growth rate. A curve can be fitted through these test data to get the Paris relation. The Paris-law is the crack growth rate function of the SERR.

The standard test method for mixed Mode I-Mode II interlaminar fracture toughness of unidirectional fibre reinforced polymer matrix composites (ASTM-D6671) is used [29]. According to the standard the $G_{I,Max}$ and $G_{II,Max}$ is calculated as follows:

$$G_{I,Max} = \frac{12P^2(3c-L)^2}{16b^2h^3L^2E_{1f}}(a+\chi h)^2 \tag{28}$$

$$G_{I,Max} = \frac{9P^2(c+L)^2}{16b^2h^3L^2E_{1f}}(a+0.42\chi h)^2 \tag{29}$$

where P is the applied load, c is the lever length of the MMB test apparatus, L is the half span length of the MMB test apparatus, b is the width of the specimen, h is half the thickness of the test specimen, E_{1f} is the modulus of elasticity of the MMB test specimen, a is the crack length, and χ is the crack length correlation parameter. Calculations of the individual parameters can be found in the test standard.

The aluminium alloy 5745-H22 samples are 6mm thick, 185mm long and 25mm in width, Figure 5.13. The dimensions are different from the test standard due to the use of aluminium instead of fibre composite laminate samples. The samples are sandblasted as pre-treatment. A thin film inserts of 45 mm long 0.05 mm thick Teflon was added to create an initial crack length, ending up with a joint length of 140 mm. The adherends are bonded with Araldite AW4858/HW4858 two-component epoxy[30]. This adhesive contains spacers (glass beads) to ensure a minimum bond line thickness. This is beneficial for the bond line thickness of the wrapped structure because it prevents squeezing out of the adhesive under pressure. Curing is done at room temperature, 21 degrees Celsius for a minimum of 30 hours. The adhesive is applied within 2 hours after sandblasting preventing oxidation of the aluminium. According to the manufacturer, a shear strength of 37 MPa can be achieved. It is assumed that this high-strength adhesive can yield significant fatigue resistance, hence the motivation for the choice of this adhesive.

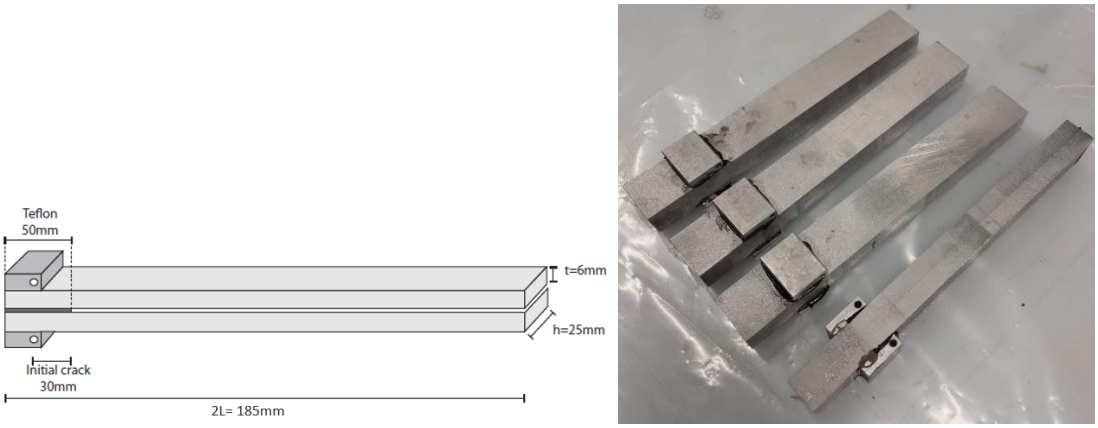

Figure 5.13 Dimensions test sample (left) [2]*. Actual test specimen (right)*

The Mode Mix is obtained from the FEA model and has a mode mix of 70%, as explained in paragraph 5.4. This means that the dominant crack opening mode is in the in-plane shear direction. This mode mix must be recreated in this test. This can be done by setting the right lever dimensions. These values must be obtained prior to testing the MMB samples. Initial calculations resulted in an arm-length, C, of 46.5 mm.

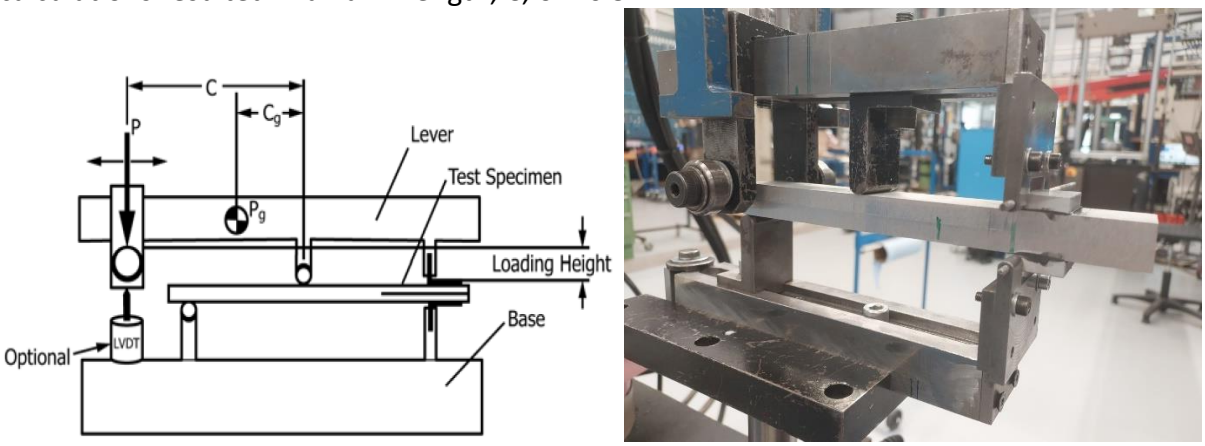

Figure 5.14 Mixed Mode-I Mode-II test setup schematic (left) and actual setup including test specimen (right) [29]

Four test samples were made. First, each specimen is quasi-statically loaded in displacement control mode to find the maximum load at crack initiation. The remaining joint length is used for fatigue testing. Testing is done at a frequency of 5 Hz, [2]. The upper load limit and a load ratio, R = 0.1, are used to set the maximum and minimum displacement boundaries. After a sequential number of fatigue cycles, a picture is taken to measure the crack length along with the maximum measured load and displacement. Each specimen is tested at the same mode mix, but at different loads to get four different G_{Max} values. A straight power law curve is fitted through the data points on a logarithmic scale. The parameters of the power law, C and m, are later employed to predict the fatigue life of the helically wrapped structure.

5.5.1 Quasi-Static Results Mixed Mode-I Mode-II Bending Test

The quasi static and fatigue test are executed on the 10 kN MTS fatigue bench. Testing is done on hot summer day so the average temperature during testing was 30 degrees Celsius. First the quasi-static maximum load test results are presented followed by the fatigue test results.

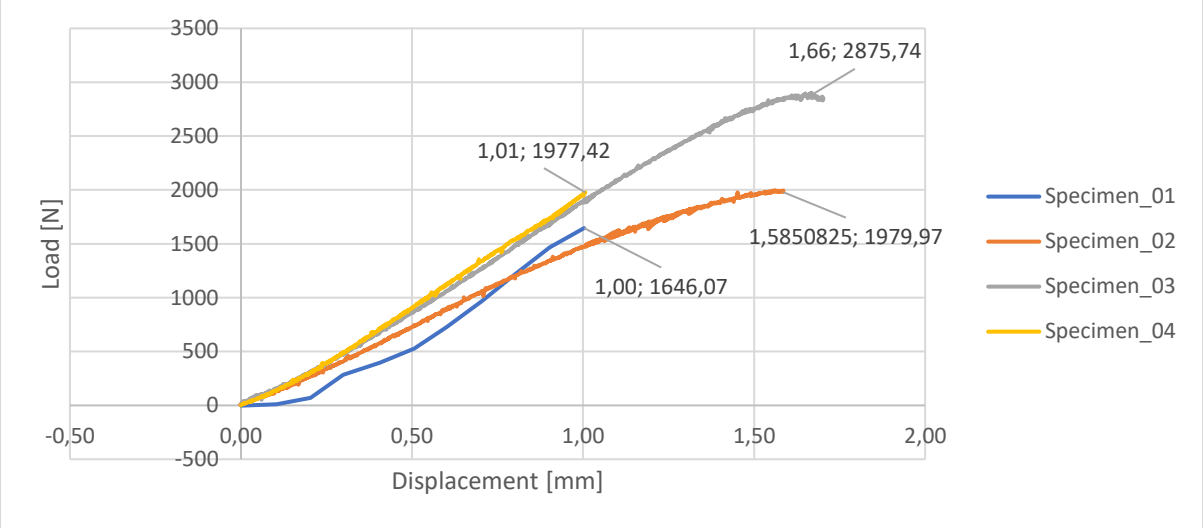

Figure 5.15 Recorded Load vs Displacement curve from the 70% Mix Mode-I Mode-II test.

The recorded load displacement data is shown in Figure 5.15. The maximum load, until crack initiation, was reached at 1.65, 1.59, 2.88, and 1.98 kN for specimen 1 till 4, respectively. This corresponds to a total maximum SERR, G_{Max}, of 0.9, 1.040, 1.546, and 0.439 $\frac{kJ}{m^2}$. A mode mix of 40%, 70%, 71% and 70% is reached for specimen 1 till 4 respectively. The maximum mode-I SERR, $G_{I,Max}$, reached a value of 0.55, 0.31, 0.45, 0.13 $\frac{kJ}{m^2}$. The maximum mode-II SERR, $G_{II,Max}$, reached a value of 0.36, 0.73, 1.1, and 0.31 $\frac{kJ}{m^2}$. These maximum SERR together, $G_{Tot_{Max}}$, summates to a value of 0.9, 1.04, 1.55, and 0.44 $\frac{kJ}{m^2}$. These results are all summarised in Table 3.

Table 3 Quasi static maximum load test results

Specimen	1	2	3	4
Slope	1744.7	1348.1	1860.2	2004.2
Mode-mix [%]	39.5	70.4	70.9	70.1
Max load [N]	1646.07	1979.97	2875.74	1977.42
Max Displacement [mm]	1.00	1.585	1.66	1.01
$G_{I,Max}\left[\frac{N}{mm}\right]$	0.544	0.308	0.449	0.131
$G_{II,Max}\left[\frac{N}{mm}\right]$	0.356	0.733	1.097	0.308
$G_{Tot_{Max}}\left[\frac{N}{mm}\right]$	0.9	1.040	1.546	0.439

5.5.2 Fatigue Results Mixed Mode-I Mode-II Bending Test

The first specimen was completely cracked in the first test because the displacement rate was set too high. Therefore, only specimen 2 till 4 were used for the fatigue tests. Figure 5.16 shows the crack propagation per fatigue cycle. Data was capped beyond a crack length of 65 mm because at this location the crack approached the compression zone of the test setup, Figure 5.14. This would influence the crack growth and is therefore neglected. The step size between consecutive pictures for specimen 2 was taken too large resulting in a less accurate result. Specimen 3 endured a high quasi static load and therefore a higher fatigue stress range, because for all specimen the stress range was derived from the maximum quasi static load test. Specimen 4 endured a lower fatigue stress range which resulted in more stress cycles.

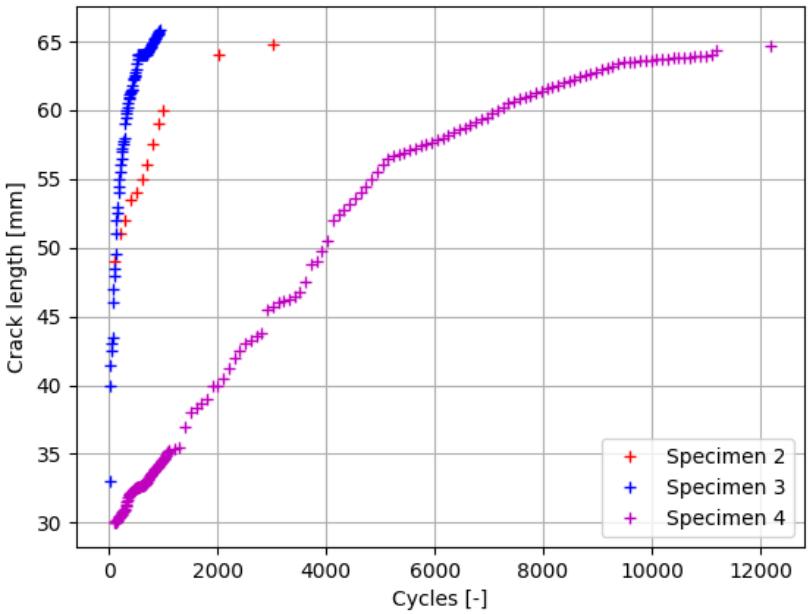

Figure 5.16 Recorded crack length data of the 70% Mixed Mode-I Mode-II test

The derivative, $\frac{da}{dN}$, of this crack vs cycle data is calculated according to ASTM standard E647 [31]. It employs a least squares regression method to minimize the error between the fitted curve and the data point. A second-order polynomial function is fitted through 7 consecutive data points. The form of this equation for the local fit is as follows:

$$a_i = b_0 + b_1 x_i + b_2 x_i^2 \tag{30}$$

where x_i is given by the standard to be:

$$x_i = \frac{N_i - C_1}{C_2} \tag{31}$$

where C_1 and C_2 are scaling parameters that avoid numerical difficulties in determining the regression parameters. The scaling parameters are as follows:

$$C_1 = \frac{1}{2}(N_{i-1} + N_{i+1}) \; and \; C_2 = \frac{1}{2}(N_{i+1} - N_{i-1}) \tag{32}$$

The scaling is only valid if the difference between successive cycle data points is within a range specified as:

$$-1 \leq \left(\frac{N_i - C_1}{C_2}\right) \leq +1 \tag{33}$$

The residual between the actual and this fitted function becomes:

$$r(x_i) = f(x_i) - a(x_i), i = 1, \dots, N, \tag{34}$$

where N would be 7 in this case. Then with the least squares principle the sum of the squares must be minimised. This is done by differentiation with respect to $b_0, b_1, and \; b_2$ and solve for them:

$$\Phi(b_0, b_1, b_2) = \sum_{i=1}^{N} r(x_i)^2 = \sum_{i=1}^{N} \big(f(x_i) - a(x_i)\big)^2 \tag{35}$$

$$\begin{cases} \dfrac{d\Phi}{db_0} = -2\sum_{i=1}^{N}(f_i - b_0 - b_1x_i - b_2x_i^2) = 0 \\ \dfrac{d\Phi}{db_1} = -2\sum_{i=1}^{N}(f_i - b_0 - b_1x_i - b_2x_i^2)(x_i) = 0 \\ \dfrac{d\Phi}{db_2} = -2\sum_{i=1}^{N}(f_i - b_0 - b_1x_i - b_2(x_i)^2)(x_i)^2 = 0 \end{cases} \tag{36}$$

In matrix-form this becomes:

$$2\begin{pmatrix} \sum_{i=1}^{7} 1 & \sum_{i=1}^{7} x_i & \sum_{i=1}^{7} x_i^2 \\ \sum_{i=1}^{7} x_i & \sum_{i=1}^{7} x_i^2 & \sum_{i=1}^{7} x_i^3 \\ \sum_{i=1}^{7} x_i^2 & \sum_{i=1}^{7} x_i^3 & \sum_{i=1}^{7} x_i^4 \end{pmatrix}\begin{pmatrix} b_0 \\ b_1 \\ b_2 \end{pmatrix} = 2\begin{pmatrix} \sum_{i=1}^{7} f_i \\ \sum_{i=1}^{7} f_i x_i \\ \sum_{i=1}^{7} f_i x_i^2 \end{pmatrix} \tag{37}$$

This system of equations is solved by basic linear algebra rules to get the regression parameters. These parameters are filled in the second-order polynomial function corresponding to its local domain range. Each separate local polynomial fit is shown as a whole in Figure 5.17.

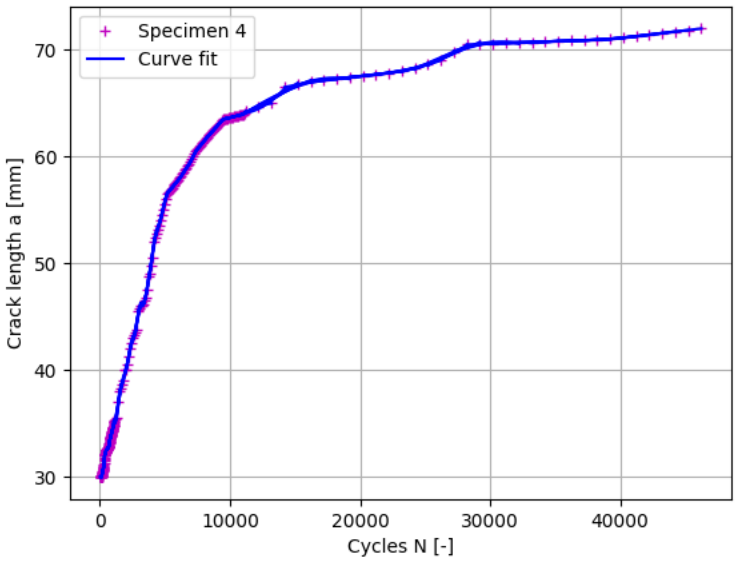

Figure 5.17 Least squares curve fit through 7 successive crack growth data points. All consecutive curve fits are plotted on top of each other representing a complete curve.

These parameters are used to calculate the derivate at each local curve fit (38).

$$\left(\frac{da}{dN}\right)_{a_i} = \frac{b_1}{C_2} + \frac{2b_2(N_i - C_1)}{(C_2)^2} \tag{38}$$

The result of the crack growth rate per crack opening mode, $\frac{da}{dN}$, is plotted against the matching G_{Max}, Figure 5.18 and Figure 5.19. Hence the Paris relation is found for aluminium alloy AL5745-H22 adhesively joined with Araldite AW4858/HW4858 two-component epoxy. A straight line on a logarithmic scale is fitted through the $\frac{da}{dN}$ and G_{Max} data. The power law is

a straight line on a logarithmic scale. The parameters of this power law, C and m, for each crack opening mode is given in equation (39), and (40).

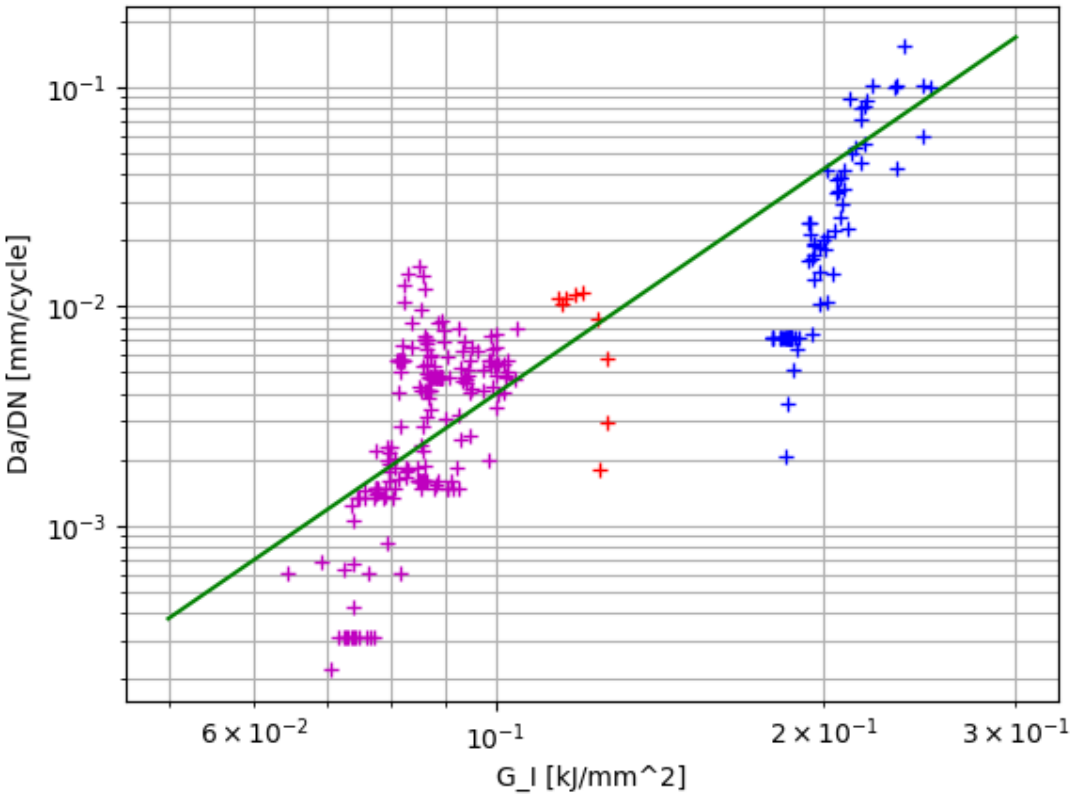

Figure 5.18 $\frac{da}{dN}$ against $G_{I,Max}$ $\left[\frac{N}{mm}\right]$ Mode-I Paris relation.

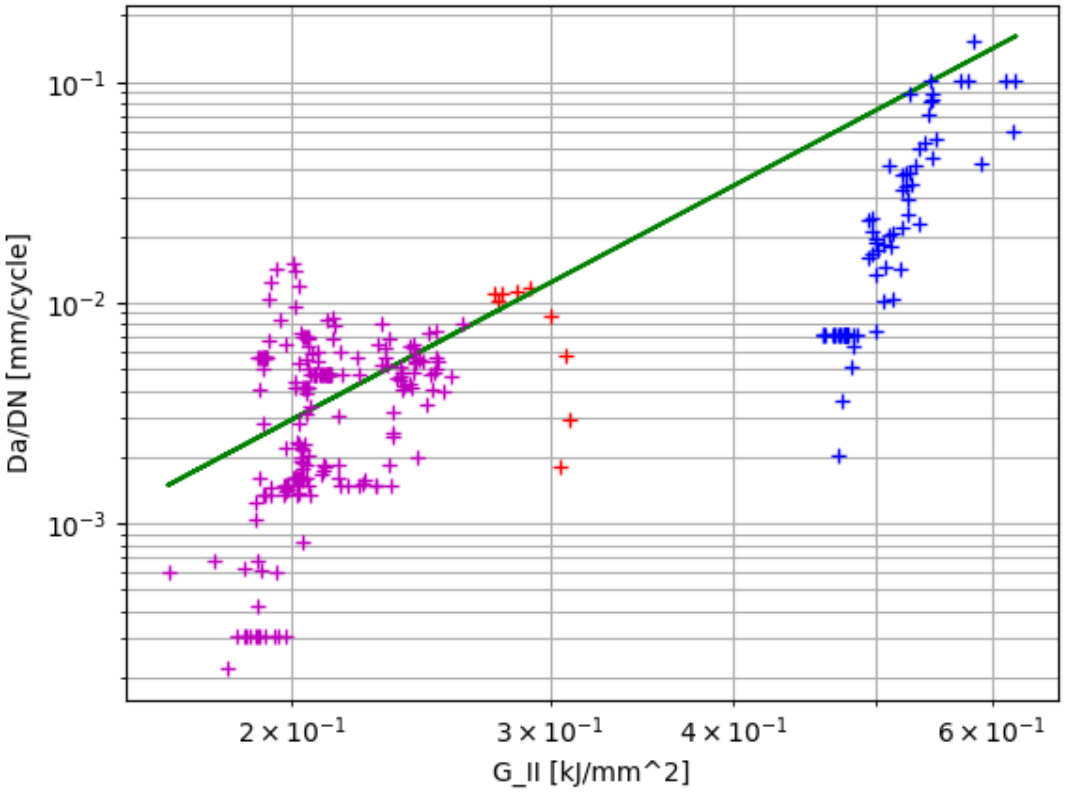

Figure 5.19 $\frac{da}{dN}$ against $G_{II,Max}$ $\left[\frac{N}{mm}\right]$ Mode-II Paris relation.

$$\left(\frac{da}{dN}\right)_I = 10.304371\ G_{I_{Max}}^{3.4110413} \quad (39)$$

$$\left(\frac{da}{dN}\right)_{II} = 0.854051\ G_{II_{Max}}^{3.5203273} \quad (40)$$

Reflecting on these results, the Paris relation obtained from the MMB test results for $G_{I,Max}$ and $G_{II,Max}$ show much scatter. The G_{Max} range for both modes calculated from specimen 2 show a negative trend of the Paris relation and should be neglected. However, the G_{Max} range from specimen 3 (blue points) is narrow and can be used. The G_{Max} range for specimen 4 (purple points) is not narrow, but a quantitative power law can be curve fitted through it to be useful. Therefore, a curve fit through the individual points per specimen per mode to obtain two Paris relations would have been better. It was thought that for a stress ratio $R = 0.1$, the G_{Max} results from each specimen would appear underneath each other, because different load levels were tested, such that one overall power law could be curve fitted through it. It turned out that the stress ratio might have been different, causing a shift of the power law per specimen in the diagram. This happened due to the displacement-controlled fatigue testing. After some cycles the minimum stress decreased to zero meaning a deviation in stress ratio.

Nevertheless, a quantitative overall Paris relation is still curve fitted through all data points. The obtained $G_{I,Max}$ values from FEA results never reached values higher than $0.016\ \frac{N}{mm}$. The obtained $G_{II,Max}$ values from FEA results never reached values higher than $0.1\ \frac{N}{mm}$. This would mean that the predicted fatigue crack growth for $G_{I,Max}$ and $G_{II,Max}$ values, below these FEA results, overestimate the fatigue crack growth rate.

5.6 Fatigue Prediction Employing the Paris Relations

The two equations (26) and (27), given in the beginning of this chapter are used to predict the fatigue life of the helically wrapped structure. The G_{Max} distribution along the crack front dependent on the crack length is obtained from finite element analysis, described in paragraph 5.4. The Paris relations resulted from testing are described in paragraph 5.5.

The highest value of the G_{Max} distribution along a crack front at fixed delamination area is substituted in the Paris relation. This provides the fatigue crack growth rate, $\frac{da}{dN}$, for this single highest G_{Max} value along the crack front. This fatigue crack growth rate value is divided by a crack size propagation of 5mm to obtain the amount of fatigue cycles. The remaining but lower G_{Max} values along the crack front are also substituted in the Paris relation to get the fatigue crack growth rate at the remaining nodes along the crack front. These are then multiplied with the obtained required fatigue cycles to propagate the crack. This results in the remaining nodes along the crack front to propagate as well but less then 5mm. When the entire overlap length is cracked, the structure is considered as end of fatigue life. The fatigue crack growth per iteration is shown in Figure 5.20.

The first method had one initial node disconnected. The crack progressed slowly to the neutral axis, and then progressed in axial direction. An oval crack front was obtained and continued to propagate along the axial direction. Since the G_{Max} distribution along the crack

front was highest at the edges of the front. Crack propagation only occurred along the circumferential length and minor in axial direction.

The second method started with an entire edge as initial crack. After the first iteration the crack progressed just like the first method from iteration 7. So, the methods merged. This is because the first method only cracked in circumferential direction until it became the initial crack of this second method. In other words, the second method skipped the delamination from one node. The result of the second method required less fatigue cycles to propagate the crack up to the 7th iteration from method 1. Method 1 had a very low G_{Max} distribution for the first iteration taking longer to propagate the crack for the obtained amount of fatigue cycles.

Method 1 started with one node delaminated. The second method started with an entire edge delaminated of the tension side of the bent helically wrapped structure as initial crack. The initial crack is required when using the VCCT in FEA. I think that a mixture of both methods is more realistic. Method 2 shows a smooth distribution along the crack front resulting from the smooth stress distribution along the pipe structure. Without initial crack, this distribution would still be there, shaped like an oval crack progressing in axial direction. Method 1 stating with 1 node delaminated is too non-conservative while method 2 possibly skipped too many initial cracked nodes meaning too rapid propagation and thus conservative.

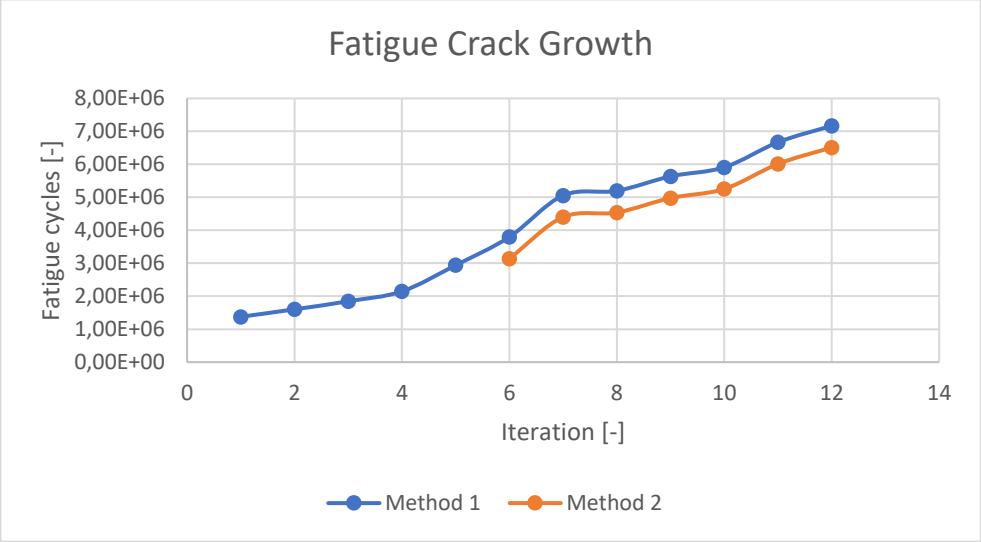

Figure 5.20 Fatigue Crack Growth prediction from FEA-results

The overlap length is 30mm so it would take 6.5e6 to 7.1e6 fatigue cycles to completely break through the joint. This number of cycles can never be reached since the aluminium alloy Al5754-H22 tested on fatigue with R=0.1 at a maximum stress level of 171 MPa, can only withstand $4 * 10^5$ cycles, paragraph 5.2. Even the first iterations required too many fatigue cycles to crack the adhesive to a next iteration. Therefore, the aluminium is critical for the fatigue estimation of this structure tested at 90% of the yield strength.

Quasi-static testing at a stress level close to the yield strength of the adherend causes the adhesive to fail instantly. Fatigue testing above the fatigue limit of the adherend but below the yield strength, causes the adherend to fail sooner than the adhesive. Fatigue testing below the fatigue limit of the aluminium must result in the adhesive to fail after a high amount of fatigue cycles but this is not tested.

6 Validation

To validate if the predicted number of fatigue cycles is valid, a full-scale test is executed. The helically wrapped structures are manufactured in the wrapping machine, Figure 6.1. A test rig was designed to allow using a 60 kN fatigue bench to apply four-point bending to the wrapped structure. To control the area of fatigue failure in the joint, a non-adhesive film was inserted in the middle of the structure, locally weakening the structure where the stress due to bending will be highest. This insert acts as the initial crack at a focussed area of the structure. Digital Image Correlation is used to view and obtain the crack growth rate in a non-destructive manner.

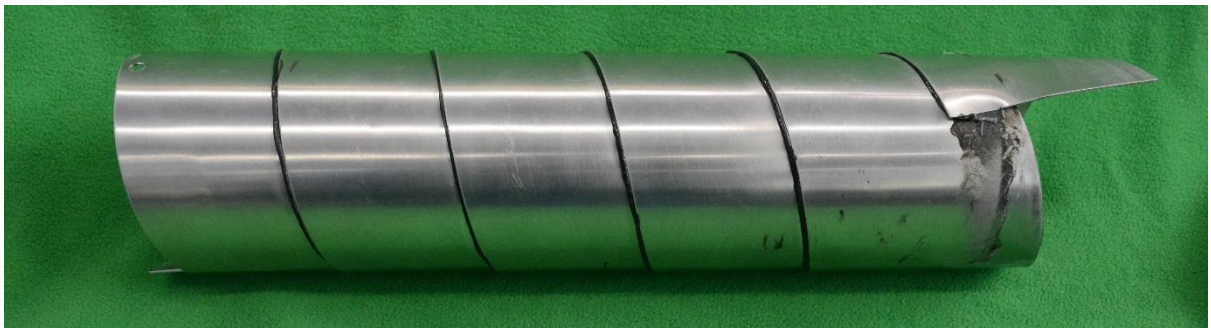

Figure 6.1 Helically wrapped structure.

A total of 9 samples were manufactured, Figure 6.2. The first sample is a double layered helically wrapped structure and made with a different wrapping technique. This sample is wrapped around a solid cylinder without sheet guidance. The first layer is helically wrapped and fixed to the mould. Then a second layer is wrapped around and glued to the first layer. A gap of 7mm between the edges of one metal strip is created. Sample 2 to 9 are helically wrapped around a cylinder with helical guidance in the mould. This is the main wrapping technique which contains only one strip of material. Sample 2 and 3 are used for ultimate strength test and do not contain any initial cracks. Sample 3 was cut to obtain flush ends of the tube. Samples 4,5, and 6 are helically wrapped structures with an initial crack of 10mm. A non-adhesive film insert was wrapped along with the helical wrapped structure. A green coloured diamond shape was drawn on the outside of the tube to localise the insert. Samples 7,8, and 9 are helically wrapped structures with 20mm initial crack inserts. The different inserts are placed to validate the prediction at several initial crack lengths. The generated SERR values from FEA-model are validated in this way.

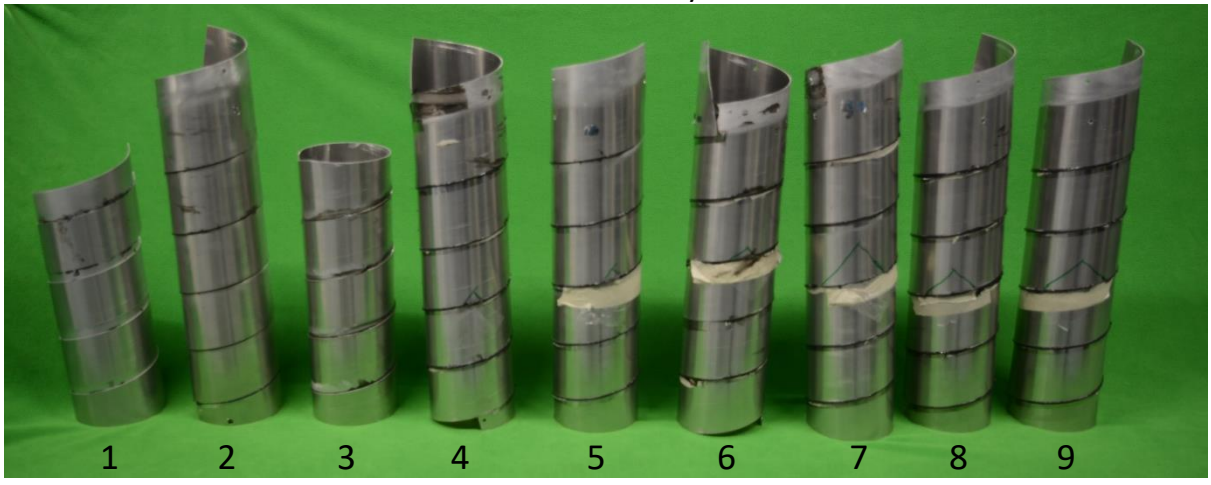

Figure 6.2 Helically wrapped test samples.

6.1 4-Point Bending Test Setup

The helically wrapped structure is placed in a 4-point bending test setup to validate the crack propagation and thus the fatigue life of the structure, Figure 6.3. The 60 kN fatigue bench has a stationary part where the loadcell is placed and another actuating part that controls the displacement. The 4-point bending setup is placed within these two parts. The stationary part is attached to the stationary forks. Hinges are placed within all the forks to allow for rotation. The clamps are attached to the hinges and clamp the complete circumference of the tube. A rubber strip was used to apply pressure and introduce the clamping forces evenly along the circumference. Loads are transferred from the actuating part through the helically wrapped structure to the stationary part connected to the loadcell. The section between the middle dynamic fluctuating clamps creates a constant moment, which mimics the physics in the FEA-model as close as possible.

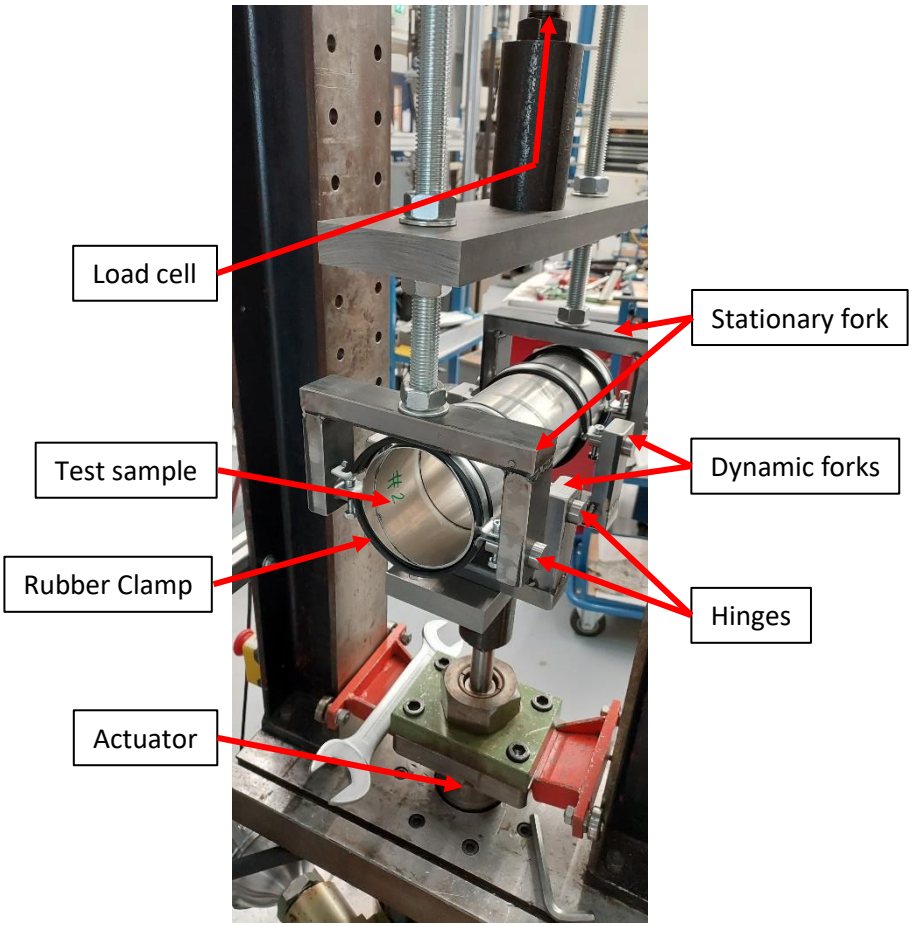

Figure 6.3 Helically wrapped structure in a 4-point bending test setup.

6.1.1 Digital Image Correlation Setup

To monitor the fatigue crack growth Digital Image Correlation (DIC) is used. The deformations and strains are measured on the surface of the helically wrapped structure. Two cameras are placed next to the fatigue bench with an angle of 35 degrees between them but both focussing on the speckle pattern on the structure. The speckle pattern is shown in Figure 6.4. The field of view on a rounded structure require a large range of focal depth. Therefore, a small aperture is required. The 23mm lens along with 5-megapixel cameras are used. Due to the 4-point bending test setup and the required focal depth, the cameras are placed 500mm from the object. The minimal working distance of the lens is 215mm.

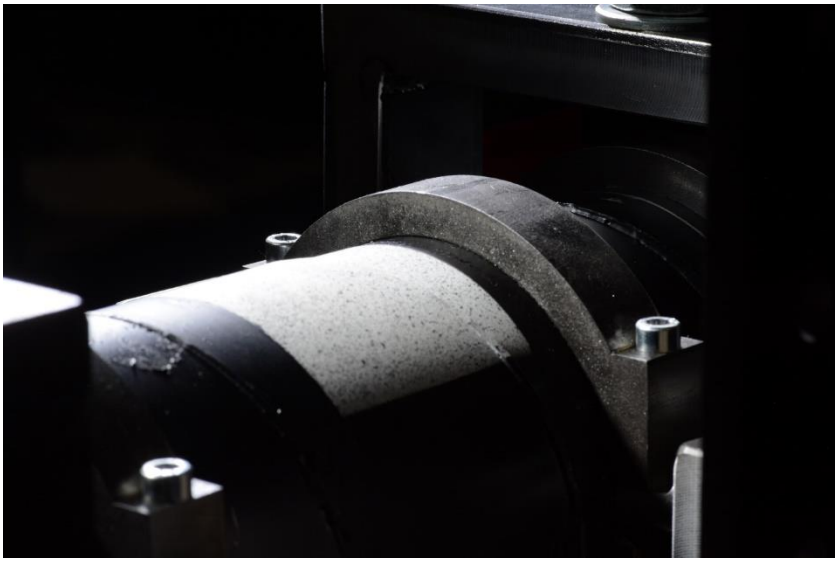

Figure 6.4 Speckle pattern on the helically wrapped structure.

6.2 Results maximum load test

The maximum load test is executed on specimen 2 and 3. According to calculations in paragraph 0, a quasi-static load of 38.62 kN was required to create a moment of 1.45 kNm in the structure. This creates a tension that meats the yield strength of the aluminium. Figure 6.5 shows the test result of the maximum load test of the helically wrapped structure. The maximum measured load was 23.69, and 27.72 kN. This applied load created a bending moment to the helically wrapped structure of 1.036, and 1.213 kNm, respectively. Hence, a tension of 136, and 159.2 MPa was applied to the furthest fibre of the bend structure. This is lower than expected since the aluminium yield strength is 190 MPa.

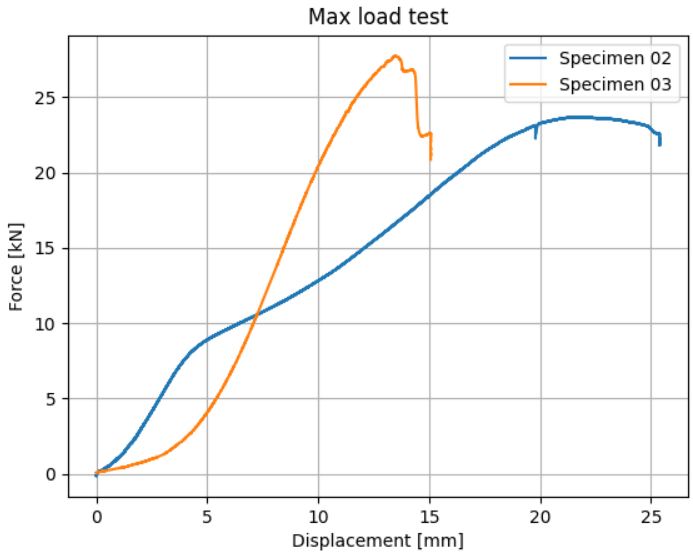

Figure 6.5 Max load test helically wrapped structure.

The cause of this lower strength can be found in two experienced problems. The first problem was that the clamps locally plastically deformed the structure. The required load to create the bending moment was too high. Only half the circumference of the structure carried the load causing larger local stresses in the structure and lead to plastic deformation. An attempt was made to locally strengthen the structure and transfer the load through the complete circumference. This was done by using larger and stronger clamps and by inserting a disk

inside the structure. This led to a higher max load for specimen 3 as shown in Figure 6.5, but still not sufficient to reach the 38.62 kN.

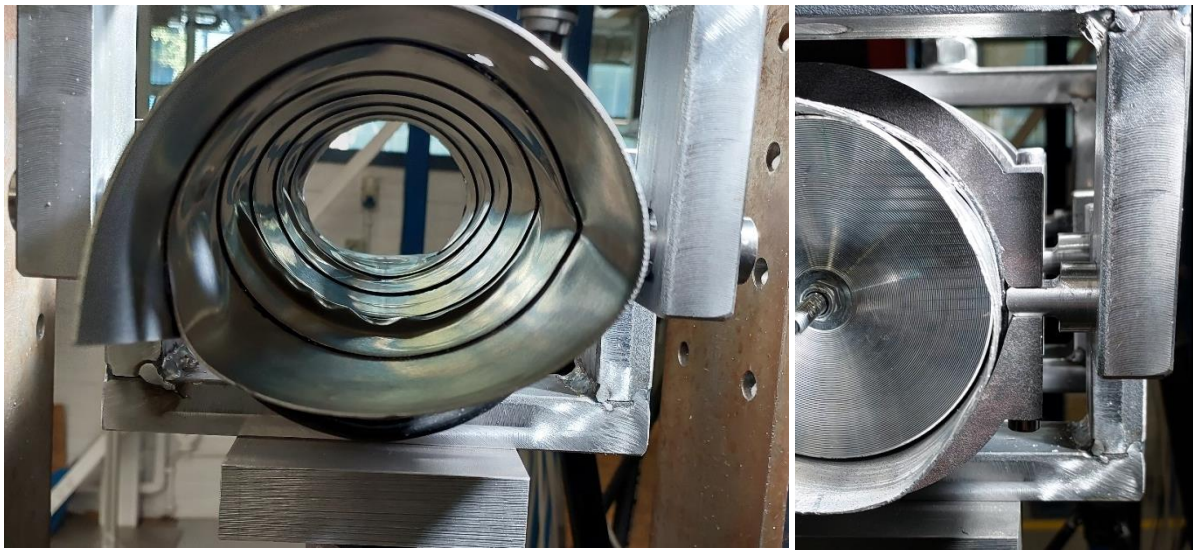

Figure 6.6 Left: Plastically deformed helically wrapped structure. The clamps locally forced itself through the structure. Right: The clamps and inserted disk locally strengthening the structure.

The second problem was the amount of displacement required to obtain the loads. From the FEA-model a displacement of 0.23 mm was obtained at an applied moment of 1.053 kNm on a helically wrapped structure of 100 mm length. The tested structure was 300mm long, meaning a displacement of roughly 3.5 times larger should be obtained in the actual test. This was clearly not the case since the displacement was much higher. This is partially caused by the insufficient stiffness of the 4-point bending test setup itself. The displacement of the structure was visually noticeable.

However, according to the FEA-model a lower bending moment is required to obtain the desired stresses in the structure. This is due to a wrong comparison with the calculations for a homogeneous pipe and the helically wrapped structure. Equation (19) is used to calculate the required stresses for a bending moment. The Inertia and distance to the furthest fibre in the structure are constant. Although, the second moment of area might be less due to the difference in diameter due to the helically wrapping of the metal strip. The bending moment equation is a linear relation between the tensile stress and the bending moment if the inertia and distance to the furthest fibre are kept constant. If one would compare the required bending moment causing a maximum stress in the furthest fibre, resulting from the FEA-model and the homogeneous pipe structure, a reduced linear relation of 80% is obtained. This reduction must be caused by the geometry of the helically wrapped structure having a transition in sheet layer thickness in axial direction due to the helix. Also, the stress concentrations cause higher stresses for the same bending moment. Conclusively, the stress in a helically wrapped structure is higher than the homogeneous pipe structure for the same bending moment.

6.3 Fatigue life

Specimen 4 with an initial crack length of 10mm and shaped like a triangle, was tested in the 4-point bending test setup. Unfortunately, the improved clamps kept breaking during testing. Also, the load level as discussed in the quasi-static load test never reached the 171 MPa maximum stress due to bending. Therefore, it was decided not to continue testing in this setup as it would not generate the result we were looking for. It was decided to keep the

remaining specimen reserved for compression test which could as well validate the crack growth rate from the FEA-model.

Although, some data was recorded and can still give some insight in the fatigue behaviour. A total amount of 216087 fatigue cycles were counted. The maximum stress of the fatigue cycles was 15 kN and the minimum was set to 1.5 kN. This caused a stress in the furthest fibre of the tube of 106.5 MPa, which is below the fatigue limit of the adherend.

The DIC setup made pictures during the test after a certain amount of fatigue cycles. The speckle pattern was sufficient for post processing to calculate the strain in the structure, Figure 6.7. The difference between picture Figure 6.8 and Figure 6.9 showed no significant difference in crack length. This would mean that no adhesive crack propagation was obtained. Also, the adherend material did not break. Although, it could be seen that the stress distribution is similar to what has been modelled in the FEA-model. The strain is highest on the edges of the bonded area, but also highest at the largest stress due to bending.

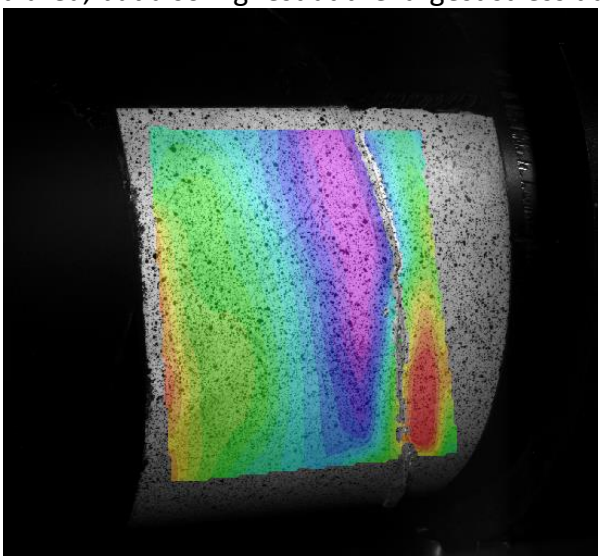

Figure 6.7 DIC image of the helically wrapped structure during 4-point bending test.

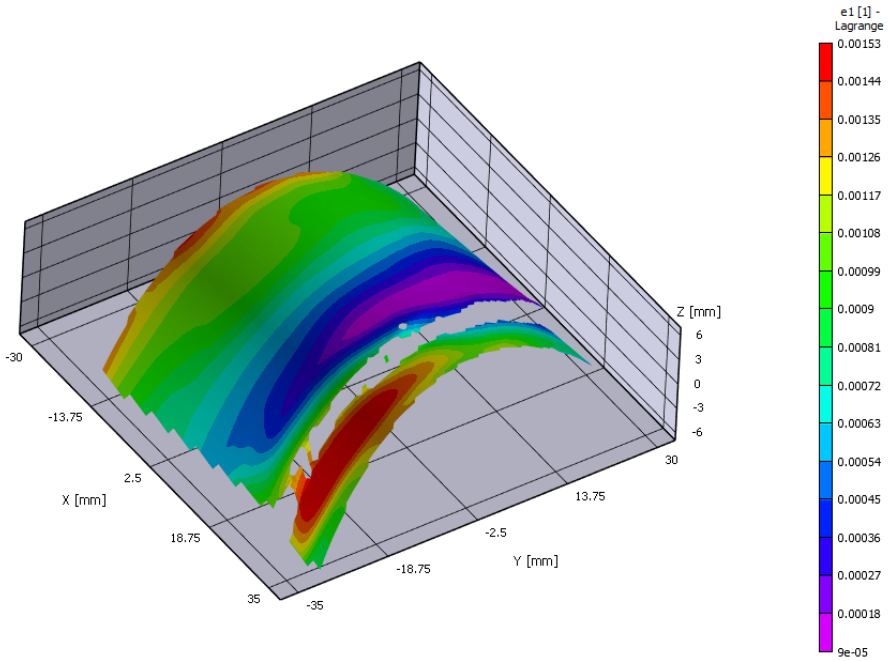

Figure 6.8 Post processed strain of the surface of the helically wrapped structure before fatigue testing.

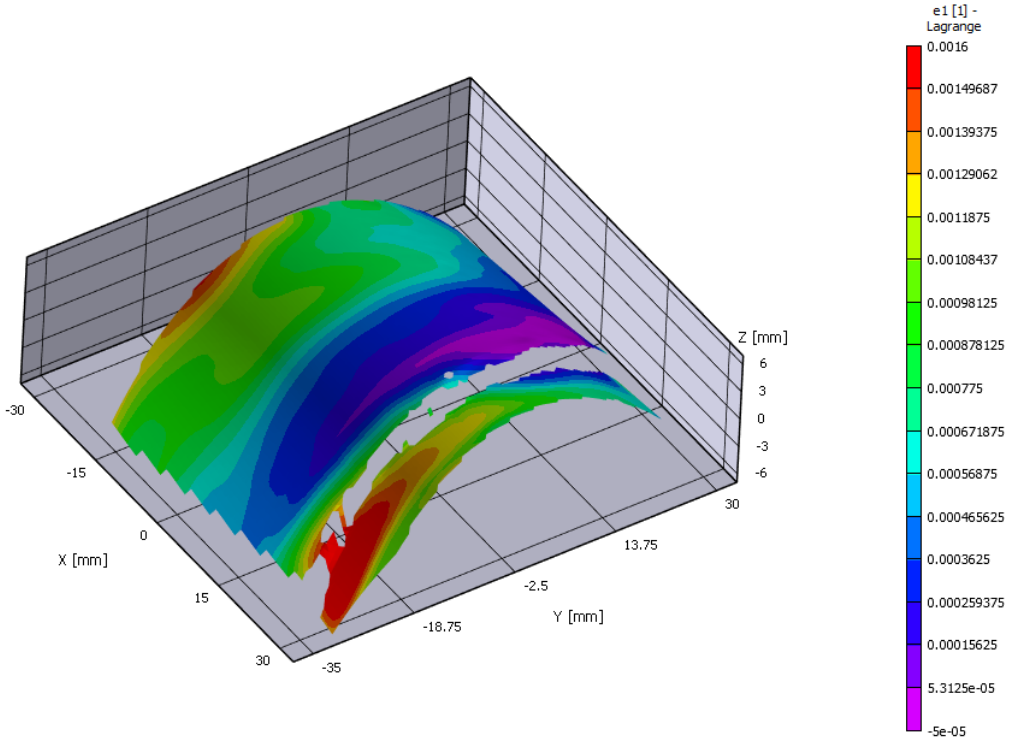

Figure 6.9 Strain of the surface of the helically wrapped structure after 216087 fatigue cycles.

It cannot be confirmed from the validation that the fatigue life was critical for either the adherend or the adhesive from this test. Neither can it be disproved that fatigue was critical for either the adherend or the adhesive. The structure endured at least $2 * 10^5$ fatigue cycles, without showing significant damage to either the adherend or the adhesive. The predicted fatigue life was higher for either the adherend and the adhesive. Therefore, the predictions are not wrong, but still require validation. If the structure would have failed within these number of cycles, it would disprove the predictions.

In future It would be better to design the test setup, being dependent on the test specimen, such that the unknown variables can be tested. During the four-point bending test I figured the setup to be unsuitable to test the unknowns I was looking for. At that moment the helically wrapped structures were already manufactured, and its geometry made it impossible to be tested. With this experience It would be better to test tubes that are either longer in length or smaller in diameter in this four-point bending test setup. This would require lower loads to be exerted on the structure at the clamps while still being able to obtain the desired stresses in the structure. Adjustments of the inner clamps might have solved the problem of high stresses at the clamps while still being able to obtain the desired stresses in the structure. However, it would be better to do the calculations beforehand to prevent adjustments on a trial-and-error base.

7 Conclusion

The objective of this project was to determine a method to calculate and predict the Quasi-static and fatigue life of the helically wrapped structure. Research was required on whether either the adherend or the adhesive would determine the strength of the structure. If the adhesive would have been critical, it was required to determine how the fatigue cracks would propagate. For validation, a helically wrapped structure must be created, but required research how to manufacture it. These points were the objectives of this research.

Manufacturability of the helically wrapped structure. A new method is developed to helically wrap a strip of material into a tubular structure and maintain an average diameter. It was found that a curved metal strip was required to manufacture the helically wrapped structure due to the conical shape. Due to wall thickness, a straight strip of sheet material cannot be helically wrapped while overlapping its own surface after one helical revolution. The solution with a curved strip resulted in a constant average tubular diameter. A helical wrapping machine was created to manufacture the structure.

Criticality of Adherend or Adhesive. It was concluded that the adherend is critical for the quasi-static strength of the joint and not the adhesive. This is true for a range of overlap length divided by adherend thickness, while being dependent on the material properties.

$$\tau_{Max}(l, t_1) * \frac{l}{t_1} > \sigma_{Yield\ strength}$$

The maximum shear stress the adhesive can withstand is dependent on the overlap length and adherend thickness, while these parameters also determine the inequality with the adherend yield strength. The adherend suffers from straining at the yield strength causing the adhesive to fail instantly. Therefore, for analyses of the quasi-static strength in an adhesive joint, one should consider these design rules and safely limit its analyses to only the adherend yield strength.

It was found that the fatigue crack growth from the finite element model of the adhesive in the helically wrapped structure were overestimated and thus underestimating the fatigue life of the adhesive. Nevertheless, these predictions were still higher than the number of fatigue cycles theoretically required to break the adherend. Therefore, it is concluded that the adherend is critical and not the adhesive for this chosen geometry of the helically wrapped structure. In practise this would mean that calculations to predict fatigue life need only be done for the adherend and not the adhesive.

Fatigue tests to validate the predictions of the fatigue crack growth of the adhesive were not disproved. However, due to the unsuitable test setup, validation is still required to demonstrate that the adherend fails earlier than the adhesive under fatigue loads. The test setup was found to be not stiff enough to apply the load to the specimen. The bending stiffness of the helically wrapped structure was higher than the bending stiffness of the test setup. The displacement in the test setup itself was too much and thus not useful. Displacements around 15mm were required to obtain the amount of stress in the structure, while not more than 2mm was expected. The clamps were unsuitable to transfer the loads through the structure. The helically wrapped structure, tested in the fatigue bench, endured a lot of fatigue cycles, but did not demonstrate significant damage to the structure. The

number of fatigue cycles required to complete the validation, were not achieved. Lessons were learned to design a test setup such that it is suitable to test the specimen to obtain the intended results. Due to the limited validation process it was not determined if analyses can be limited to only the adherend and thus neglecting the analyses of complex fatigue crack growth of the adhesive, while taking design rules into account.

Adhesive data. The manufacturer presented maximum adhesive shear stress cannot be used as a design parameter, but merely be used for comparison. Due to specified specimen dimensions from test standards, the presented maximum shear strength of an adhesive might be higher. Once the adherend material reaches the yield strength, due to loading, failure of the joint occurs.

Mixed mode bend test. The mixed mode bending test were executed on a 10kN test bench. The gathered data was used to obtain the Paris relations for two crack opening modes. The test specimens loading points were misaligned causing the test results to contain a lot scatter. It was found that the curing temperature was not high enough to ensure good bonding. The obtained strain energy release rate for the two crack opening modes versus fatigue crack growth per fatigue cycle contained data for different R ratios.

Crack propagation. A FEA-model of the helically wrapped structure employing the VCCT was found suitable to obtain the necessary SERR distribution along the crack front as a function of the delamination area. Due to the complex three-dimensional shape of the structure a stepwise approach to manually delaminate a crack surface is required. If fatigue crack initiated at the location analysed in this thesis, a oval shaped delamination area propagates in axial direction ultimately leading to failure of the structure.

Validation. It was found that the geometry of the helically wrapped structure was too short in length or the diameter was too large. The structure close to the clamps showed local buckling and thus limiting the desired stress at the desired location of the structure. The digital image correlation was setup correctly, but due to the large displacements in the test setup, too much scatter was obtained in the post processing. Only an indication of the amount of stress through the structure showed resemblance to the FEA-model results.

8 Recommendations

Geometry of the helically wrapped structure. A longer length or a smaller diameter of the helically wrapped structure is recommended to be tested on bending for future testing. Either a longer length or smaller diameter result in a lower required load to apply the desired bending moment on the structure. A longer helical wrapped structure could become impractical to be manufactured or tested in a 4-point bend test setup. A reduction in diameter is a practical solution but might alter the fatigue properties because the strip of material must be bent to a smaller radius. Hence higher springback tension occurs that applies a higher peel stress on the adhesive thus altering the fatigue life. Though, for testing purpose and the ability to quantify the amount of limiting springback, it is recommended to choose a smaller diameter.

Adhesive data sheets. Manufacturers of adhesives should include the strain energy release rate or stress intensity factor for design purpose. A double cantilever beam test or an end-notched flexure test can deliver sufficient information about the SERR per mode. This will increase the introduction of adhesives in areas of engineering, like aerospace, automotive, marine industry, or civil engineering.

Compression testing. To avoid the difficulty of testing a tubular structure in a 4-point bending test setup and dealing with round clamps, it is recommended to test the structure on compression in axial direction. The tubular structure ends should be fixed in a mould to transfer the compression forces through. The fatigue crack growth can still be validated because the non-adhesive insert still locally weakens the structure focussing the area of delamination. One should account for the possible effect of torsion due the helical structure. This can be addressed by allowing one compression side to be rotated freely.

Multiple attached single lap joints. When multiple single lap joints are joined in sequence an axial representation of the cross section of a helical structure is created. It would be interesting to see the resemblance to the helically wrapped structure. With only this simpler setup and a correction factor the analyses of the helically wrapped structure can be avoided.

Workshop DEMO. It is recommended that the workshop, Demo, at the flight hall of the TUDelft continue their work with students. This project could not be realised without the help of these people.

Bibliography

[1] J. Schijve, *Fatigue of structures and materials*. 2008.

[2] D. Bürger, *Mixed-Mode Fatigue Disbond on Metallic Bonded Joints*. 2015.

[3] HVACDIRECT.COM, "Gauge Spiral Pipe." 2022.

[4] M. Chopra, "United States Patent : 5861366 United States Patent : 5861366," *New York*, vol. 1, no. 19, pp. 1–29, 2010, [Online]. Available: https://patentimages.storage.googleapis.com/30/f4/62/e9b75605352fb0/US10679987.pdf.

[5] O. Volkersen, "Die Schubkraftverteilung in Leim-, Niet-und Bolzenverbindungen," *Energ. und Tech.*, vol. 5, no. 68, p. 103, 1938.

[6] L. F. M. da Silva and R. D. S. G. Campilho, *Design of adhesively-bonded composite joints*. Elsevier Ltd, 2015.

[7] A. V Pocius, "Adhesion and Adhesives Technology: An Introduction, Hanser," *New York*, 1997.

[8] R. D. Adams, J. Comyn, and W. C. Wake, *Structural adhesive joints in engineering*. Springer Science \& Business Media, 1997.

[9] M. Goland and E. Reissner, "The Stresses in Cemented Joints," *J. Appl. Mech.*, vol. 11, no. 1, pp. A17–A27, 1944, doi: 10.1115/1.4009336.

[10] L. J. Hart-Smith, "Adhesive-Bonded Single-lap Joint," *Natl. Aeronaut. Sp. Adm.*, 1973, doi: 19740005083.

[11] R. D. Adams and V. Mallick, "A method for the stress analysis of lap joints," *J. Adhes.*, vol. 38, no. 3–4, pp. 199–217, 1992, doi: 10.1080/00218469208030455.

[12] Surjya Kumar Maiti, "Fracture Mechanics : Fundamentals and Applications," pp. 8–9, 2015.

[13] A. . A. . Griffith, "The Phenomena of Rupture and Flow in Solids Author (s): A . A . Griffith Source : Philosophical Transactions of the Royal Society of London . Series A , Containing Papers of a Mathematical or Physical Character , Vol . 221 (1921), pp . 163-198 Publish," *Philos. Trans. R. Soc. london. Ser. A, Contain. Pap. a Math. or Phys. character*, vol. 221, no. 1921, pp. 163–198, 1921.

[14] N. Perez, *Fracture Mechanics*, vol. 23, no. 6. 2006.

[15] G. R. Irwin, "Analysis of Stresses and Strains Near the End of a Crack Traversing a Plate," *J. Appl. Mech.*, vol. 24, no. 3, pp. 361–364, 1957, doi: 10.1115/1.4011547.

[16] J. Pascoe, "Characterisation of Fatigue Crack Growth in Adhesive Bonds," *TU Delft Univ.*,

p. 289, 2016, doi: 10.4233/uuid.

[17] W. A. P. Paris, M. Gomez, P. C. Paris, M. P. Gomez, and W. E. P. Anderson, "A Rational Analytic Theory of Fatigue," *The Trend in Engineering*, vol. 13. pp. 9–14, 1961.

[18] René C. Alderliesten, *Fatigue and Fracture of Fibre Metal Laminates*. Springer, 2017.

[19] J. Pascoe, "How to set up a cohesive zone model for an LEFM dominated problem : a detailed analysis for first time users," no. mm, pp. 1–17.

[20] DSS dassault systems, "Crack propagation analysis." 2023.

[21] D. Algemene *et al.*, "Technische gegevens aluminium," pp. 1–5, 2021, [Online]. Available: https://salomons-metalen.nl/datasheets/aluminium.pdf.

[22] Huntsman Corporation, "Araldite® AW4858/ Hardener HW4858 Technical Datasheet," no. June, pp. 1–7, 2014, [Online]. Available: https://www.viba.nl/nl/catalog/lijmen-tapes/twee-componentenlijmen/twee-componenten-epoxylijmen/twee-componenten-epoxylijmen/araldite-aw4858-hw4858-epoxylijm/groups/g+c+p+t+a+view?selectedartnr=220485850.

[23] E. F. Karachalios, R. D. Adams, and L. F. M. da Silva, "Single lap joints loaded in tension with high strength steel adherends," *Int. J. Adhes. Adhes.*, vol. 43, pp. 81–95, 2013, doi: 10.1016/j.ijadhadh.2013.01.016.

[24] R. C. Hibbeler, *Sterkteleer, 2/e*. Pearson Education, 2006.

[25] ASTM D6272-02, "Standard Test Method for Flexural Properties of Unreinforced and Reinforced Plastics and Electrical Insulating Materials by Four-Point Bending ASTM D6272-02," *Annu. B. ASTM Stand.*, pp. 1–9, 2002, doi: 10.1520/D6272-17E01.1.

[26] J. A. Pascoe, "Delamination of Bonded Repairs," no. May, 2012, doi: http://resolver.tudelft.nl/uuid:38e5d9ac-8c04-48d5-801f-b0c9308f67fa.

[27] J. X. Li, X. Y. Wen, C. S. Man, and T. Zhai, "Fatigue of continuous cast AA5754 Al alloy sheet," *Mater. Sci. Technol.*, vol. 23, no. 3, pp. 324–332, 2007, doi: 10.1179/174328407X158677.

[28] J. Lukács, Á. Meilinger, and D. Pósalaky, "High cycle fatigue and fatigue crack propagation design curves for 5754-H22 and 6082-T6 aluminium alloys and their friction stir welded joints," pp. 737–749, 2018.

[29] A. D6671M, "Standard Test Method for Mixed Mode I-Mode II Interlaminar Fracture Toughness of Unidirectional Fiber Reinforced Polymer Matrix Composites," *ASTM Int.*, no. Mode I, p. 15, 2006, doi: 10.1520/D6671.

[30] Huntsman Corporation, "Araldite® AW4858/ Hardener HW4858 Technical Datasheet," no. June, pp. 1–7, 2014.

[31] ASTM E647−13, "Standard Test Method for Measurement of Fatigue Crack Growth

Rates," *Am. Soc. Test. Mater.*, pp. 1–50, 2014, doi: 10.1520/E0647-15E01.2.

Appendix A: Python code least squares regression to calculate delamination growth rate da/dN

```
import numpy as np
import matplotlib.pyplot as plt
import pandas as pd

# This script is used to fit a function through 7 successive data points
# ASTM E647-15 Appendix x1.2 is used as reference.
# a second order polynomial function is fitted through measured crack vs cycles
data
# Import data, N, a, G_I, G_II and G_tot
df = pd.read_excel(r'Fatigue_results.xlsx',
sheet_name='Cam_Specimen_04_Fatigue',header=1)
data = np.array([df['counts'],df['crack'], df['G_I'], df['G_II'],df['G_tot']])
data = np.transpose(data)

# Set the matrix regression summation indices
k11 = 0
k12 = 0
k13 = 0
k23 = 0
k33 = 0
# polynomial parameters:
b1 = 0
b2 = 0
b3 = 0
c1 = 0
c2 = 0
n = 3
x = np.array([[], [], [], [], [], [], [], [], [], [], [], [], [], [], [], [],
[], [], []])
y = np.array([[], [], [], [], [], [], [], [], [], [], [], [], [], [], [], [],
[], [], []])
a = np.array([[], [], []])
dadn = np.array([[]])

for i in range(len(data)-2*n):
    i = i + n
    c1 = 0.5 * (data[i - n, 0] + data[i + n, 0])
    c2 = 0.5 * (data[i + n, 0] - data[i - n, 0])
    k11 = k12 = k13 = k21 = k22 = k23 = k31 = k32 = k33 = b1 = b2 = b3 = 0

    for j in range(-3, 4):
        scaling = ((data[i+j, 0]-c1)/c2)
        if -1 > scaling > 1:
            print(scaling)
        k11 = k11 + 1
        k12 = k12 + ((data[i+j, 0]-c1)/c2)
        k13 = k13 + ((data[i+j, 0]-c1)/c2)**2
        k23 = k23 + ((data[i+j, 0]-c1)/c2)**3
        k33 = k33 + ((data[i+j, 0]-c1)/c2)**4
        b1 = b1 + data[i+j, 1]
        b2 = b2 + data[i+j, 1]*((data[i+j, 0]-c1)/c2)
        b3 = b3 + data[i+j, 1]*((data[i+j, 0]-c1)/c2)**2

    k21 = k12
    k22 = k31 = k13
```

```
    k32 = k23
    k = np.array([[k11, k12, k13], [k21, k22, k23], [k31, k32, k33]])
    b = np.array([[b1], [b2], [b3]])
    a = np.c_[a, np.linalg.solve(k, b)]
    dadn1 = a[1, i-n] / c2 + 2 * a[2, i-n] * ((data[i, 0] - c1) / (c2 ** 2))
    dadn = np.c_[dadn, np.array([dadn1])]
    x1 = np.transpose(np.array([np.linspace(data[i-n, 0], data[i+n, 0], 20)]))
    x = np.c_[x, x1]
    y1 = []
    for m in range(len(x1)):
        y1.append(a[0,i-n]+((x1[m]-c1)/c2)*a[1, i-n]+((x1[m]-c1)/c2)**2*a[2, i-n])
    y = np.c_[y,y1]


plt.figure(1)
plt.plot(data[:,0],data[:,1],'m+', label='Specimen 4')
plt.ylabel('Crack length a [mm]')
plt.xlabel('Cycles N [-]')
plt.plot(x[0, 0:20], y[0, 0:20], 'b', label='Curve fit')
plt.plot(x, y,'b')
plt.legend()
plt.grid()

plt.figure(2)
plt.plot(data[3:-3,0],np.transpose(dadn))
plt.grid
plt.show()
```

Appendix B: Technical Drawings Wrapping Machine

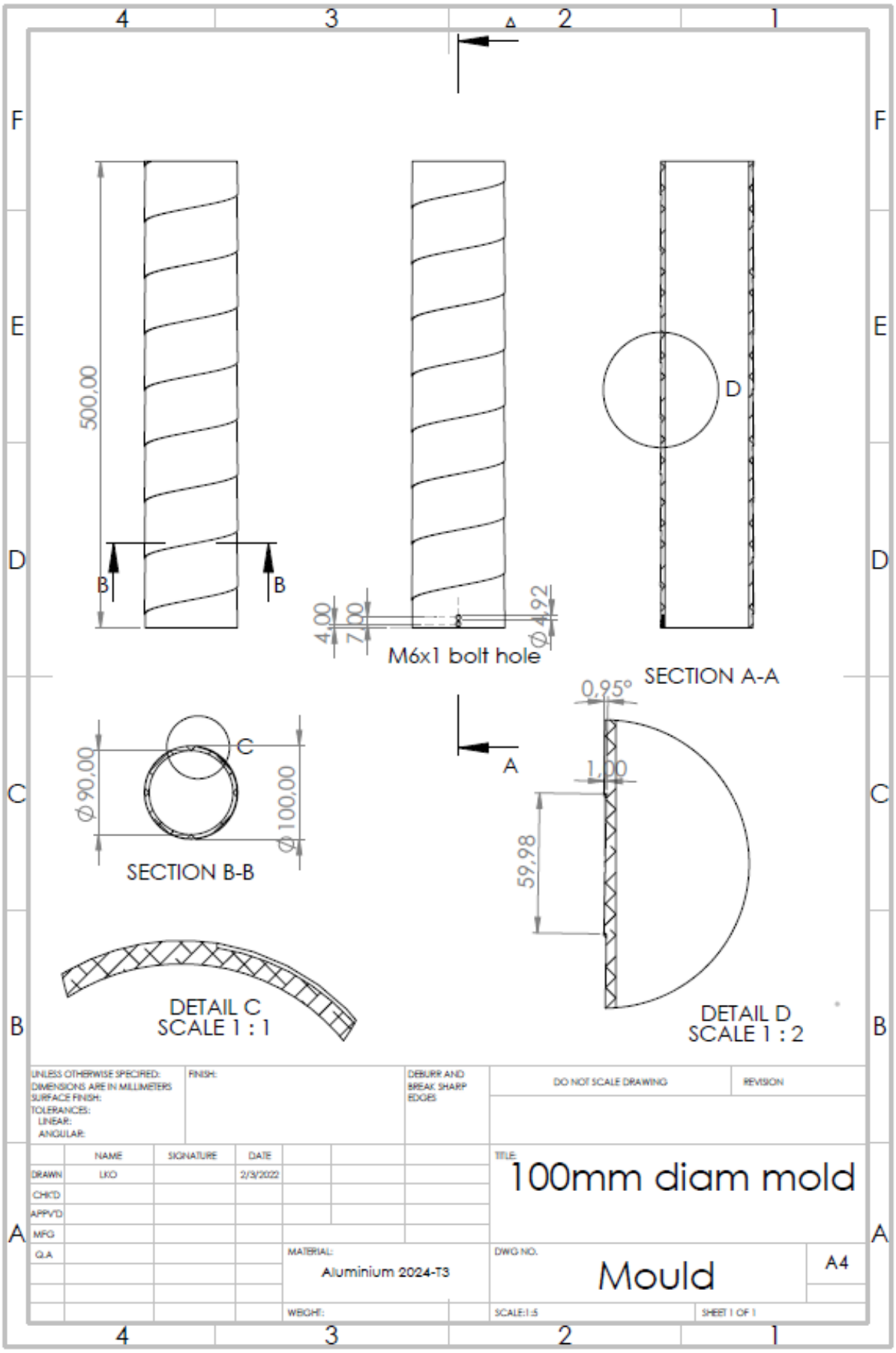

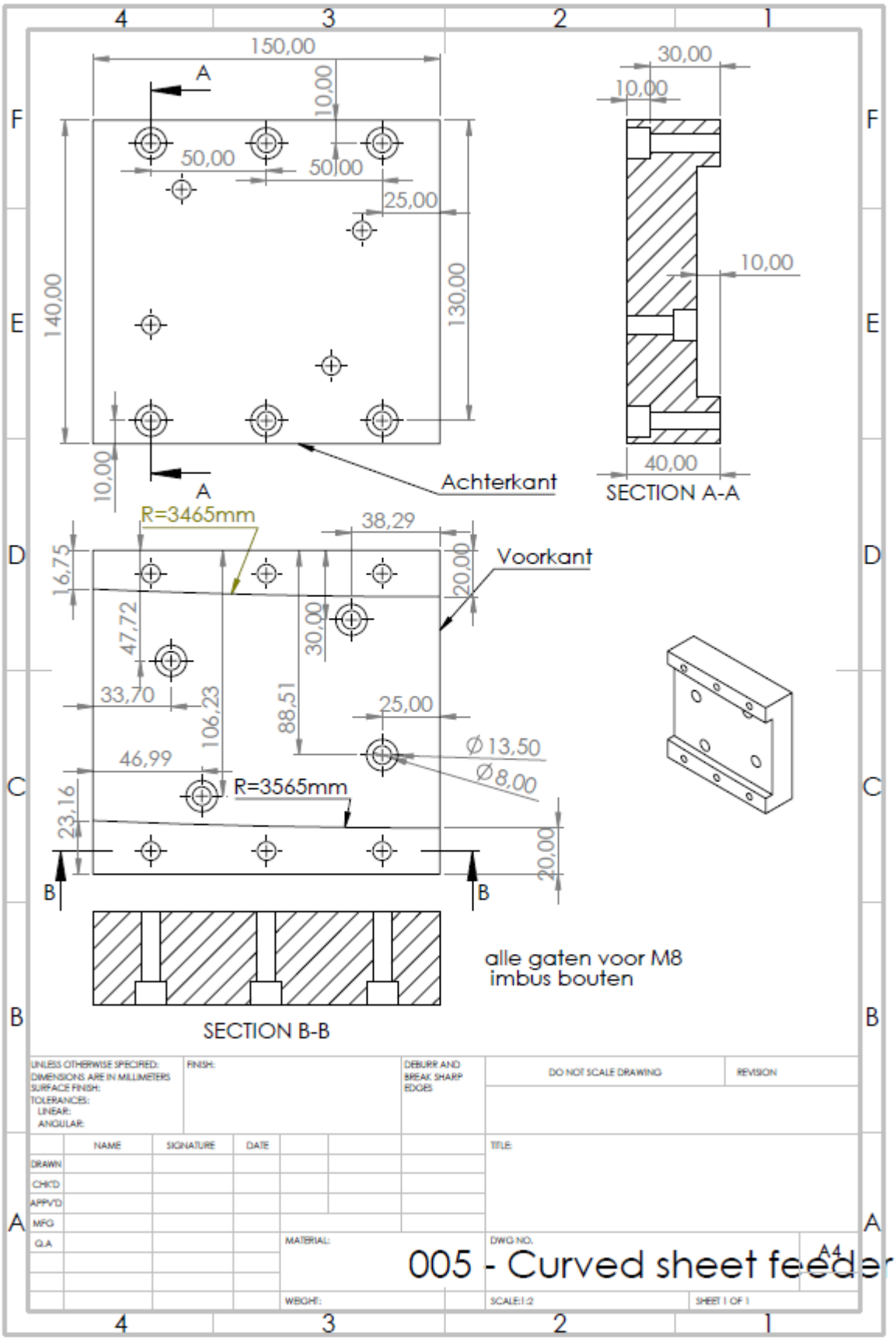
150,00
A
10,00
50,00
50,00
25,00
140,00
130,00
10,00
A
Achterkant
30,00
10,00
10,00
40,00
SECTION A-A
R=3465mm
38,29
16,75
20,00
Voorkant
47,72
30,00
33,70
106,23
88,51
25,00
Ø13,50
Ø8,00
46,99
R=3565mm
23,16
20,00
B
B
SECTION B-B
alle gaten voor M8
imbus bouten
UNLESS OTHERWISE SPECIFIED:
DIMENSIONS ARE IN MILLIMETERS
SURFACE FINISH:
TOLERANCES:
LINEAR:
ANGULAR:
FINISH:
DEBURR AND BREAK SHARP EDGES
DO NOT SCALE DRAWING
REVISION
NAME
SIGNATURE
DATE
DRAWN
CHK'D
APPV'D
MFG
Q.A
TITLE:
MATERIAL:
DWG NO.
005 - Curved sheet feeder
A4
WEIGHT:
SCALE:1:2
SHEET 1 OF 1

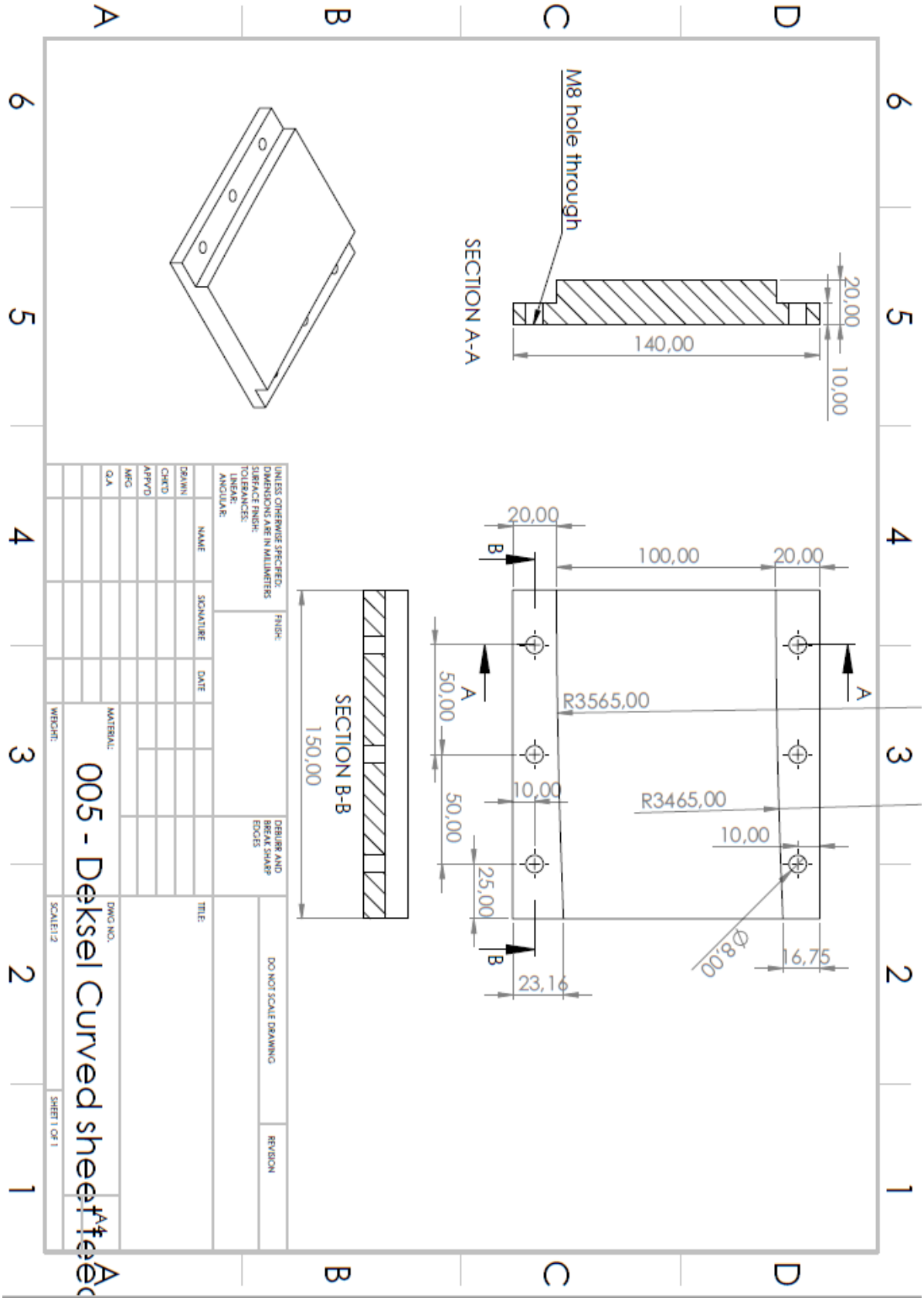
M8 hole through
SECTION A-A
20,00
140,00
10,00
SECTION B-B
150,00
20,00
100,00
20,00
50,00
R3565,00
10,00
50,00
R3465,00
10,00
25,00
16,75
23,16
005 - Deksel Curved sheet
A4

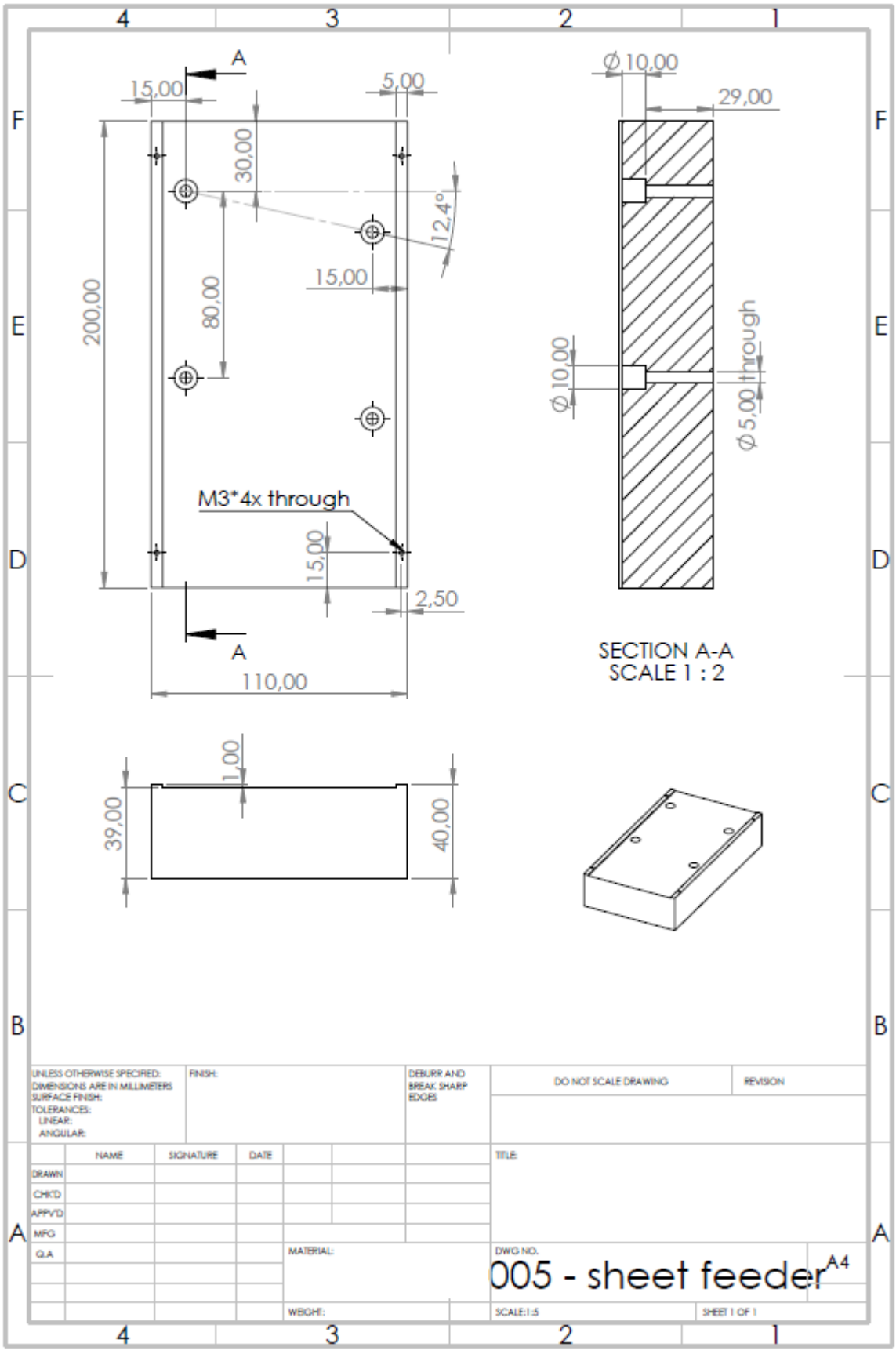
A
15,00
5,00
30,00
12,4°
15,00
200,00
80,00
M3*4x through
15,00
2,50
A
110,00
Ø 10,00
29,00
Ø 10,00
Ø 5,00 through
SECTION A-A
SCALE 1 : 2
1,00
39,00
40,00
UNLESS OTHERWISE SPECIFIED:
DIMENSIONS ARE IN MILLIMETERS
SURFACE FINISH:
TOLERANCES:
LINEAR:
ANGULAR:
FINISH:
DEBURR AND BREAK SHARP EDGES
DO NOT SCALE DRAWING
REVISION
NAME
SIGNATURE
DATE
DRAWN
CHKD
APPVD
MFG
Q.A
TITLE:
MATERIAL:
DWG NO.
005 - sheet feeder
A4
WEIGHT:
SCALE:1:5
SHEET 1 OF 1

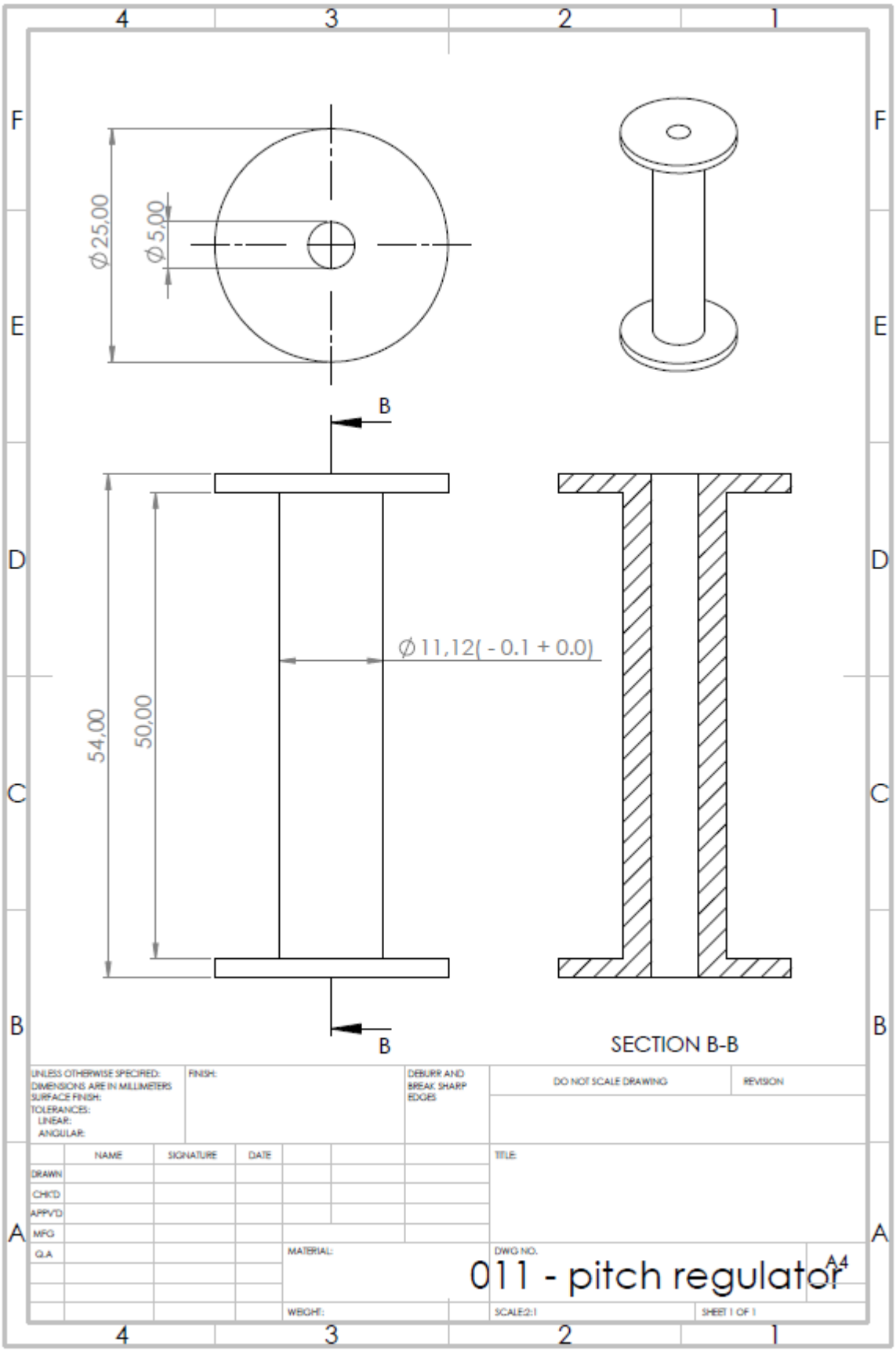
4
3
2
1
F
E
D
C
B
A
Ø25,00
Ø5,00
B
B
Ø11,12(- 0.1 + 0.0)
54,00
50,00
SECTION B-B
UNLESS OTHERWISE SPECIFIED:
DIMENSIONS ARE IN MILLIMETERS
SURFACE FINISH:
TOLERANCES:
LINEAR:
ANGULAR:
FINISH:
DEBURR AND BREAK SHARP EDGES
DO NOT SCALE DRAWING
REVISION
NAME
SIGNATURE
DATE
DRAWN
CHK'D
APPV'D
MFG
Q.A
TITLE:
MATERIAL:
DWG NO.
A4
011 - pitch regulator
WEIGHT:
SCALE:2:1
SHEET 1 OF 1

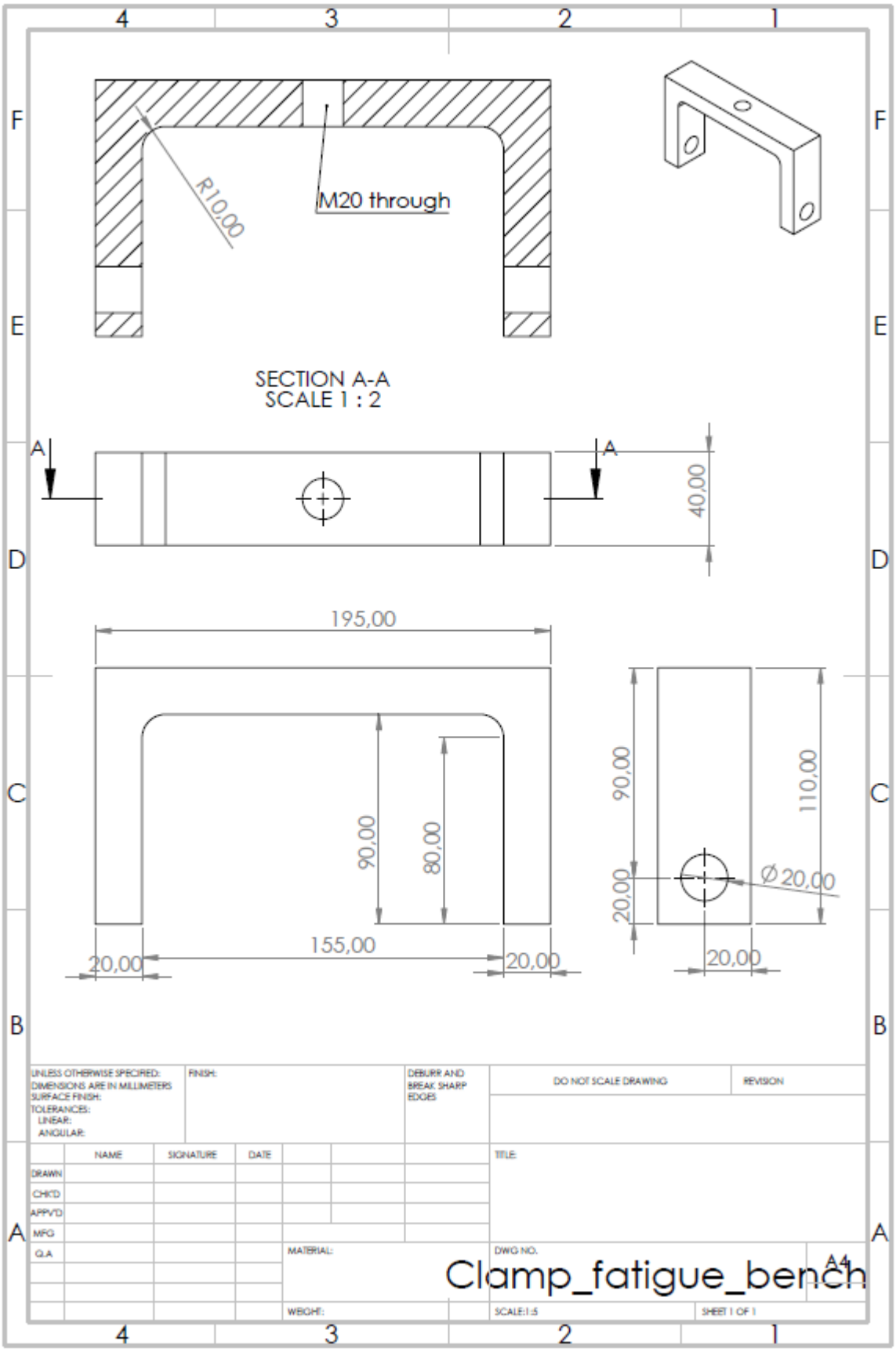
R10,00
M20 through
SECTION A-A
SCALE 1 : 2
A
A
40,00
195,00
90,00
80,00
155,00
20,00
20,00
90,00
110,00
20,00
Ø 20,00
20,00
UNLESS OTHERWISE SPECIFIED:
DIMENSIONS ARE IN MILLIMETERS
SURFACE FINISH:
TOLERANCES:
LINEAR:
ANGULAR:
FINISH:
DEBURR AND BREAK SHARP EDGES
DO NOT SCALE DRAWING
REVISION
NAME
SIGNATURE
DATE
DRAWN
CHK'D
APPV'D
MFG
Q.A
TITLE:
MATERIAL:
DWG NO.
A4
Clamp_fatigue_bench
WEIGHT:
SCALE:1:5
SHEET 1 OF 1

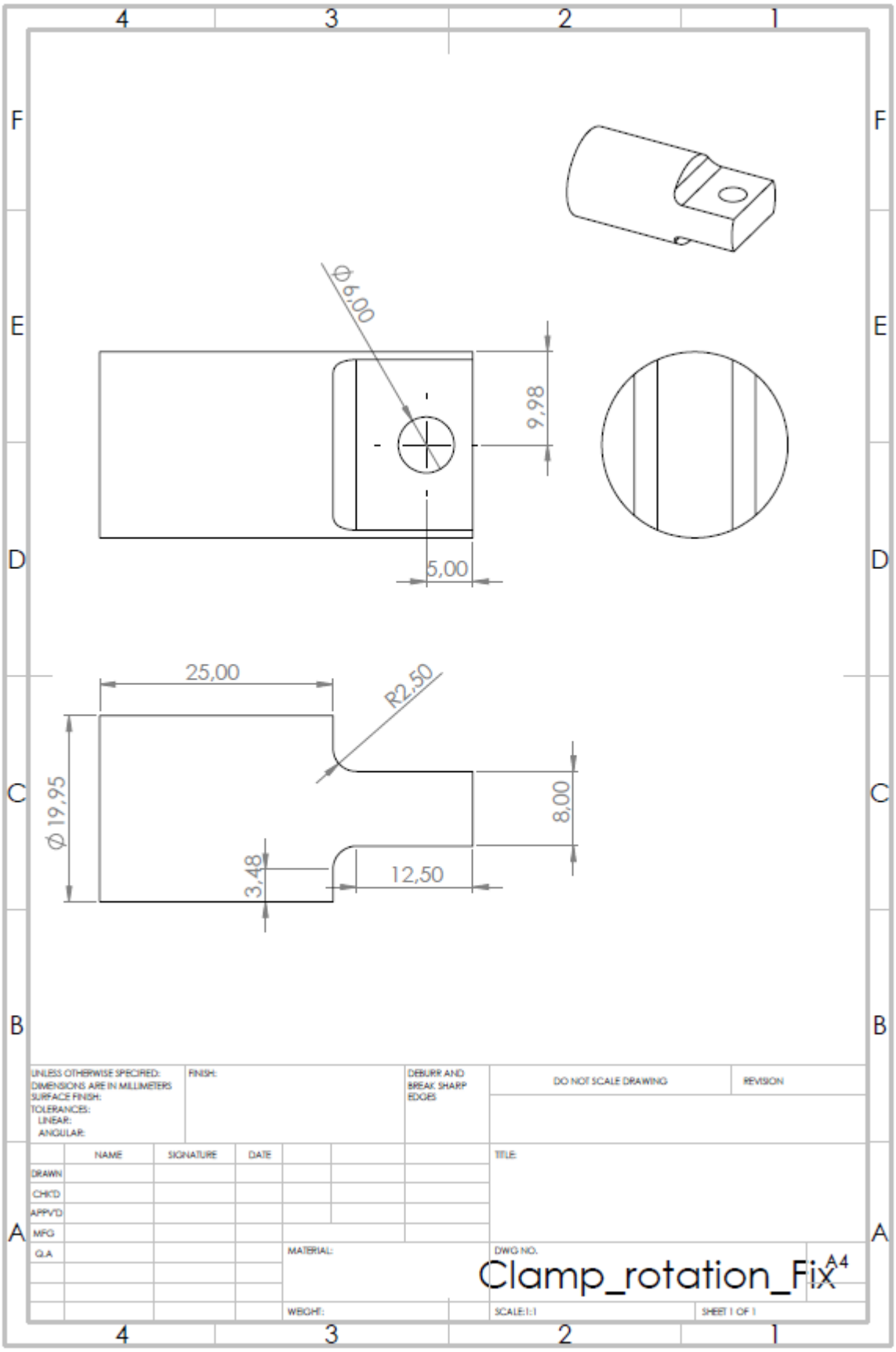
Ø6,00
9,98
5,00
25,00
R2,50
Ø 19,95
8,00
3,48
12,50
UNLESS OTHERWISE SPECIFIED:
DIMENSIONS ARE IN MILLIMETERS
SURFACE FINISH:
TOLERANCES:
LINEAR:
ANGULAR:
FINISH:
DEBURR AND BREAK SHARP EDGES
DO NOT SCALE DRAWING
REVISION
NAME
SIGNATURE
DATE
DRAWN
CHK'D
APPV'D
MFG
Q.A
TITLE:
MATERIAL:
DWG NO.
Clamp_rotation_Fix
A4
WEIGHT:
SCALE:1:1
SHEET 1 OF 1

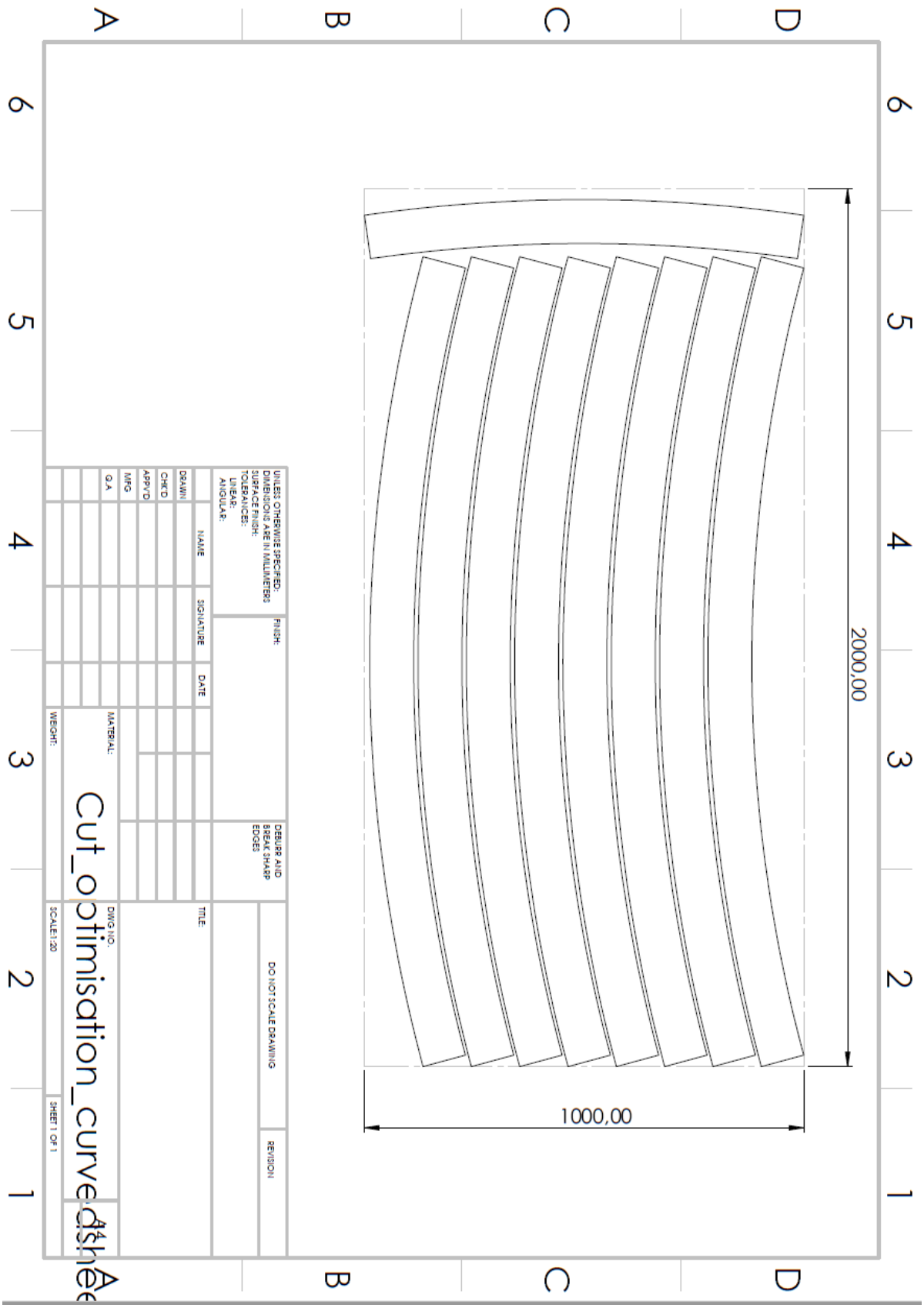
2000,00
1000,00
UNLESS OTHERWISE SPECIFIED:
DIMENSIONS ARE IN MILLIMETERS
SURFACE FINISH:
TOLERANCES:
LINEAR:
ANGULAR:
FINISH:
DEBURR AND BREAK SHARP EDGES
NAME
SIGNATURE
DATE
DRAWN
CHK'D
APP'D
MFG
Q.A
MATERIAL:
WEIGHT:
TITLE:
Cut_optimisation_curved_sheet
DWG NO.
SCALE:1:20
SHEET 1 OF 1
DO NOT SCALE DRAWING
REVISION
A4